University of Windsor
Scholarship at UWindsor

Electronic Theses and Dissertations

2002

Fluid inclusion studies of the Pea Ridge iron-oxide-rare earth elements deposit, Missouri.

Xinyu. Song
University of Windsor

Follow this and additional works at: http://scholar.uwindsor.ca/etd

Recommended Citation

Song, Xinyu., "Fluid inclusion studies of the Pea Ridge iron-oxide-rare earth elements deposit, Missouri." (2002). *Electronic Theses and Dissertations.* Paper 2130.

This online database contains the full-text of PhD dissertations and Masters' theses of University of Windsor students from 1954 forward. These documents are made available for personal study and research purposes only, in accordance with the Canadian Copyright Act and the Creative Commons license—CC BY-NC-ND (Attribution, Non-Commercial, No Derivative Works). Under this license, works must always be attributed to the copyright holder (original author), cannot be used for any commercial purposes, and may not be altered. Any other use would require the permission of the copyright holder. Students may inquire about withdrawing their dissertation and/or thesis from this database. For additional inquiries, please contact the repository administrator via email (scholarship@uwindsor.ca) or by telephone at 519-253-3000ext. 3208.

INFORMATION TO USERS

This manuscript has been reproduced from the microfilm master. UMI films the text directly from the original or copy submitted. Thus, some thesis and dissertation copies are in typewriter face, while others may be from any type of computer printer.

The quality of this reproduction is dependent upon the quality of the copy submitted. Broken or indistinct print, colored or poor quality illustrations and photographs, print bleedthrough, substandard margins, and improper alignment can adversely affect reproduction.

In the unlikely event that the author did not send UMI a complete manuscript and there are missing pages, these will be noted. Also, if unauthorized copyright material had to be removed, a note will indicate the deletion.

Oversize materials (e.g., maps, drawings, charts) are reproduced by sectioning the original, beginning at the upper left-hand corner and continuing from left to right in equal sections with small overlaps.

ProQuest Information and Learning
300 North Zeeb Road, Ann Arbor, MI 48106-1346 USA
800-521-0600

UMI®

Fluid Inclusion Studies of the Pea Ridge Fe-Oxide-REE Deposit, Missouri

by

Xinyu Song

A Thesis
Submitted to the Faculty of Graduate Studies and Research
through the Department of Earth Sciences in
Partial Fulfillment of the Requirements for
the Degree of Master of Science at the
University of Windsor

Windsor, Ontario, Canada

2002

National Library of Canada
Acquisitions and Bibliographic Services
395 Wellington Street
Ottawa ON K1A 0N4
Canada

Bibliothèque nationale du Canada
Acquisitions et services bibliographiques
395, rue Wellington
Ottawa ON K1A 0N4
Canada

Your file Votre référence

Our file Notre référence

The author has granted a non-exclusive licence allowing the National Library of Canada to reproduce, loan, distribute or sell copies of this thesis in microform, paper or electronic formats.

The author retains ownership of the copyright in this thesis. Neither the thesis nor substantial extracts from it may be printed or otherwise reproduced without the author's permission.

L'auteur a accordé une licence non exclusive permettant à la Bibliothèque nationale du Canada de reproduire, prêter, distribuer ou vendre des copies de cette thèse sous la forme de microfiche/film, de reproduction sur papier ou sur format électronique.

L'auteur conserve la propriété du droit d'auteur qui protège cette thèse. Ni la thèse ni des extraits substantiels de celle-ci ne doivent être imprimés ou autrement reproduits sans son autorisation.

0-612-75852-4

Canada

972993

© Xinyu Song, 2002
All Rights Reserved

Abstract

The Pea Ridge iron oxide-REE deposit is hosted by the Mesoproterozoic St. Francois granite-rhyolite terrane in southeast Missouri and is considered to be an example of an Olympic Dam-type deposit. Primary aqueous, liquid-vapour (LV) inclusions in apatite from the early amphibole stage have salinities of 14 to 24 equiv. wt. % $NaCl+CaCl_2$ and Th (L-V) values of 130°C to 180°C. Primary fluid inclusions in quartz from the post-magnetite hematite stage comprise aqueous liquid-only and liquid-vapour inclusions. This association, and homogenization temperatures of around 100°C for many of the LV inclusions, indicates low depositional temperatures. The LV inclusions have salinities of 21 ± 3 equiv. wt. % $NaCl+CaCl_2$.

Primary inclusions in quartz from the silicification stage, which surrounds the magnetite and hematite zones, comprise liquid-vapour-halite (LVH) inclusions that have salinities between 34 and 48 equiv. wt. % NaCl. These inclusions homogenize by halite dissolution, with TmH values of between 245°C and 422°C. These high salinity inclusions also occur as secondary inclusions in the earlier amphibole, magnetite, and hematite stages. LVH inclusions may also contain trapped hematite or calcite crystals. CO_2-bearing inclusions occur as secondary inclusions in quartz of the silicification stage. These comprise both halite-bearing, aqueous, liquid-rich inclusions and CO_2-rich, aqueous-poor inclusions. No CH_4 has been detected by Raman spectroscopy.

Primary inclusions in quartz from late-stage REE-rich breccia pipes consist of LV inclusions that exhibit two salinity populations; one is moderately saline (~20 wt. %) and one is dilute (0-5 wt. %). Where consistent, Th (L-V) values for these inclusions have a mode at 230°C. There are also abundant primary, liquid-only fluid inclusions within quartz growth zones in the breccia pipes, indicating low formation temperatures during the later stages of quartz deposition.

Microthermometry data suggest that there are three types of fluids responsible for the formation of the Pea Ridge deposit. A moderate salinity fluid (~20 wt. %) formed the amphibole-apatite and hematite zones and was also present during formation of the breccia

pipes. The temperature of this fluid was at least 300°C during amphibole formation, decreased to 150°C or less during hematite formation and increased again to approximately 320°C during breccia pipe formation. Between hematite and breccia pipe formation, a high salinity (average 40 wt. %), high temperature (270°C to 450°C) fluid formed the silicification stage. During breccia pipe formation, a low salinity fluid infiltrated the system.

These data suggest the following. a) the fluid responsible for hematitic alteration of the magnetite zone was similar to that which deposited the amphibole and possible magnetite, except that it may have been more oxidizing; this fluid was moderately saline and low temperature and may have been derived from evaporite-related brines. b) a second fluid was responsible for silicification and was hypersaline. The common occurrence of CO_2-rich inclusions in these samples suggests that immiscibility occurred during infiltration of this hypersaline fluid, and by analogy with other deposits, may have been magmatic. c) The third fluid responsible for the REE-rich breccia pipes is a mixture of the first fluid with a distinct, late, lower-salinity, possibly meteoric, fluid.

These results differ from preliminary fluid inclusion data obtained by Sidder et al. (1993), which indicated that the salinity of the fluids responsible for the early stages (amphibole, magnetite, and hematite) were significantly higher than the estimates reported here. This is likely due to a different interpretation of the origin of LVH inclusions in the early zones and/or to the timing of the quartz from which they obtained their data.

Comparison of the ore-forming fluids at Pea Ridge with other Proterozoic Fe-Oxide Cu-Au-(REE) deposits suggest that they have the same types of fluids present, i.e., (1) high temperature and hypersaline aqueous fluids coexisting with carbonic fluids, which are thought to be magmatic, and (2) low temperature and very dilute fluids, which are thought to be derived from meteoric water. However, the Pea Ridge deposit differs in that it has moderate salinity and low to moderate temperature fluids in the early alteration and hematite stages, and possibly in the magnetite stage.

TABLE OF CONTENTS

Dedication

To my parents, my sister and brother.

Acknowledgments

Sincerest thanks go to Dr. Iain Samson and Dr. Brian Fryer for their support and instruction on this project. Special thanks go to Cheryl Seeger from Missouri Geologic Survey for her assistance with field work, sample collection, and discussions on the deposit geology, to Mark Marikos at the University of Arizona for his discussion on the paragenesis, to Joel Gagnon for his assistance in Laser ICP/MS experiments and to Nik Pieczonka for his assistance with the Raman spectrometer. Thanks also go to my fellow colleagues Sean Crowe, Shanmugam (Johari) Pannalal and Magdalena Scarlat for their help during my stay in the department. Special thanks go to Dr. Phil Graniero, Dr. Michael Harris, Dr. Phil McCausland and Misuk Yun for their kind help with graphing, sample processing, data searching and presentation.

Abbreviation

Abbreviation	Mineral Name	Abbreviation	Microthermometry term
ab	Albite	Tn	Nucleation temperature of phase
act	Actinolite	Te	Eutectic temperature
all	Allanite	TmICE	Ice melting temperature
amph	Amphibole	TmHh	Hydrohalite melting temperature
and	andalusite	TmNaCl	Halite dissolution temperature
anh	anhydrite	Th (L-V)	Liquid-vapour homogenization temperature
ap	apatite	Td	Decrepitation temperature
bar	barite	$TnCO_2$	Nucleation temperature of carbon dioxide
bio	biotite	$ThCO_2$	Homogenization temperature of carbon dioxide
cal	calcite	$TmCO_2$	Melting temperature of carbon dioxide
chl	chlorite	TmCLATH	Clathrate melting temperature
cp	chalcopyrite		
fl	fluorite	ppl	Plane polarizer light
gn	galena	xpl	Cross plane light
hbl	hornblende		
hl	halite		
hm	hematite		
kfs	K-feldspar		
mnz	monazite		
ms	muscovite		
mt	magnetite		
px	pyroxene		
py	pyrite		
po	pyrrhotite		
qtz	quartz		
Rt	rutile		
Ser	sericite		
Sd	siderite		
Sph	sphalerite		

List of Figures

List of Tables and Appendices

1 Introduction

1.1 Introduction to the Pea Ridge deposit

The Pea Ridge Fe oxide-REE (rare earth element) deposit is hosted by the Mesoproterozoic, 1.45-1.48 Ga (Bickford, 1988) St. Francois granite-rhyolite terrane in Southeast Missouri (Kisvarsanyi and Proctor, 1967; Kisvarsanyi and Kisvarsanyi, 1989a, b). The St. Francois terrane consists mainly of rhyolite that was intruded by coeval subvolcanic granite plutons (Figure 1). In addition, granite porphyries and an iron-rich trachyte suite were emplaced as ring-dike intrusions around the margins of caldera complexes (Sidder et al., 1993a,b) (Figure 2). This igneous suite hosts numerous iron-oxide ± Cu ± REE deposits that some workers have included in an important class of deposits variably referred to as Proterozoic Fe-oxide-Cu-Au-U-REE or Olympic Dam-type deposits. This class includes the Olympic Dam Fe oxide-Cu-U-Au-REE deposit, South Australia, the Kiruna iron ore district, Sweden, and the Bayan Obo Fe-REE-Nb deposit, China (e.g. Sims et al., 1987; Einaudi and Oreskes, 1990; Hitzman et al., 1992; Oreskes and Hitzman, 1993, Williams et al., 1999).

This comparison has generated a significant amount of research interest in the Pea Ridge and other deposit in the St. Francois terrane (e.g., Day et al., 1989a,b; Hauck et al., 1989; Hauck, 1990; Kisvarsanyi, 1990; Sidder et al., 1991; Nuelle et al., 1991a,b; Menuge et al., 1997; Kerr, 1998; Kerr and Samson, 1998; Gleason et al., 2000). There are, however, still many fundamental questions that need to be addressed that relate to: 1) the nature and source of the fluids responsible for the various stages of mineralization at Pea Ridge; and 2) the relationship between Pea Ridge and the other deposits of the Olympic Dam class.

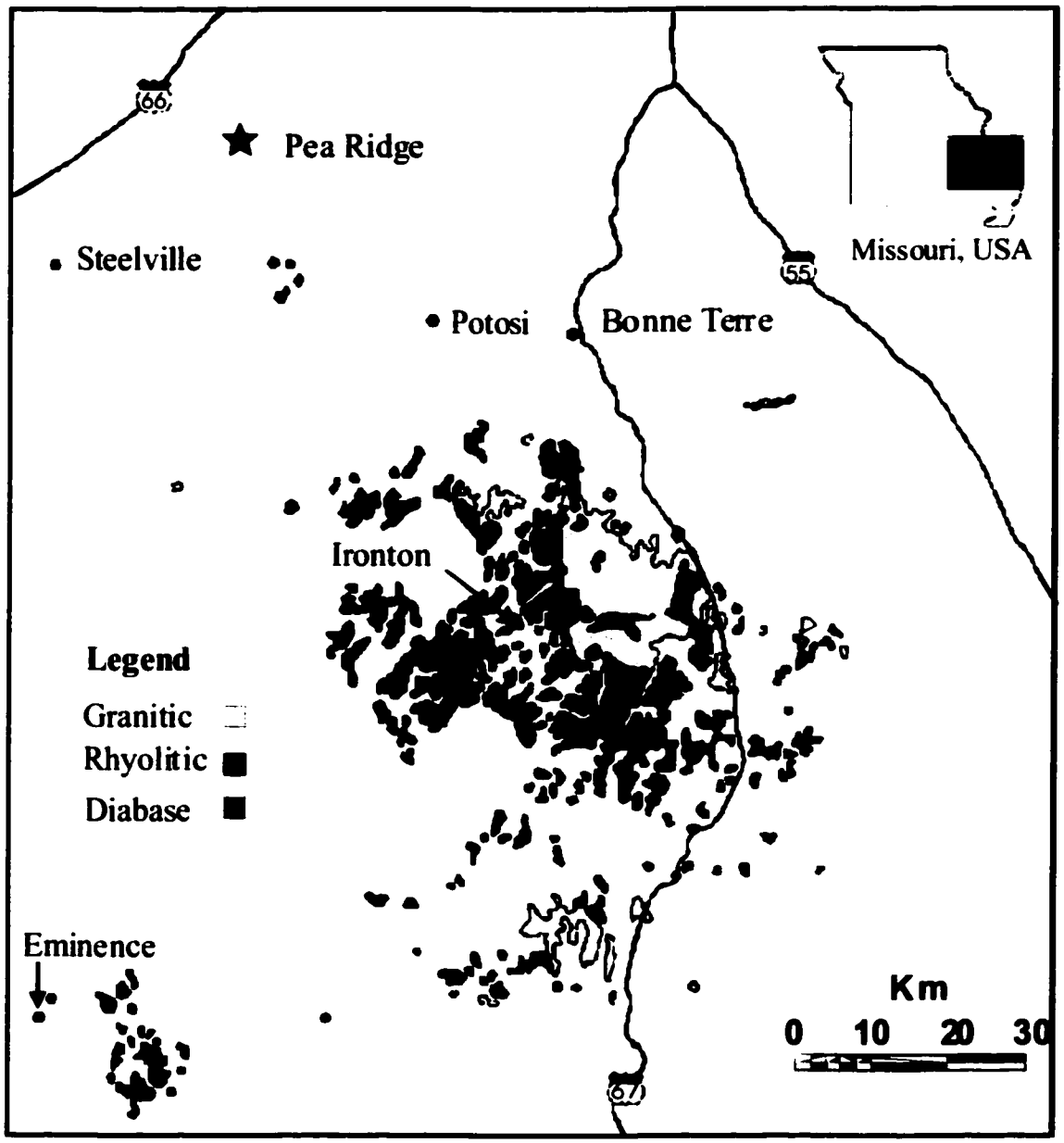

Figure 1 Exposed Precambrian rocks in the St. Francois Mountains and the location of the Pea Ridge deposit, Missouri (Cited from Kerr, 1998, after U.S.G.S. Missouri Geology Map)

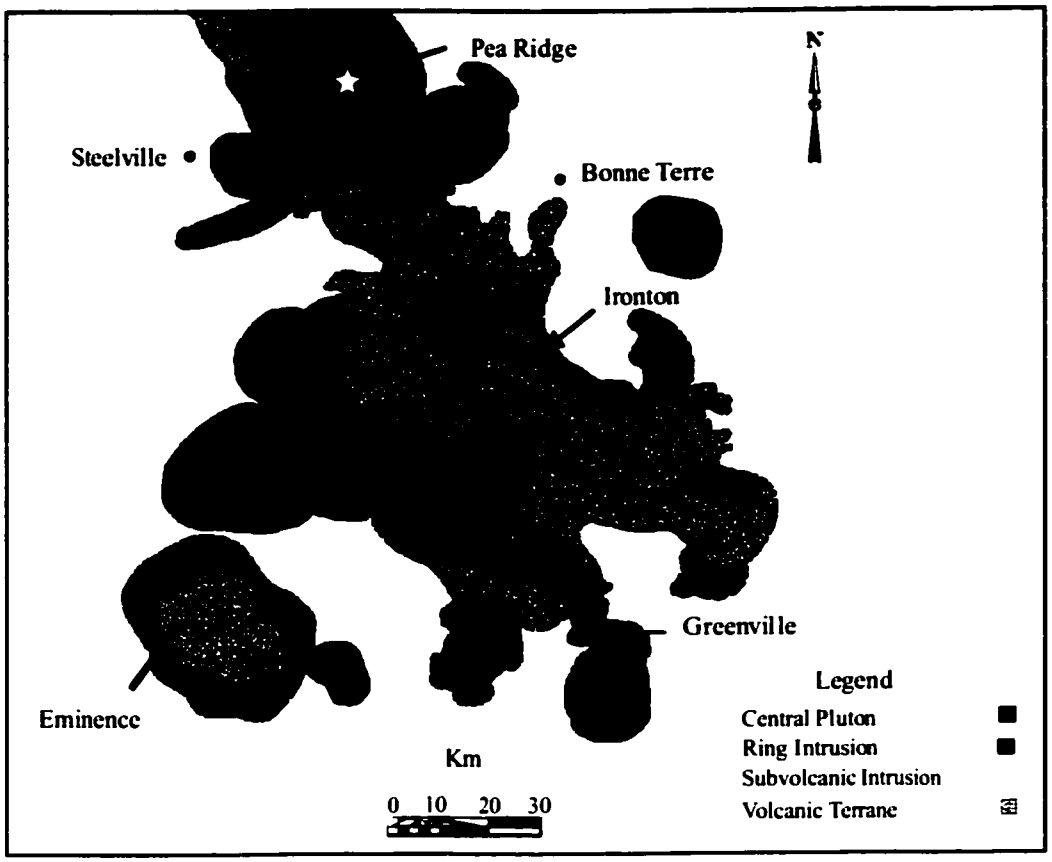

Figure 2 Geological map of the middle Proterozoic St. Francois terrane, Missouri showing locations of eight known magnetite and hematite deposits (Cited from Kerr, 1998. after Kisvarsanyi and Kisvarsanyi, 1989)

1.2 Olympic Dam-type Deposits

Hitzman et al. (1992) and Oreskes and Hitzman (1993) proposed that the following deposits and districts comprise a single class, named Olympic Dam Class Deposits, also known as Proterozoic Fe oxide Cu-U-Au-REE deposits:

- the Olympic Dam Cu-U-Au-Ag deposit, South Australia
- the Cloncurry District, North Queensland, Australia
- the Wernecke Mountain Breccia, Yukon
- the Kiruna iron ore district, Sweden
- the Bayan Obo district, China

- the Southeast Missouri iron district (including Pea Ridge)
- the Great Bear magmatic zones, Northwest Territories, Canada

The characteristics of this class of deposits have been generalized by Hitzman et al (1992) as follows:

- **Age.** Most examples of this class of deposit are found within early to middle Proterozoic host rocks (1.1-1.8 Ga).
- **Tectonic setting.** The deposits have a spatial and temporal association with extensional tectonics.
- **Host rocks.** These may be igneous or sedimentary. Many of the deposits occur in anorogenic silicic to intermediate igneous rocks.
- **Mineralogy.** The dominant minerals are magnetite and hematite. The former is found at deeper levels than the latter. Carbonates, barium, phosphorous, or fluorine minerals are common and many of the deposits contain anomalous abundances of REE.
- **Alteration.** There is a general trend from sodic alteration at deep levels, to potassic alteration at intermediate to shallow levels, to sericitic alteration and silicification at very shallow levels.

Hitzman et al. (1992) proposed that these deposits are formed in shallow crustal environments (< 4 – 6 km), where deep-seated, volatile-rich igneous-hydrothermal systems have been tapped by deep crustal structures. Oreskes and Hitzman (1993) further proposed that exploration criteria should include the recognition of characteristic alteration and associated geochemical anomalies and the regional structure that focused the hydrothermal fluids, rather than the recognition of a particular igneous association.

The type member of this class of deposit is the Olympic Dam deposit, which is located in the mid-Proterozoic granite basement of the Stuart shelf region of South Australia. It contains over 2 billion tons of Cu-U-Au-Ag-REE mineralization hosted by hematite-rich breccias in fractured granite (Robert and Hudson, 1983; Reeve et al., 1990; Oreskes and Einaudi, 1990). Oreskes and Einaudi (1992) conducted fluid inclusion and stable isotope studies on the Olympic Dam and the nearby Acropolis deposit and proposed that two sources of fluids of contrasting temperature,

composition, and oxygen isotope characteristics were involved in their formation. They showed that early magnetite was formed from fluids with high $\delta^{18}O$ values (~10 ‰) at temperatures of about 400°C and concluded that the fluids had a deep source and possibly were magmatic in origin. They also showed that later hematite in the ore-bearing breccias was formed from fluids with lower and more variable $\delta^{18}O$ values (+4.5 to –2.5 ‰) and at lower temperatures of between 200°C and 400°C. They also concluded that these fluids had salinities ranging from 31 to 42 wt. % and that these waters had a surficial origin, such as seawater, closed-basin water, or ground water. Late-stage fluorite veins were formed at temperatures of between about 90°C and 210°C and the fluids had salinities ranging from 6.6 to 22.8 wt. %.

Oreskes and Hitzman (1993) proposed that the Olympic Dam-type deposits were formed primarily from hydrothermal processes operating in shallow crustal environments. Igneous intrusions may be critical in supplying heat and/or volatile-rich solutions and possibly metals to the systems, but the ore deposits form at higher structural levels than the magmas. Variations in deposit mineralogy, alteration assemblages and parageneses are suggested to be related to depth of formation and the nature of the host rocks (Hitzman et al., 1992; Oreskes and Hitzman, 1993). They proposed that the hematite-bearing deposits with associated sericitic alteration and silicification and the highest concentrations of Cu, Au and U, are formed at the shallowest levels, as typified by the Olympic Dam deposit. At greater depths, magnetite is the dominant Fe-oxide with potassic (K-feldspar-sericite-magnetite-quartz (biotite, actinolite, chlorite), and sodic (albite-magnetite-actinolite) alteration being more important than sericitization and silicification.

Haynes et al. (1995) presented a fluid mixing model for the Olympic Dam deposit, in which the mixing of hot, saline, reduced magmatic or deeply circulated meteoric water and cooler, moderately saline, more oxidized meteoric water was responsible for the formation of the deposit.

Johnson and McCulloch (1995) used Nd isotopic evidence to propose that two fluids were involved in the genesis of the Olympic Dam deposit. They found εNd values of -2.5 for the hematite breccia ores that are more positive than the εNd values of -5 obtained from the magnetite ores. They present a model in which an early, granite-related fluid precipitated

magnetite, and a later "ore-forming" fluid oxidized the magnetite to form hematite, and introduced Cu and REE. They further suggest that the εNd signature of -2.5 for the hematite breccia ores cannot be derived from preexisting crustal rocks, and must have involved a contribution from mantle-derived source rock or magma, i.e. the altered alkaline mafic/ultramafic dykes within the deposit.

Gow et al. (1994) studied the Emmie Bluff deposit near Olympic Dam and found that it has similar characteristics to Olympic Dam. Magnetite and pyrite were deposited from magmatic fluids with $\delta^{18}O$ values of ~8 to 9 ‰ at temperatures of 400°C to 600°C. Later, hematite-associated Cu mineralization, formed from lower-temperature, Cu-rich fluids that had a meteoric component, as indicated by $\delta^{18}O$ values of between 0 and 2 ‰.

Barton and Johnson (1996) proposed that evaporites may be involved in the ore-forming process in providing the highly saline fluids that are thought to be responsible for the formation of these deposits. These authors include many Phanerozoic deposits in this class and propose that examples of these deposits may be as young as Holocene, rather than being all Proterozoic, as proposed by Hitzman et al. (1992). Barton and Johnson (1996) also inferred that the Fe oxide-REE-Cu-Au-U deposits may form in various tectonic environments, such as within and behind oceanic and terrestrial arcs, failed continental rifts, active rifts, and on stable platforms associated with hot-spot volcanism. They argue that magmatism provides the necessary heat to drive fluid circulation and igneous rocks may host the mineralization. However, they do not exclude the possibility that immiscible oxide melts or magmatic-hydrothermal fluids were involved in the formation of these deposits.

Fluid inclusion data on a variety of iron-oxide Cu-Au-REE deposits in this class, such as Olympic Dam, Australia, Candelaria, Chile, the Cloncurry district, Australia (Maramungee Creek, Little Eva, Ernest Henry, Mount Elliot, Osborne, Lighting Creek, Starra, Eloise), and Pahtohavare, Kiruna, Sweden indicate that the fluids responsible for the main stage of mineralization had high temperatures (300-600°C) and were a combination of hypersaline, aqueous and carbonic fluids. Late or post ore-stage fluids were low temperature (100-300 °C) and more dilute (0-28 wt. %). Workers on these deposits generally concluded that the main-

stage ore-forming fluids were magmatic, and that the post ore fluids were meteoric (Marschik et al., 2000; Marschik & Fontbote, 2001; Ullrich and Clark, 1999; Xu, 2000; Adshead et al., 1998; Adshead, 1995; Perring et al., 1999; Perring et al., 2000; Rotherham et al., 1998; Baker, 1998; Lindblom et al., 1996)

The above case studies regarding the ore forming fluids in different Olympic Dam-type deposits in different parts of the world demonstrate that they are all formed from hydrothermal fluids. This is contrary to the view held by some workers that the magnetite in some of the deposits is orthomagmatic; i.e. was formed from oxide magmas.

2 Deposit Geology

The Pea Ridge Iron oxide-REE deposit is composed of apatite-bearing high grade (~55 %) Fe oxide ores (Emery, 1968) and high grade REE ores (>10 wt. % REE_2O_3) (Kisvarsanyi, 1990; Marikos et al., 1990; Sidder et al., 1993a,b). Detailed descriptions are provided in Emery (1968), Nuelle et al. (1989a), Sidder et al. (1993a) and Kerr (1998), and only a summary is given here. The Fe mainly occurs as magnetite in an elongate, cross-cutting tabular body that is hosted by broadly coeval rhyolite flows (Seeger et al., 1989; Marikos et al., 1990; Day et al., 1989a, b; Sidder et al., 1993a, b; Figure 3). The REE mainly occur in breccia pipes that crosscut the Fe oxide ores (e.g., Seeger et al., 1989; Marikos et al., 1990; Day et al., 1991). This association of Fe oxide and REE enrichments at Pea Ridge, along with Fe-Cu-Au mineralization at the nearby Boss-Bixby deposit have, in part, led to direct comparisons with the high-grade, Fe oxide-Cu-Au-U-REE-enriched deposits at Olympic Dam, Australia (e.g., Einaudi and Oreskes, 1990; Hagni and Brandom, 1990; Hitzman et al. 1992). Nuelle et al. (1989a, b) described a variety of mineralogically distinct zones from the deposit that they interpreted to have formed in the following order: amphibole zone, magnetite zone, specular hematite zone, silicified and quartz vein zone and breccia pipes (Figure 3, 4 and Table 2). Other rock types include aplite dikes, and mafic dikes. Below is a brief description of the various stages of the Pea Ridge deposit.

2.1 Paragenesis

Amphibole zone: The amphibole zone occurs in both the hanging wall and foot wall of the deposit (Nuelle et al., 1989a, b). It is composed of massive, coarse-grained actinolite with interstitial apatite (Figure 5B), magnetite, pyrite, chalcopyrite, and calcite. Quartz occurs as interstitial grains and massive pods (Nuelle et al., 1989a, b; Sidder et al., 1993a, b). Contacts between the amphibole zone and the host rhyolite (Figure 5A) are generally gradational; some wall rock exhibits minor replacement by actinolite (Nuelle et al., 1989a, b; Sidder et al., 1993a, b). The amphibole stage is interpreted to represent a metasomatic alteration front that preceded emplacement of the magnetite ores (Sidder et al., 1993a, b).

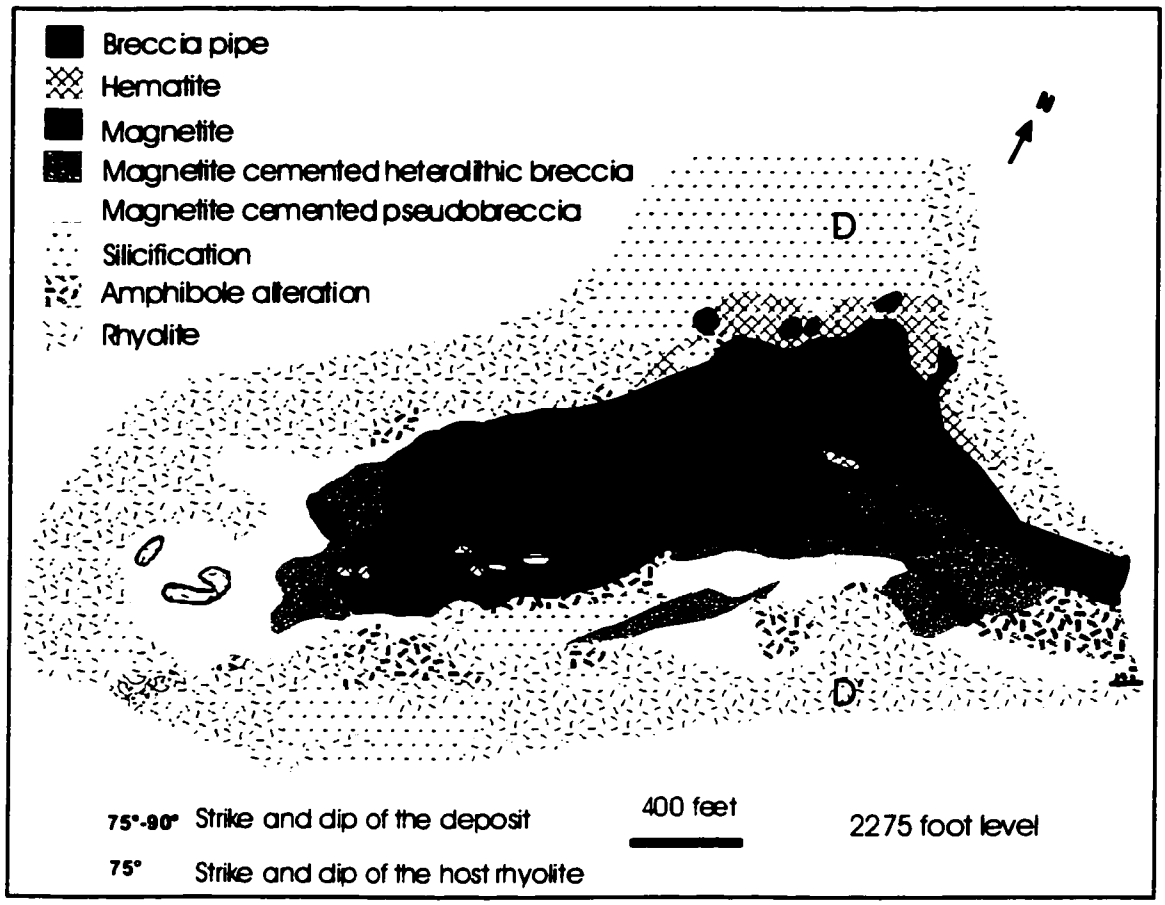

Figure 3 Geological map of the 2275 ft. level of the Pea Ridge deposit (Modified from Seeger et al., 2001)

Magnetite zone: The magnetite zone comprises massive magnetite ores (Figure 5D), magnetite-cemented breccias (magnetite heterolithic breccias), and magnetite pseudobreccia (Nuelle et al., 1989a). Massive magnetite ores consist of 60 to 90 modal percent magnetite, the remainder comprising gangue minerals such as apatite, quartz (Figure 5E), phlogopite, chlorite, pyrite, calcite, chalcopyrite, fluorite, barite, and potassium feldspar. In the main magnetite orebody, the magnetite is generally massive, coarse to fine grained, and granular. The gangue minerals form interstitial intergrowths, net-textured veinlets, and pods within the massive magnetite ores.

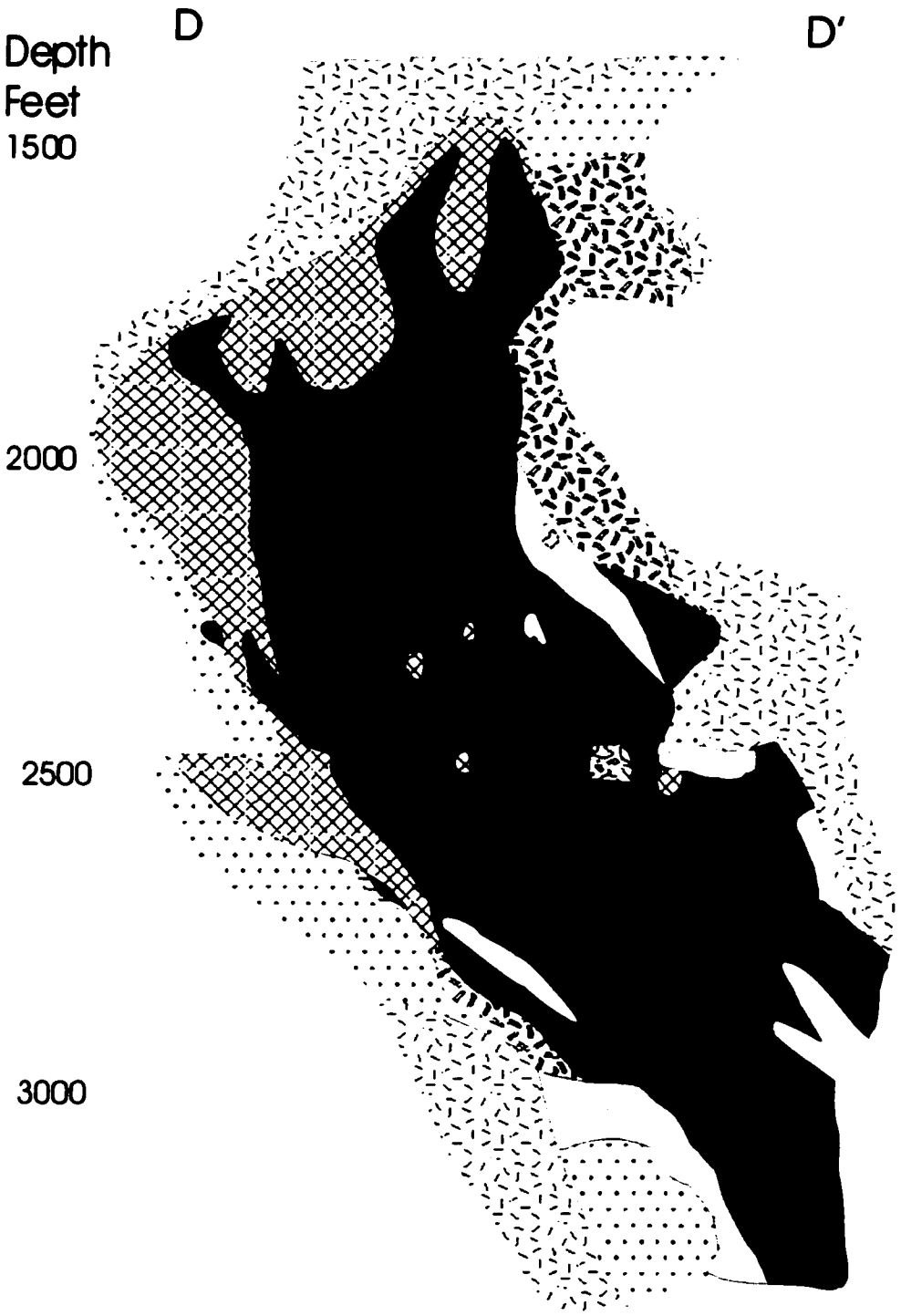

Figure 4 Cross section of D-D' showing the vertical occurrence of various zones. Legend is the same as Figure 3 (Modified from Seeger et al., 2001)

Figure 5 Microphotographs of minerals and their textures

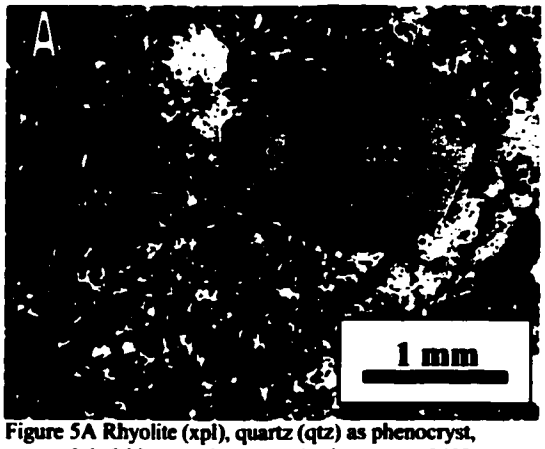

Figure 5A Rhyolite (xpl), quartz (qtz) as phenocryst, quartz & k-feldspar (Kfs) as matrix, image # pr0492, sample # PR95-1.

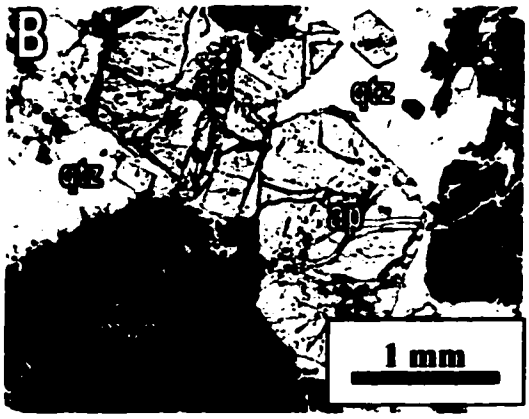

Figure 5B Amphibole stage (xpl), amphibole (amph) coexisting with apatite (ap), image # pr0493, sample # PR95-25.

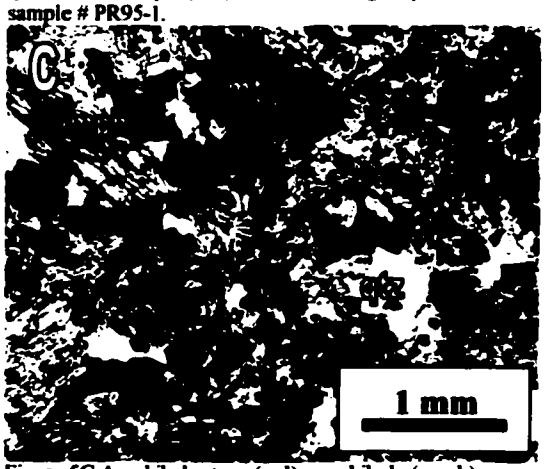

Figure 5C Amphibole stage (ppl), amphibole (amph) replaced by quartz (qtz)(white) and magnetite (mt) (black). Image # pr0484, sample # PR95-10.

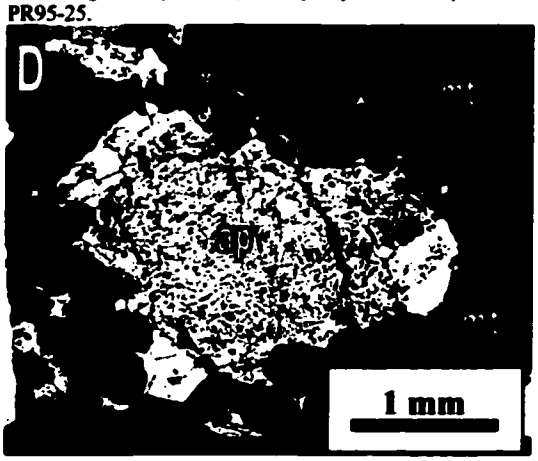

Figure 5D Magnetite stage (ppl), apatite (ap) coexists with magnetite (mt)(black), but replaced by magnetite, image # pr0485, sample # PR95-12

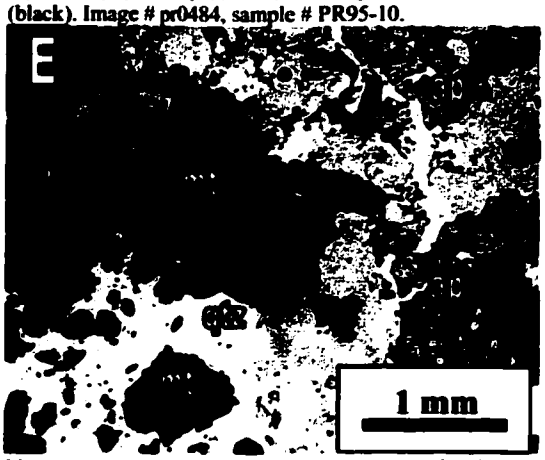

Figure 5E Magnetite stage (ppl), magnetite (mt)(black) & apatite (ap) replaced by quartz (qtz), image #pr0486, sample #PR95-14.

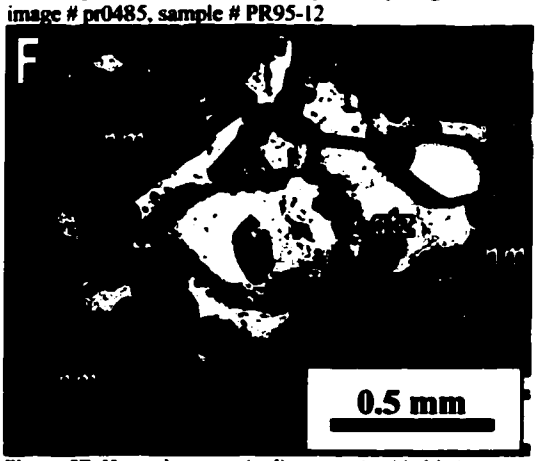

Figure 5F Hematite stage (xpl), quartz (qtz)(white) co-precipitating with hematite (hm)(black), image #pr0494, sample # PR01-69.

Figure 5 continued

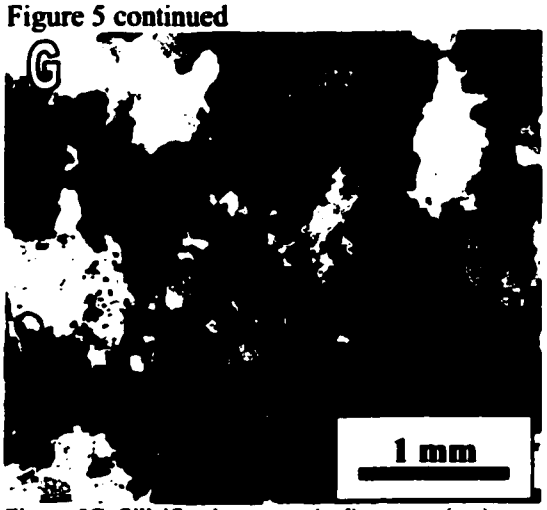

Figure 5G Silicification stage, (xpl), quartz (qtz) coexisting with monazite (mnz), image # pr0489, sample # PR95-28.

Figure 5H Silicification stage (xpl), quartz (qtz) and monazite (mnz), image # pr0491, sample # PR95-28.

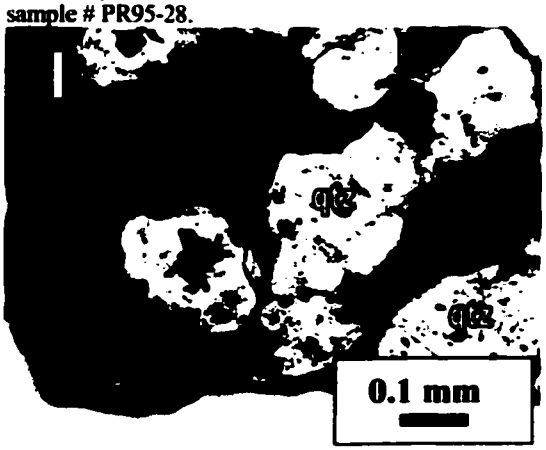

Figure 5I Breccia pipe stage (ppl), quartz (qtz) occurring as matrix and with clear growth zones, image # pr0471, sample # PR95-35.

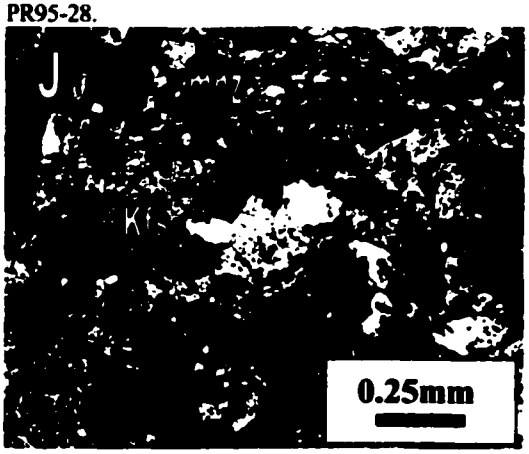

Figure 5J Breccia pipe stage (xpl), monazite(mnz) in k-feldspar (Kfs) fragments, image # pr0496, sample # PR95-16.

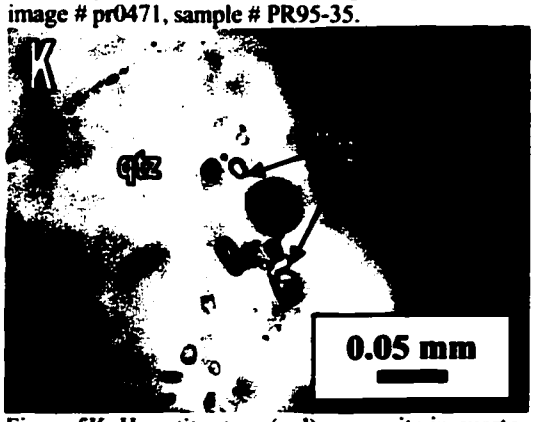

Figure 5K Hematite stage (ppl), monazite in quartz (qtz), showing quartz and monazite coprecipitation, image # pr0502, sample # PR01-69.

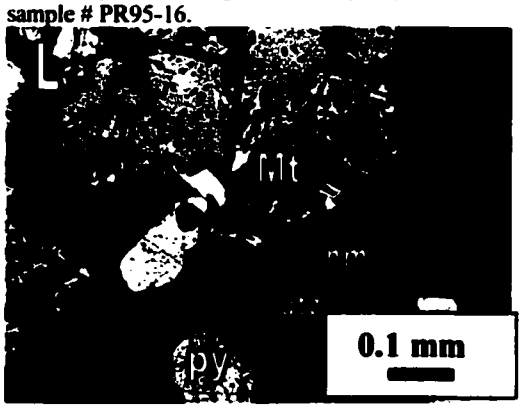

Figure 5L hematite stage, reflecting light, quartz – pyrite-hematite replacing magnetite. Image # pr0500, Sample #PR95-7

Magnetite-cemented breccias consist of variably altered fragments of rhyolite and amphibole-stage rocks in a matrix of magnetite and actinolite (Nuelle et al., 1989a). These breccias occur along the margins of the magnetite ore body and are particularly well-developed in the hanging wall (Nuelle et al., 1989a). Magnetite pseudobreccia refers to where the host rhyolite has been partially replaced by magnetite along fractures and has a breccia-like appearance (Nuelle et al., 1989a).

Hematite zone: The hematite zone irregularly envelopes the margins of the magnetite zone (Figure 3). Contacts between the hematite and magnetite zones are commonly gradational, but sharp contact occurs locally (Nuelle et al., 1989a). Most hematite is an alteration product of magnetite (Figure 5L) (Nuelle et al., 1989a). The hematite stage mainly consists of hematite (80 modal percent) and gangue minerals such as quartz (Figure 5F), apatite, pyrite, and calcium sulphate (Nuelle et al., 1989a; Sidder et al., 1993a).

Table 1 Paragenesis of the Pea Ridge deposit

Stages	Early → Late
Amphibole apatite	
Magnetite	
Hematite	
Silicification	
Breccia pipe	
Quartz vein	
Mafic dike	
Aplite dike	

(Modified from Nuelle et al., 1992)

Silicified zone and quartz veins: The silicified zone occurs between the Fe oxide stages (hematite/magnetite) and the host rhyolites and is the product of both open-space filling and replacement (Nuelle et al., 1989a). This stage is characterized by massive quartz (Figure 5G) that replaces the host rhyolite wall rock to different degrees (Nuelle et al., 1989a). Potassic alteration

is associated with the silicification and is characterized by K-feldspar. Accessory minerals in the silicification stage include fluorite, muscovite, biotite, tourmaline, chlorite, epidote, calcite, barite, rutile, pyrite, chalcopyrite, monazite, apatite, and topaz (Nuelle et al., 1989a; Sidder et al., 1993a). Nuelle et al. (1989a) defined a separate quartz vein stage at Pea Ridge. Quartz veins are common in the silicified zone and have a similar mineralogy to the silicified zone rocks. In addition to the minerals described previously, Kerr (1998) discovered that andalusite is moderately abundant (up to 20 modal %) in some silicified zone rocks. The silicification stage is interpreted to have formed later than the hematite stage (Nuelle et al., 1989a, b; Seeger et al., 2001; Seeger, Pers. Comm., 2002). According to C. Seeger (Pers. Comm, 2002) this is indicated by the indurated nature of the hematite zone rocks in the vicinity of the silicified zone, reflecting higher quartz contents.

REE-rich breccia pipes: REE-rich breccia pipes cut the iron ores and altered rhyolite wall rocks and occur at the contacts between the hematite zone and the rhyolite host, between the hematite and silicified zones, and within the hematite zone (Nuelle et al., 1989a) (Figure 3 Table 1). The breccia pipes contain fragments of rhyolite, magnetite-hematite ore, and silicified zone rocks. The matrix of the breccias is dominantly composed of rock flour, feldspar, chlorite, barite, apatite, monazite, quartz (Figure 5I), and calcite. Total averaged REE oxide (REE_2O_3) in the breccia pipes reaches 20.3 wt. % (Nuelle et al., 1989a). Monazite is the predominant REE-bearing mineral in the breccia pipes (Kerr, 1998) (Figure 5J). Other REE-bearing minerals include allanite, xenotime, bastnasite, britholite, florencite, synchysite, parisite, tengerite, and cheralite (Husman, 1989; Kerr, 1998).

2.2 Previous work on fluids of the Pea Ridge Deposit

Little work has been done on the fluids responsible for the formation of the Pea Ridge deposit. Sidder et al. (1993a, b) published the only paper with fluid inclusion data, but studied less than 20 fluid inclusions (Table 2). They found that quartz is the only fluid-inclusion-bearing mineral, and noted that primary fluid inclusions in quartz in the amphibole, magnetite, hematite, and silicification stages consist of three or more phases, with liquid, vapour, halite, and one or more other daughter minerals. The fluid inclusions range in size from less than 5 μm to 16 μm. They

also found that the fluid inclusions in quartz in the REE-breccia pipes contain only liquid and vapour, and that their ratios vary considerably. They identified secondary fluid inclusions in all stages and noted that they are generally less than 7 μm in size and only contain liquid and vapour. They calculated that the fluids responsible for the various stages were high temperature, high salinity, and had a heavy $\delta^{18}O$ signature (14.5 ~15.7 ‰) (Table 2). Based on this data, they interpreted the Pea Ridge deposit as a magmatic hydrothermal deposit.

Day et al. (1989a) calculated $\delta^{18}O$ quartz-magnetite equilibrium temperatures for the magnetite ores and found that the ore fluids were as hot as 680°C, and had a $\delta^{18}O$ signature of +15 ‰. They concluded that the fluids responsible for the magnetite ores were in equilibrium with a magma with a heavy $\delta^{18}O$ signature.

Gleason et al. (2000) conducted Nd isotope studies on the Pea Ridge deposit and found that the ε_{Nd} isotopic values for apatite, monazite, and xenotime separates (+3.5 to +5.1) are similar to the associated felsic to intermediate igneous rocks of the same age (ε_{Nd} = +2.6 to +6.2) and concluded that the coeval igneous host rocks were the primary source for the REE.

Table 2 Fluid inclusion and stable isotope data on Pea Ridge deposit *

Stage	Amphibole stage	Magnetite stage	Hematite stage	Silicified stage	Breccia pipes stage
Mineral	qtz	qtz	qtz	qtz	Qtz
Primary	LVH	Rare LVH	Rare LVH	LVHS	LV varied L/V ratio
Th	Halite not disappeared by 530°C	480C and 530°C some not dissolved by 530°C	About 410°C	Between 320°C and 430°C	
Salinity (NaCl wt%)	52 to >56%	54 to >60%	47%	39 to 49%	
Isotopic temperature	qtz-Mt 680°C	qtz-Mt480°C	qtz-hem 395°C		Brt-Py 305°C
Isotope values	$\delta^{18}O$ of qtz 14.5‰	$\delta^{18}O$ of qtz 15.2‰		$\delta^{18}O$ of qtz 15.7‰	

* (after Sidder et al., 1993a)

Kerr (1998) studied the mineralogy, mineral chemistry and hydrothermal evolution of the Pea Ridge deposit and found that in the early amphibole-apatite-magnetite alteration and magnetite-apatite stages, the REE are concentrated in apatite and in monazite inclusions within the apatite. The early magnetite was then altered to hematite around the margin of the magnetite ore body. Subsequent alteration (silicification) of the host rhyolites produce an assemblage of quartz-andalusite-muscovite-K-feldspar, which indicates an acidic fluid of over 341°C. Later quartz veins are similar to the silicified rocks but do not contain andalusite. The late-stage breccia pipes were divided into two types: in type I, the REE mineral assemblage includes allanite, apatite, and fluorocarbonates as well as the dominant monazite-xenotime assemblage and feldspar and barite clasts are absent, whereas, the type II pipe contains feldspar and barite clasts and the matrix consists of monazite, xenotime, rutile, thorite, hematite, and quartz, with up to 90 % monazite and xenotime.

Monazite-xenotime geothermometry (Kerr, 1998) indicates that the type I breccia pipes were formed at lower temperatures than the type II pipes. Chlorite geothermometry indicates that chlorite-bearing assemblages, which are characteristic of the late-stage breccia pipes, were precipitated at temperatures of 100-220°C. Kerr (1998) suggests that this chlorite alteration, along with associated hematite, may be related to a regional event. Kerr (1998) also concluded that the variation from apatite as the dominant REE-bearing phase in the early amphibole and magnetite stages to monazite and xenotime in the breccia pipes reflects a decrease in the Ca/REE ratio of the hydrothermal fluids. Similarly, the appearance of REE-flurocarbonate in the late stages suggests that the PO_4^{2-}/CO_3^{2-} and PO_4^{-2}/F^- ratios of the hydrothermal fluids decreased in the late stages of deposit formation.

In comparing Pea Ridge with the Olympic Dam deposit, Kerr (1998) concluded that Pea Ridge is comparable to Olympic Dam, but that there are notable differences. These include the presence of andalusite and abundance of K-feldspar, abundant apatite and monazite rather than bastnasite, the abundance of actinolite instead of chlorite, negative instead of positive Eu anomalies in chondrite-normalized REE profiles, higher Th/U ratios, and much lower Cu. Kerr (1998) further proposed that these differences indicate that the chemistry and temperature of the fluids were substantially different from those at Olympic Dam and that the mineralization at Pea Ridge

represents a series of fluid infiltration events in which the fluids became sequentially lower temperature and more alkaline, which might be related to a differentiating magma underneath.

This brief review shows that some work had been carried out that addresses the questions regarding the nature and origin of the ore-forming fluids at Pea Ridge. However, the fluid inclusion data is extremely limited and little is known about the chemistry of the fluids responsible for Pea Ridge.

2.3 Objectives

In order to further understand the genesis of the Pea Ridge deposit, the following questions need to be addressed:

1. What are the physico-chemical characteristics of the fluid responsible for the various stages of mineralization? Such data will be important for placing constraints on models of fluid origins and evolution, and for processes that may lead to mineral precipitation (see below). In this study, the physico-chemical characteritics of the fluids responsible for the Pea Ridge mineralization have been determined by carrying out a detailed fluid inclusion study of a variety of hydrothermal minerals from Pea Ridge.

2. How are the fluids responsible for the various stages related to one another? It is possible that the fluids responsible for different zones had the same source or that they had different sources. If they had the same source, they may either have the same or similar characteristics or they may represent the evolution of fluids from that source. For example, their physico-chemical characteristics should be consistent with the changes expected from magmatic degassing or water-rock interaction. Fluids from different sources would be expected to have different physico-chemical characteristics from one another. The data obtained from the fluid inclusion study is used to address this question.

3. What are the origins of the fluids that formed the different zones?
Three different sources for the fluids involved in Olympic Dam-type deposits have been proposed: (1) hydrothermal fluids derived from a silicate magma (e.g., Nuelle et al., 1989a,b; Johnson and McCulloch, 1995; Menuge et al., 1997; Gleason et al., 2000); (2) hydrothermal fluids that started life as meteoric water (e.g., Oreskes and Einaudi, 1992; Gow et al., 1994; Haynes et al., 1995; Perring et al., 2000); and (3) hydrothermal fluids derived from evaporite brines (Barton and Johnson, 1996). The physico-chemical characteristics of the fluids will help to constrain the origin of the fluids at Pea Ridge. Because these characteristics are predicted to be very different for the various fluids, the fluid inclusion data is used to test these models.

4. What caused hydrothermal mineral precipitation in the various zones ? Mineral precipitation can be caused by many different processes, including adiabatic cooling, boiling, and fluid mixing. Because these processes change the physico-chemical characteristics of the fluids, evidence that these processes operated may be recorded in the fluid inclusion data.

5. Is Pea Ridge a member of the Olympic Dam class of deposits? Previous studies on Pea Ridge have demonstrated that it is a similar age, occurs in a similar geotectonic setting, and has common mineralogical characteristics to the Olympic Dam deposit (Einaudi and Orekes, 1990). However, there are sufficient differences between the two deposits to question the relationship. It is reasonable to suggest that if Pea Ridge is a variant of the Olympic Dam type, it should have similar fluid characteristics and sources and that similar precipitation mechanisms for the hydrothermal minerals should have been in operation. An important consequence of this is that the genetic and exploration model proposed for Olympic Dam should also be applicable to the Pea Ridge deposit.

This thesis reports the results of a detailed fluid inclusion analysis of the Pea Ridge deposit. These data are used to better understand the chemistry, temperature, and evolution of the hydrothermal fluids responsible for the deposit and to attempt to answer the questions posed above.

3 Methodology

3.1 Sampling

One hundred and sixty two samples have been collected from the Pea Ridge deposit from both underground workings and from drill core by Ian Kerr, Iain Samson, Brian Fryer and the author (Appendix I). These include samples of the rhyolite wall-rock, the amphibole alteration assemblages, the magnetite zone, the hematite zone, the silicified zone, quartz veins, and the REE-breccia pipes. Thin and polished thin sections were prepared for most of these samples and forty seven samples were selected for the preparation of doubly polished wafers for the fluid inclusion study.

3.2 Fluid inclusion petrography

Optical microscopy and image analysis were used to characterize and record the distribution of fluid inclusions in minerals from the various stages in the Pea Ridge deposit. This involved documenting the origin (primary, secondary, and pseudosecondary), distribution, shape, size, and the number, type, and abundance of phases in the inclusions at room temperature.

3.3 Fluid inclusion chemistry

The chemical composition of fluid inclusions can be obtained using a wide variety of methods that partly depend on the nature of the inclusions. Fluid inclusions generally consist of a liquid aqueous phase that contains a complex mixture of dissolved ions and a vapour phase that may simply be water vapor, or may contain a variety of gases (some gases will also reside in the aqueous phases depending on the solubility of the gas). Inclusions may also contain one or more solid phases (crystals) that may have been trapped with the fluid or may have been precipitated in the fluid inclusion after entrapment (daughter minerals).

The methods used in assessing the bulk chemical composition of inclusions will depend on the nature of the inclusions, determined through careful petrography. The methods used were microthermometry and Raman spectroscopy. Laser-ablation ICP-MS analysis of the inclusions was attempted in order to determine the elemental composition of the inclusions. The preli-

minary attempts at such analyses were largely unsuccessful, probably because of the small size of most inclusions in the Pea Ridge samples, and the results of these attempts have been omitted from this thesis.

3.3.1 Microthermometry

Doubly-polished sections with a thickness of about 100 μm were prepared for microthermometric analysis. Fluid inclusions were measured using a Linkam THMS 600 heating-freezing stage mounted on a Leitz optical microscope and fitted with a video monitor for observation of phase behavior over a temperature range of −100°C to 500°C. The stage was repeatedly calibrated using synthetic fluid inclusions containing water and carbon dioxide. Heating rates were normally lower than 10°C/min and were 0.5°C/min during phase changes. As simple one-stage cooling and heating of the fluid inclusions does not typically make large crystalline phases that allow unambiguous observations of the disappearance temperature of the phase, the technique of sequential freezing (Haynes, 1985) was used in measuring the low-temperature phase transitions in some fluid inclusions.

3.3.2 Salinity calculation

Salinities in aqueous, halite-undersaturated inclusions were calculated from final ice melting temperatures (TmICE) in the H_2O-NaCl-$CaCl_2$ system (Oakes et al., 1990) using a regression equation in which salinities represent the median salinity for a given TmICE. Salinities of halite-saturated inclusions were calculated from halite dissolution temperatures (TmH) using the regression equation of Sterner et al. (1988). The results are shown in Table 4 and Table 5.

3.3.3 Raman spectroscopy

Raman spectroscopy can be used to identify solids, gases, and dissolved molecular species within individual inclusions, and to quantify the composition of the latter two components. Spectra were collected using a Renishaw RM2000 micro-Raman system equipped with a computer-controlled three-axis encoded (XYZ) motorized stage at the University of Windsor. The RM2000 uses a Leica microscope and a Peltier cooled CCD array detector. Each spectrum represents five accumulated spectra using an integration time of ten seconds. Data acquisition was carried out using the Galactic Industries GRAMS/32© software.

4 Results

4.1 Petrography of the Host Minerals

Fluid inclusions have been observed in actinolite, quartz, apatite, monazite, and barite. However, microthermetric measurements were only carried out on inclusions in quartz, apatite and barite because the actinolite crystals are too dark and inclusions in monazite are too small (less than 1 μm) to observe phase changes.

Amphibole-Apatite and Magnetite Stages: Rocks from the amphibole zone are primarily characterized by the assemblage actinolite-apatite-quartz. In the amphibole zone rocks, actinolite occurs as euhedral to subhedral, prismatic crystals. Actinolite crystals are widely replaced by magnetite and quartz (Figure 5C). Apatite occurs as subhedral to euhedral crystals that are in equilibrium with actinolite. There appear to be two generations of quartz in amphibole zone rocks: an early generation of subhedral quartz that appears to be in equilibrium with actinolite (Figure 5B), and a later generation of anhedral quartz, together with magnetite, which replaces actinolite (Figure 5C).

Apatite crystals in magnetite zone rocks are anhedral and are invariably replaced by magnetite and/or hematite (Figure 5D). They resemble apatite crystals that occur in amphibole zone rocks where magnetite replacement has been significant. Apatite within the magnetite zone rocks is therefore considered to predate magnetite deposition and be equivalent to the apatite-amphibole assemblages that occur outside of the magnetite zone (Samson et al., in prep). For this reason, all apatite from these two zones is considered to have been formed in a single event and will be referred to as the amphibole-apatite stage.

Quartz in the magnetite zone rocks appears to either be a relict of the replaced rhyolite (Samson et al., in prep) or to be replacing magnetite and therefore to have formed later than magnetite (Figure 5E). Consequently, there are no minerals that can be unequivocally tied to magnetite

deposition and no information on the physiochemical nature of the fluids that deposited magnetite is available from fluid inclusions.

Hematite stage: Quartz in hematite zone rocks is anhedral and fills the interstices between euhedral hematite crystals. Some of these quartz crystals contain hematite inclusions and growth zones that are defined by fluid inclusions and hematite inclusions (Figure 5F). These textures require that the quartz was formed at the same time as the hematite. Barite occurs as subhedral crystals in some hematite-zone rocks and grain boundaries between barite, hematite and quartz are commonly linear, suggesting co-precipitation. Because hematization is not restricted to the main hematite zone and is temporally later than magnetite precipitation, massive hematite-formation will be referred to as the hematite-stage.

Silicification stage: In silicified rocks and in the quartz veins, quartz is euhedral to anhedral, massive, and coarse grained. Quartz may contain solid inclusions such as hematite, anhydrite and tourmaline (Kerr, 1998).

Breccia pipe stage: In the breccia pipes, quartz occurs as irregular clasts and as anhedral crystals in the matrix (Kerr, 1998). Quartz clasts often have an ovoid or hexagonal core which is rimmed by an overgrowth containing fine hematite, monazite, and other, unidentified acicular minerals (Kerr, 1998). Quartz in the matrix occurs as rounded grains which may have euhedral, including hexagonal, overgrowths in which fine hematite crystals define the growth zones (Kerr, 1998). Barite occurs as subhedral clasts in the breccia pipes, it may be probably formed at the early breccia pipe stage as matrix, but later brecciated into clast. There are massive barite-carbonate veins spatially associated with breccia pipes and they are genetically related to the formation of breccia pipes (Nuelle et al., 1991b).

4.2 Fluid inclusion types

Liquid-Vapour aqueous inclusions (LV): Liquid-vapour aqueous inclusions (Figure 6A, B, C, F, G, M) contain a volumetrically-dominant aqueous liquid and a smaller vapour bubble (5-10 volume %).

Liquid-Vapour Carbonic inclusions (C): Type C (carbonic) fluid inclusions comprise a liquid carbonic phase and a vapour phases (5-10 volume %) (Figure 6L). No aqueous phase is optically resolvable around the edge of such inclusions. However, as will be shown later, Raman spectroscopic evidence indicates the presence of a thin, aqueous sheath around some of these inclusions.

Liquid-Vapour-Solid inclusions (LVS): Liquid-Vapour-Solid inclusions contain an aqueous liquid, a vapour bubble, and one or more solids (Figure 6H, I, N, O, P). Most LVS inclusions contain one or two solids, but some inclusions contain as many as five solids. Halite is the only crystal that shows consistent liquid/solid ratios in inclusion groups and is interpreted as a daughter mineral. Such inclusions will be referred to as LVH (Liquid-Vapour-Halite) inclusions. Other solids are irregularly distributed as a result of having been trapped during inclusion formation or through necking. Trapped solids may occur in LV or LVH inclusions and where this occurs the inclusions are referred to as Liquid-Vapour-Solid (LVS) or Liquid-Vapour-Halite-Solid (LVHS) inclusions.

Liquid inclusions (L): These are fluid inclusions that contain only a single aqueous liquid phase.

Liquid-Halite-Carbonic inclusions (LVHC): These inclusions contain an aqueous liquid, a halite crystal, and a carbonic bubble (Figure 6N). The latter comprises both liquid and vapor at room temperature, but vapour dominates.

Vapour-Liquid aqueous inclusions (VL): These are aqueous fluid inclusions in which the vapour phase occupies 75 to 90 % of the volume of the inclusion.

4.3 Fluid inclusion assemblages and distributions

Fluid inclusions have been observed in a number of the minerals from Pea Ridge, namely, amphibole, apatite, quartz, barite, and monazite. However, quartz contains the largest number of

fluid inclusions. The distributions of the various inclusion types in terms of mineral, stage, and origin are summarized in Table 3.

In the early amphibole-apatite alteration stage, LV inclusions are found as isolated inclusions in amphibole (Figure 6A) and apatite (Figure 6B) or as three dimensional arrays in apatite, and are interpreted as primary in origin. Some other LV inclusions occur in planar arrays that do not cut grain boundaries and are interpreted as pseudosecondary in origin. No secondary inclusions of any type were found in either apatite or amphibole. The size of these LV inclusions is quite variable, but they are generally less than 5 microns in diameter (Figure 6 C). Quartz in the

Table 3 Fluid inclusions in the Pea Ridge deposit

Stages	Host	Primary	Pseudosecondary	Secondary
Breccia pipe	Quartz	LV, L		L, LV
	Barite	LV, L	LV	
	Apatite	LV		
	Monazite	LV		
Silicification	Quartz	LVH(S)	LVH(S)	L, LV, LVHS, LVCH, LVS, LVC
Hematite	Quartz	LV, L	LV, LVH	LV, LVH, LVS
Magnetite	Apatite	LV	LV	
	Quartz			LVH, LVS, LV, L
Amphibole	Amphibole	LV		
	Apatite	LV		
	Quartz		L, LV, LVH	L, LV, LVH, LVS

amphibole-apatite-rich rocks contains LV, LVH, LVS (Figure 6M, P), and L inclusions, which occur in planar arrays (healed microfractures) and are interpreted as secondary inclusions. No primary LV inclusions were found in quartz, but there are many L inclusions present in quartz growth zones. In sample PR95-11, the quartz contains growth zones defined by irregular-shaped L inclusions. The inclusion assemblages inside and outside the growth zones are different. Inside the growth zones, the quartz contains planes of LV, LVS, LVH, and L inclusions that are interpreted to be pseudosecondary (they truncate at the growth zone) but most of the inclusions are L inclusions within the growth zone. Outside the growth zone inclusions occus as L inclusions.

Figure 6 Fluid inclusion images from various stages

Figure 6A LV primary fluid inclusion in amphibole from amphibole-apatite stage, image # pr0014, sample # PR95-10.

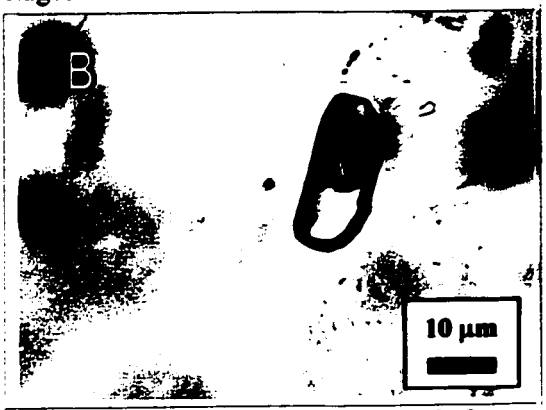

Figure 6 B LV primary fluid inclusion in apatite from amphibole-apatite stage, image # pr0068, sample # PR95-25.

Figure 6C LV primary fluid inclusions in apatite from magnetite stage. image # pr0468, sample # PR01-33.

Figure 6D hematite and quartz in hematite stage. Quartz with a growth zone enclosing a hematite crystal. image # pr0352, sample # PR01-69.

Figure 6E numerous small red hematite crystals within the growth zone of quartz. image # pr0456, sample # PR01069.

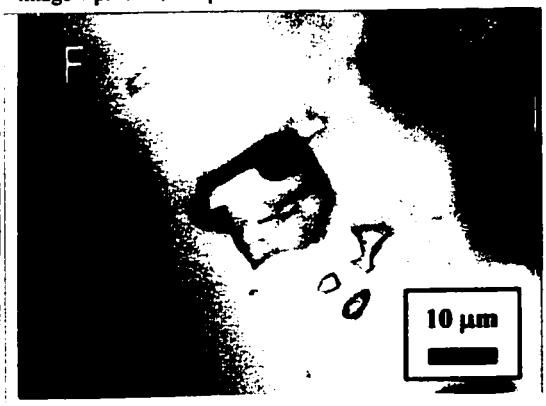

Figure 6F LV primary fluid inclusion within the growth zone of quartz. Necking of fluid inclusion. image # pr0454, sample # PR01-69.

Figure 6G another LV and L only primary fluid inclusion within the quartz growth zone. image # pr0301, sample # PR01-69.

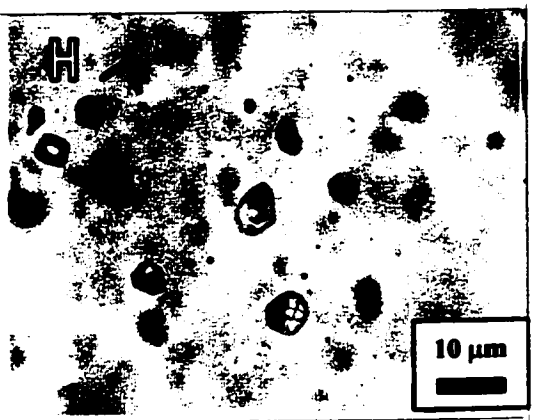

Figure 6H LVH(S) primary fluid inclusions in quartz of silicification stage image # pr0477, sample # PR95-31.

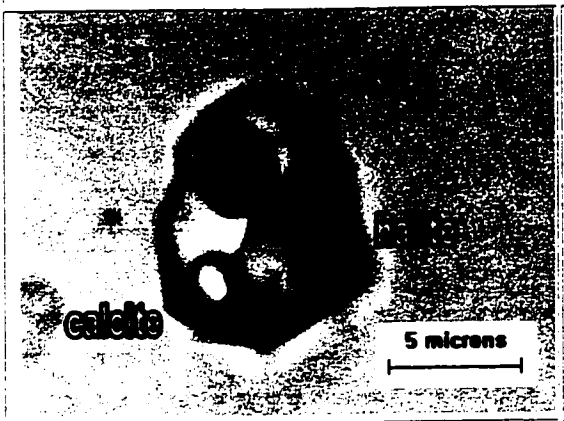

Figure 6I an example of LVHS primary fluid inclusion in quartz from silicification stage, it contains liquid, vapor, halite and calcite. image # pr0476-2, sample # PR95-31, Scale bar 5µm.

Figure 6J primary LV and L-only fluid inclusions within the core and growth zone of quartz from breccia pipe stage. image # pr0151, sample # PR95-35, Scale bar 20µm.

Figure 6K an isolated primary fluid inclusion in quartz core from breccia pipe stage. image # pr0473, sample # PR95-35.

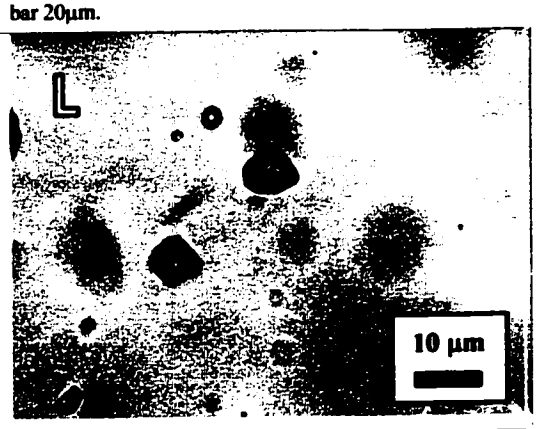

Figure 6L secondary carbonic fluid inclusions in quartz from quartz vein of silification stage. image #pr0006, sample#PR95-39.

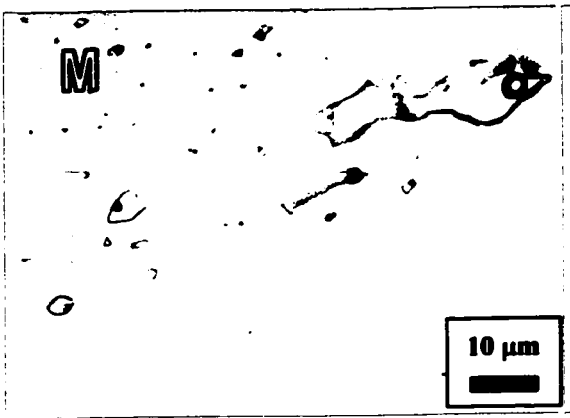

Figure 6M secondary aqueous LV fluid inclusions in quartz from quartz vein of silicification stage. image # pr0002, sample # PR95-39.

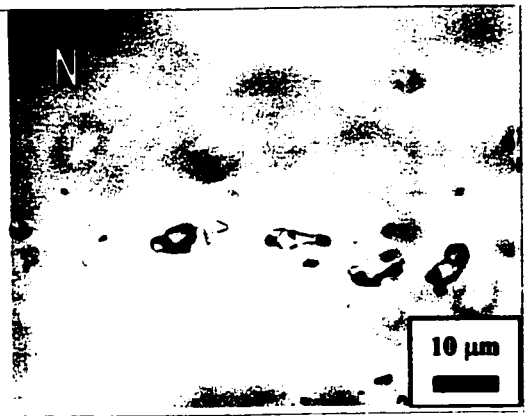

Figure 6N secondary inclusions of brine-CO_2 -halite with brine-halite-calcite-unid. unmixing of the fluids. image # pr0481, sample # PR95-39.

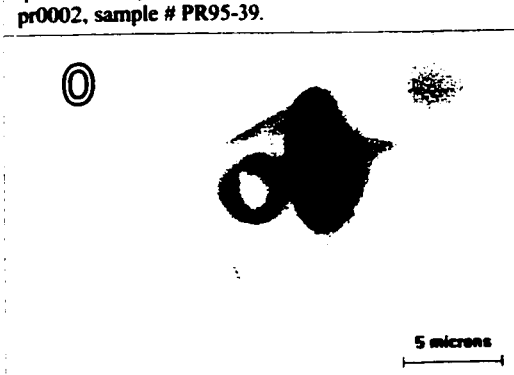

Figure 6O secondary LVS fluid inclusion in quartz from quartz vein of silicification stage. The red solid is hematite, it occurs as trapped phase. image # pr0452, sample # PR95-31.

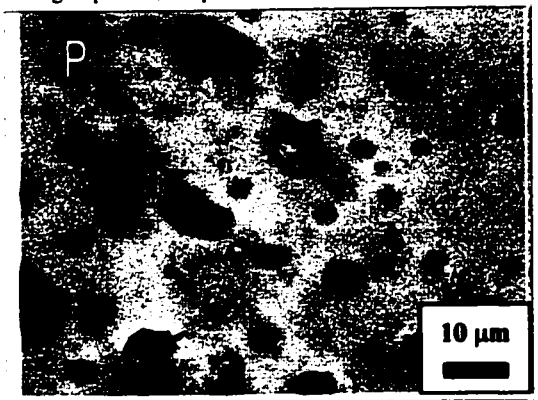

Figure 6P secondary LVS fluid inclusion in quartz from amphibole -apatite stage. The solid is identified to be barite. image # pr0463, sample # PR95-25.

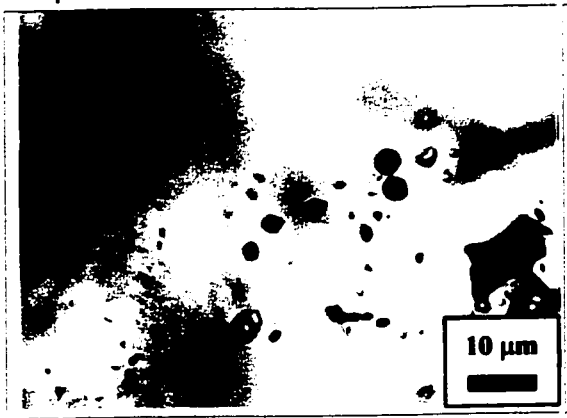

Figure 6Q Vapor rich LV inclusions in quartz growth zone of breccia pipe stage. Image # pr0497; Sample # PR95-35

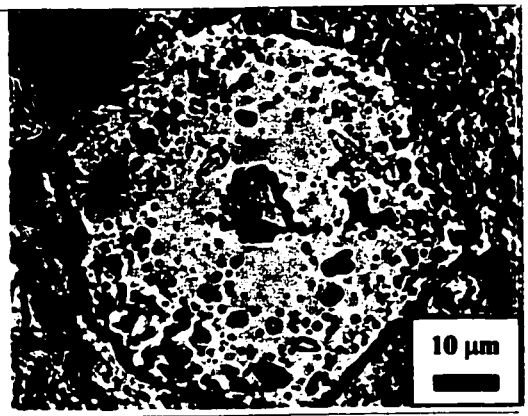

Figure 6R liquid rich inclusions in quartz growth zone of breccia pipe stage. Image # pr0498, Sample # PR95-35.

Quartz from the magnetite zone rocks contains abundant, secondary LVH, LVS, LV and L inclusions. A few LC inclusions occur in secondary planes. No primary inclusions were observed in this quartz.

Two samples from the hematite zone contain measurable fluid inclusions. Other samples contain rare and tiny fluid inclusions, which are not measurable. Quartz that is interpreted to have formed during the hematite stage occurs in sample PR01-69, and contains growth zones that contain primary inclusions (Figs. 4-1-1D, E, F, G). These are mostly small L inclusions, but some larger LV inclusions occur dispersed among the L inclusions (Figure 6G). These growth zones also contain fine-grained hematite crystals, which indicate that quartz and hematite co-precipitated in this sample. The dominance of L inclusions in these assemblages and the intimate relationship between the LV and L inclusions (Figure 6F) suggests that the LV inclusions have resulted from necking. It is possible, however, that a vapour bubble has simply not nucleated in the smaller inclusions. Most LV inclusions are 5-10 microns in diameter, but a few reach 20 microns (Figure 6B). The LV inclusions may be irregular, equant, or have a negative crystal shape. The vapour bubble generally occupies between 5 and 10 volume percent of the inclusion. The L inclusions are mostly irregular in shape.

Barite in sample PR01-69 contains LV and L inclusions, which are distributed in three dimensional arrays and are interpreted as primary inclusions. These LV and L inclusions coexist and they can be close to one another. Whether they are formed from necking or heterogeneous trapping is not clear. Quartz and barite in sample PR01-69 contains no secondary inclusions of any type. However, LV, LVH, and L inclusions are found in healed fractures in quartz from sample PR95-7. No growth zones occur in this quartz and hematite in this sample is the product of magnetite oxidation. This inclusion assemblage may therefore be a relict, and equivalent to the assemblages described above from the magnetite zone rocks.

In the silicification stage, quartz is the only mineral in which fluid inclusions were observed, and include LVH, LVHS, LVHC, LV, C and L inclusions. The distribution of these inclusions is very complicated. Most LVH and LVHS inclusions occur dispersed in three dimensional arrays and are interpreted as primary in origin; i.e. they cannot be related to planar arrays. Other LVH and

LVHS inclusions can, however, be related to planar arrays and these are interpreted as secondary inclusions. LVHC inclusions (Figure 6N), LV, C (Figure 6L), and L inclusions occur in planar arrays and are also interpreted as secondary inclusions.

Most LVH±S inclusions are 5 to 10 microns in diameter. The vapour bubble in most LVH±S inclusions occupies 5 to 10 volume %, and the solids occupy about 20 volume %. In some cases, however, the solid(s) may occupy up to 50 to 75 volume %. These inclusions with a high proportion of solids are possibly formed by necking because in an given array, only some are of this type. Carbonic inclusions may be equant or irregular in shape and most are between 1 and 5 microns in diameter, but can be up to 10 microns in size. They mostly have consistent V/L ratios (5-10 volume %) in the same co-genetic group. However, there are some carbonic inclusions in which the vapour bubble occupyes up to 90 volume percent of the inclusion.

Fluid inclusions in the breccia pipe samples occur in matrix quartz, monazite, and apatite, and also in barite clasts. Within quartz, LV inclusions occur as isolated inclusions in the core of crystals (Figure 6J, K), may be irregular, equant, or have a negative crystal shape, and range in size from 5 to 20 microns. The V/L ratio in these inclusions varies from crystal to crystal, with the volume occupied by the vapour bubble varying from 5 and 30 %. Fluid inclusions also occur in growth zones towards the edge of crystals (Figure 6J). These are mostly L inclusions (Figure 6R), but a small proportion of VL inclusions are also present. The VL inclusions are all as small as 1 to 3 microns. It is not clear whether this mixed inclusion assemblage comprising L, LV and VL inclusions are formed from boiling or necking. A mixture of L and LV inclusions also characterizes the barite, where they occur in three dimensional arrays and coexist with each other. Whether these L and LV inclusions in barite are formed from necking or boiling is not clear as no salinity data exists for the L inclusions. One tiny LV inclusion was found in a matrix monazite crystal.

4.4 Microthermometry results

LV and LVS fluid inclusions

On cooling, primary LV fluid inclusions reach complete solidification at temperatures as low as -85°C, but most crystallize in the range -65°C to -45°C. Secondary LV fluid inclusions solidify at temperatures between -85 and -35°C. Initial melting (Te, eutectic) temperatures for primary LV inclusions varied from -67 to -25°C, with the lowest value having been measured in an LV inclusion from the hematite zone. Most values lie between –60 and -30°C with one mode at -52°C and another mode at -34°C (Figure 7). Initial melting temperatures for secondary LV inclusions are mostly less than -20°C with a mode at -30°C (Figure 10 and Table 5).

These eutectic melting temperatures, which are lower than the NaCl-KCl-H_2O eutectic at -23°C, indicate that the inclusion fluids are likely to contain $CaCl_2$ (Crawford, 1981). Eutectic temperature below -52°C may indicate the presence of other solutes in the fluids or metastable equilibria (Samson and Walker, 2000).

Ice is the final phase to melt in primary LV inclusions and final ice melting temperatures (Tm ice) cover a wide range, from 0 to –28°C, with three modes at –2°C, -10°C, and -20°C (Figure 8). The LV inclusions in the breccia pipe quartz have the highest Tm ice values and those from the amphibole and hematite stage samples have the lowest. Liquid-vapour inclusions in magnetite zone apatite have intermediate values (Table 4, Figure 8, and Appendix II). The solids in LVS inclusions show no obvious change during cooling and heating up to 200°C. Ice is also the final phase to melt in secondary LV inclusions and the final melting temperatures also cover a wide range, from 0 to -26°C with one mode at 0°C and another mode at -15°C (Figure 11). Secondary LV inclusions from hematite and silicification stages do not have the TmICE mode at 0°C (Figure 11).

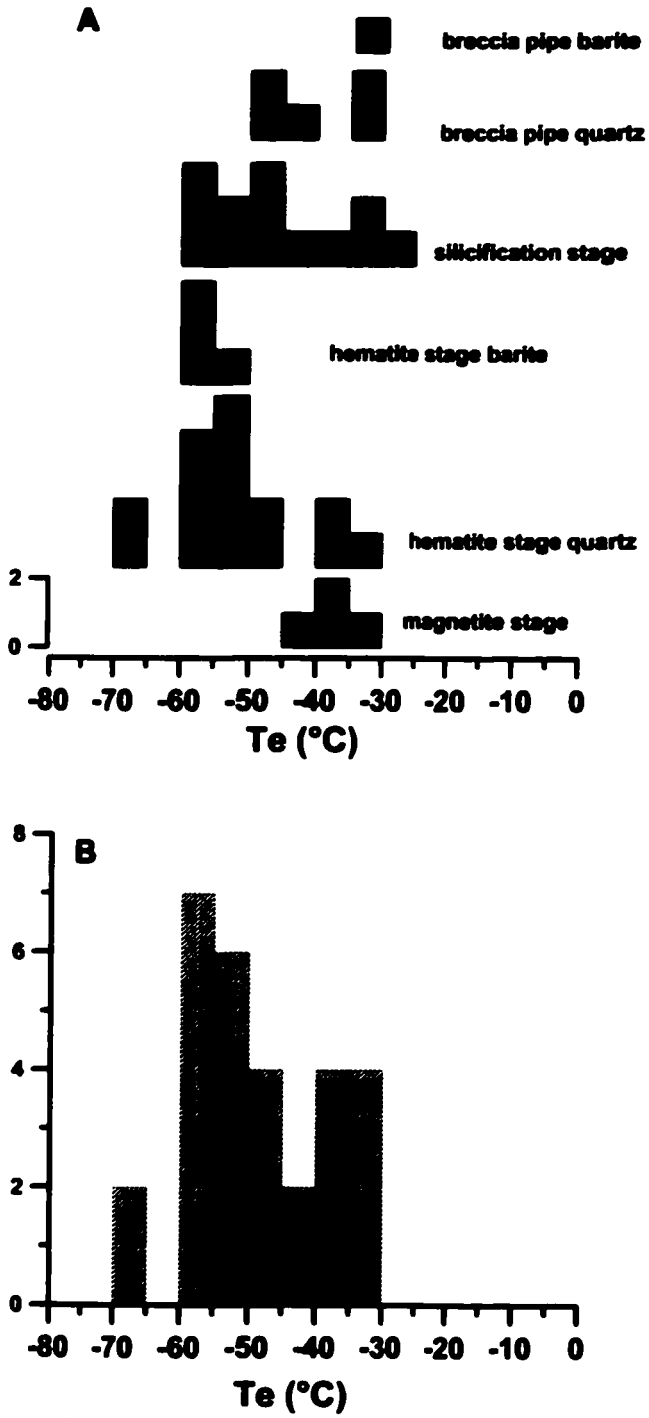

Figure 7 A. Histogram of initial melting temperatures for primary fluid inclusions from various stages. B. The combined histogram for Te of all LV inclusions

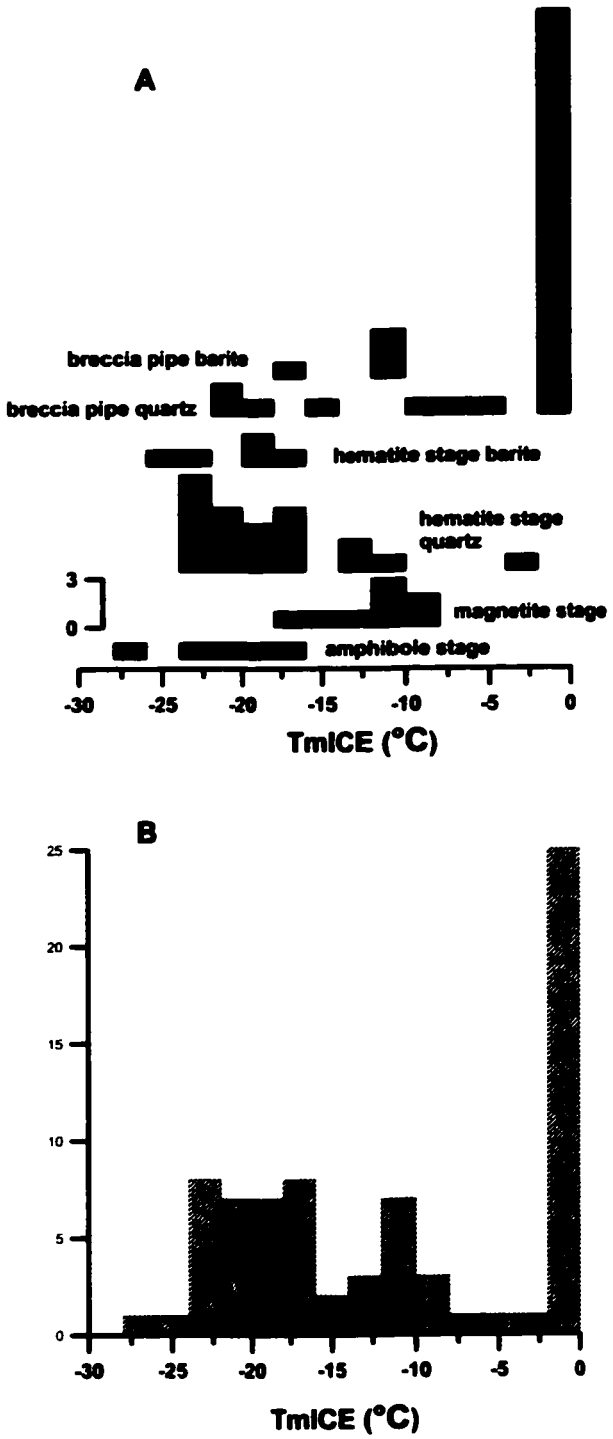

Figure 8 A. Histogram of TmICE LV primary fluid inclusions from various stages of the Pea Ridge deposit. B. The combined histogram for TmICE for all LV inclusions

In summary, primary LV inclusions differ from secondary LV inclusions in that they contain a low Te mode at -52 °C, which is not seen in secondary LV inclusions and also have a low TmICE at -70 °C, which is not seen in secondary LV inclusions.

Table 4 Summary of Microthermometry results

Zone			Amphibole	magnetite	Hematite	Silicification	Breccia pipe
Mineral			ap	ap	qtz	qtz	qtz
Origin			Primary	Primary	Primary	Primary	Primary
Type			LV	LV	LV	LVH	LV
Th	Min			-40	-67	-58	-49
	Max			-35	-33	-22	-34
	avg±δ			-37±2	-52±10	-44±11	-41±8
Th	Th (L-V)	Min	143	118	88	150	126
		Max	205	160	338	238	384
		avg±δ	160±18	144±13	243±87	194±29	276±68
	TmH	Min				245	
		max				422	
		avg±δ				311±52	
TmICE		Min	-28	-16	-24		-21
		Max	-17	-8	-3		0
		avg±δ	-21±4	-12±3	-19±5		-5±7
Salinity		Min	19	12	14	31	0
		Max	25	19	23	50	22
		avg±δ	22±2	16±2	21±3	40±4	8±8

Heating above room temperature causes the primary LV inclusions to homogenized to the liquid phase. Homogenization temperatures (Th) of primary LV fluid inclusions in apatite from the amphibole-apatite stage are quite similar, regardless of whether they are from the amphibole or magnetite zones, and have a mode at 150°C (Figure 9).

Primary LV fluid inclusions in quartz from hematite zone and breccia pipe samples are quite varied but have similar modes. In the hematite stage sample, Th values have three modes, at 90°C, 210°C, and 310°C (Figure 9). One fluid inclusion group has consistent Th values at 90°C. In the breccia pipe inclusions, however, Th values have two main modes at 210°C and 310°C, and a third mode at 380°C (Figure 9). One group of inclusions yields consistent Th values at 230

°C. Primary LV inclusions in barite from the hematite zone have consistent Th values around 310°C. However, primary LV inclusions in barite from the breccia pipes have a wider range of values from 180 °C to 350 °C (Figure 9).

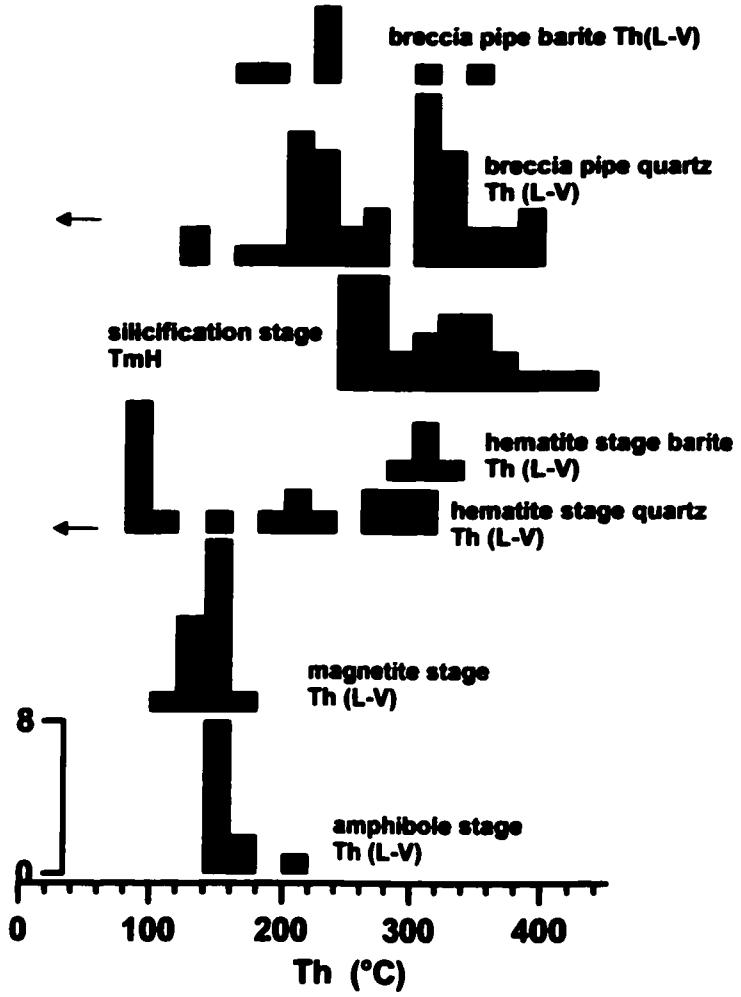

Figure 9 Histogram of homogenization temperature for primary fluid inclusion from various stages. LV inclusions from all stages except the silicification stage homogenize to liquid. LVH inclusions from the silicification stage homogenize by halite dissolution after vapour disappearance. The arrows in hematite and breccia pipe stages suggest that the liquid only inclusions from these two stages may have a low formation temperature.

Secondary LV inclusions also homogenize to the liquid phase. There are three groups of homogenization temperatures for secondary LV fluid inclusions, at 100°C, 200°C, and 300°C respectively (Figure 12). Comparing this diagram with Figure 9 for primary fluid inclusions in the breccia pipes, it can be seen that the homogenization temperatures for primary LV inclusions from the breccia pipes are similar to two of the modes of homogenization temperatures of secondary fluid inclusions from the amphibole-apatite and silicification stages. A third Th mode at about 100°C (Figure 12) is missing from the breccia pipe primary data set, but could be equivalent to the L inclusions in the breccia pipes discussed below.

LVH and LVHS fluid inclusions

On cooling, the halite and other solids in most LVH±S inclusions of both primary and secondary origin show no change, except that the vapour bubble gradually disappears. On heating from low temperatures, the first liquid appears (Te) between –58°C and –22°C. Halite generally shows no change on cooling but sometimes reacts with the aqueous liquid between –41 and –24 °C to form hydrohalite. In those inclusions where hydrohalite forms from halite, halite reappears between 2 and 10°C with the corresponding disappearence of hydrohalite. LVH and LVHS inclusions homogenize by halite dissolution, at temperatures of between 190 and 420°C (TmH) after vapour disappearance (Table 4, Figure 13). The other solids (other than halite) generally show no change on heating to the temperatures at which halite dissolves, although in some cases carbonate solids become slightly rounded.

Liquid only fluid inclusions

Liquid-only (L) inclusions are commonly present as secondary inclusions in quartz from the amphibole-apatite and silicification stages, but are particularly abundant in some samples as primary inclusions in growth zones in quartz from the hematite and breccia pipe stages. However, no measurements have been made on them to date. Liquid-only inclusions represent inclusions in which a vapour bubble has not nucleated because the magnitude of undercooling below the equilibrium homogenization temperature is insufficient to induce nucleation of a vapour bubble. Unless these inclusions were trapped at unreasonably high pressures and/or low temperatures, they should contain vapour bubbles at equilibrium. Recent studies by Roberts and

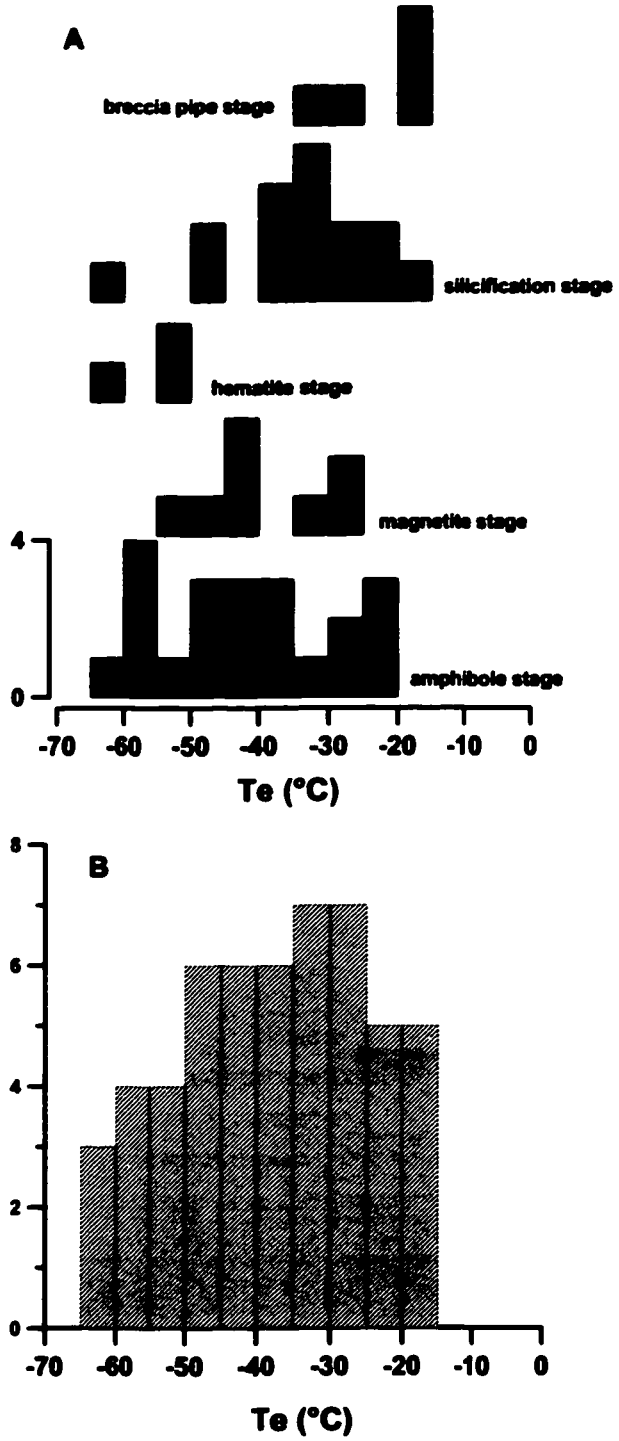

Figure 10 A. Histogram of initial melting temperature of LV secondary fluid inclusions from various stages. B. The combined histogram for Te of secondary LV inclusions

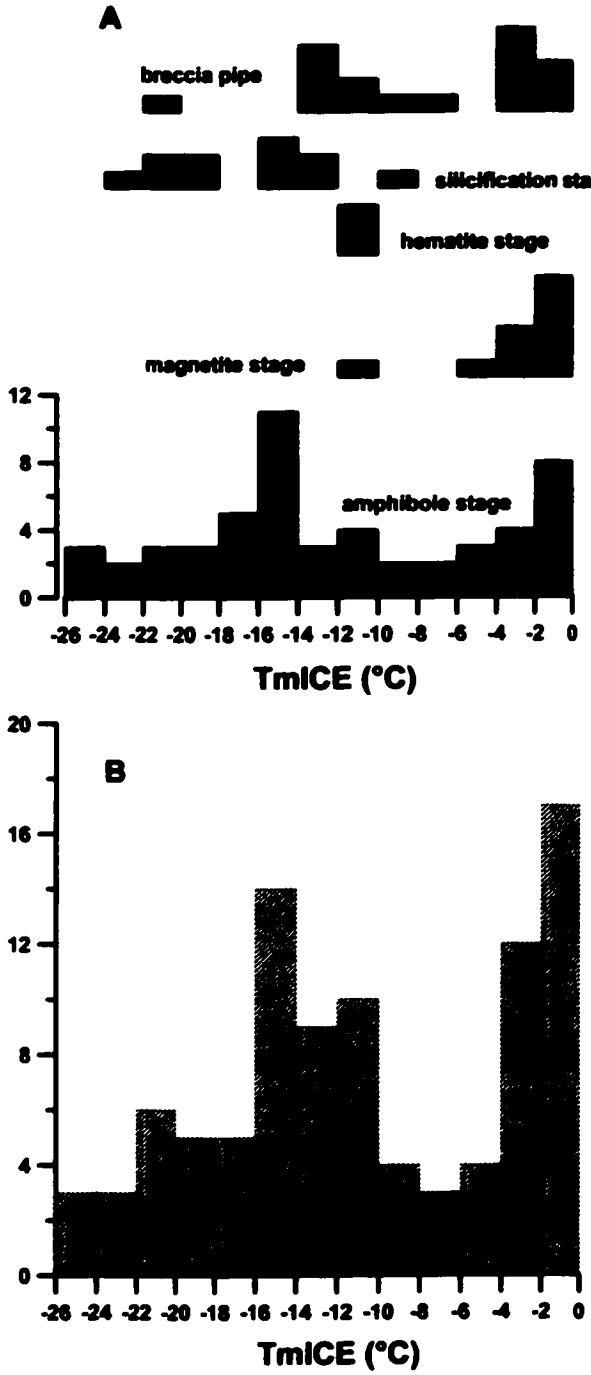

Figure 11 A. Histogram of final ice melting temperature for secondary LV fluid inclusions from various stages. B. The combined histogram for TmICE of secondary LV inclusions

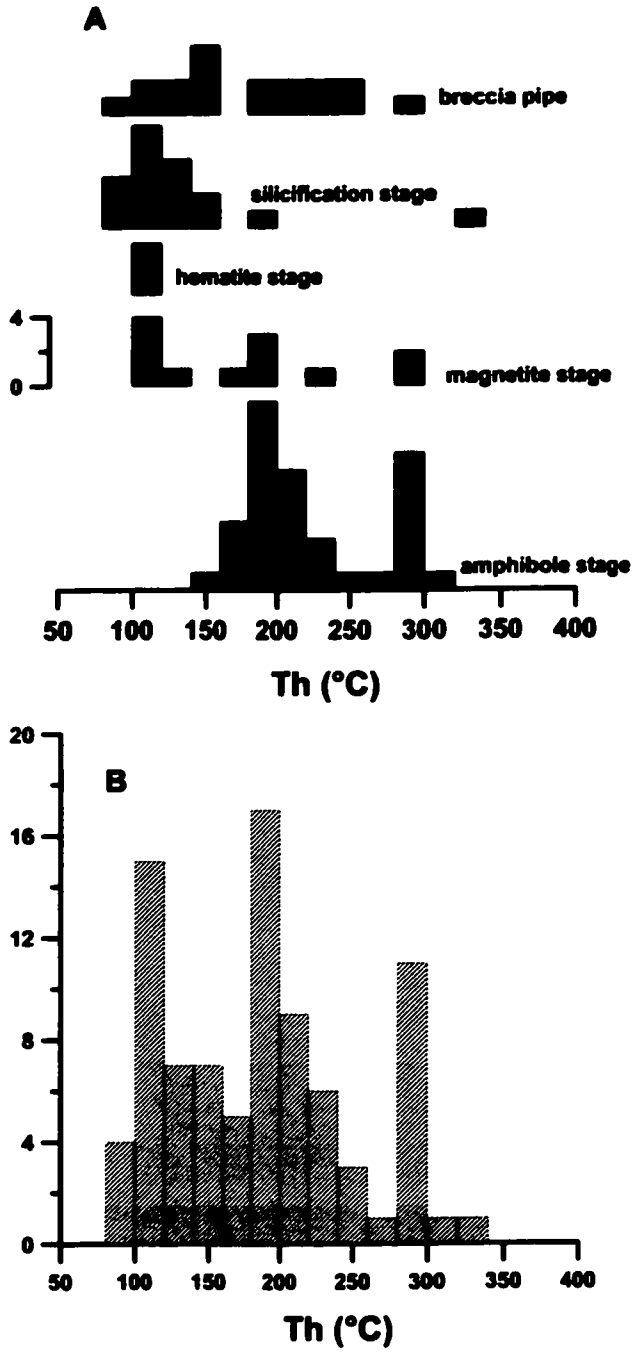

Figure 12 A. Histogram of homogenization temperature for secondary LV fluid inclusions. B. The combined histogram for Th of secondary LV inclusions

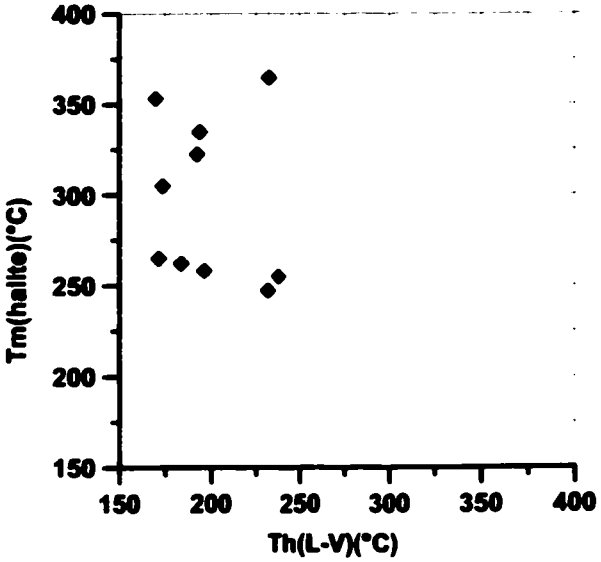

Figure 13 Halite dissolution temperature vs L-V homogenization temperature for LVH(S) inclusions

Table 5 Secondary fluid inclusion microthermometry results

Zones			Amphibole		Magnetite		Hematite	Silicification		Breccia pipe
Mineral			qtz		qtz		qtz	qtz		qtz
Origin			S		S		S	S		S
Type			LV	LVH	LV	LVH	LV	LVH	LV	LV
Te		min	-60		-53		-60		-62	-31
		Max	-19		-27		-50		-20	-19
		Avg ± δ	-42 ±13		-40 ±9		-55 ±5		34 ±13	-23 ±5
Th	Th (L-V)	Min	153		104		101		83	91
		Max	301		298		116		331	282
		Avg ± δ	220 ±46		176 ±68		110 ±8		131 ±58	177 ±56
	TmH	Min		168		168		222		
		Max		395		535		339		
		Avg ± δ		257 ±84		346 ±156		299 ±67		
salinity		Min	1	30	3	30	15	33	13	3
		Max	24	47	15	65	15	41	24	22
		Avg ±δ	14 ±7	36 ±6	5 ±4	45 ±14	15 ±0	39 ±5	19±3	11±6

Spencer (1995) and Wilson et al. (2002) have shown that inclusions that are formed at low temperatures (much lower than should be expected at Pea Ridge) can homogenize at temperatures below 35°C. In some cases, these inclusions were initially liquid-only and vapour bubble nucleation was induced by chilling the inclusions at sub-ambient temperatures in a freezer for a few hours or a few days (Roberts and Spencer, 1995).

The liquid-only inclusions at Pea Ridge represent inclusions that should probably homogenize at temperatures of less than 80°C, the minimum measured Th value. This suggests that the quartz that hosts these inclusions from the hematite and breccia pipe stages may have formed at low temperatures. Samples with abundant liquid-only inclusions from the Pea Ridge deposit are being stored in a freezer to induce vapour bubble nucleation.

Carbonic fluid inclusions

Only one sample from one of the quartz veins contained measurable secondary, carbonic fluid inclusions. On cooling, these inclusions froze at between -80°C and −100°C. On subsequent heating, final CO_2 melting (Tm CO_2) occurred at between -57.3 and -56.2°C, with an average value of -56.8°C, indicative of essentially pure CO_2. Clathrates melted at temperatures between 7.5 and 8.6 °C, averaging 8.2 °C. Homogenization temperatures ($ThCO_2$, homogenized to liquid) occur between 21.5 and 29.2 °C, averaging 25.2 °C.

4.5 Raman spectroscopy

Solids and gases within primary and secondary fluid inclusions from the silicification stage and from secondary inclusions from the amphibole and magnetite stages were identified using Raman spectroscopy. The experimental conditions and peak interpretation are given in Appendix V.

Solids

Hematite, calcite and barite were identified in fluid inclusions using Raman spectroscopy. The physical characteristics of the solids and their spectra are described below.

Hematite: Hematite in both LVS and LVHS inclusions is red in colour and anhedral. It does not occur consistently in groups of inclusions and is interpreted to be a trapped phase. Coarse hematite from the Pea Ridge deposit was used as a standard and spectra from both the coarse and inclusion-hosted hematite have peaks at 1325, 666, 410, and 295 cm^{-1} (Figure 14a).

Barite: Barite was identified in one secondary LVS inclusion in quartz from the amphibole zone. This crystal is transparent, subhedral, and birefringent. Figure 14b shows the Raman spectrum of this crystal and is characterized by a very strong peak at 989 cm^{-1}. According to Griffith (1969), barite has a very strong peak at 989 cm^{-1}, strong peaks at 462 cm^{-1} and 1142cm^{-1}, and medium intensity peak at 617 cm^{-1}. The weaker peaks are not evident, possibly because of the small size of the barite crystal and overlap with the quartz peak at 462 cm^{-1}.

Calcite: Calcite crystals in inclusions are highly birefringent, and subhedral or anhedral. They are found in LVHS fluid inclusions in the silicified rocks and in the quartz veins, not seen in LVHS inclusions from other zones. The calcite spectra have two strong peaks at 1085 cm^{-1} and 284 cm^{-1} (Figure 14C).

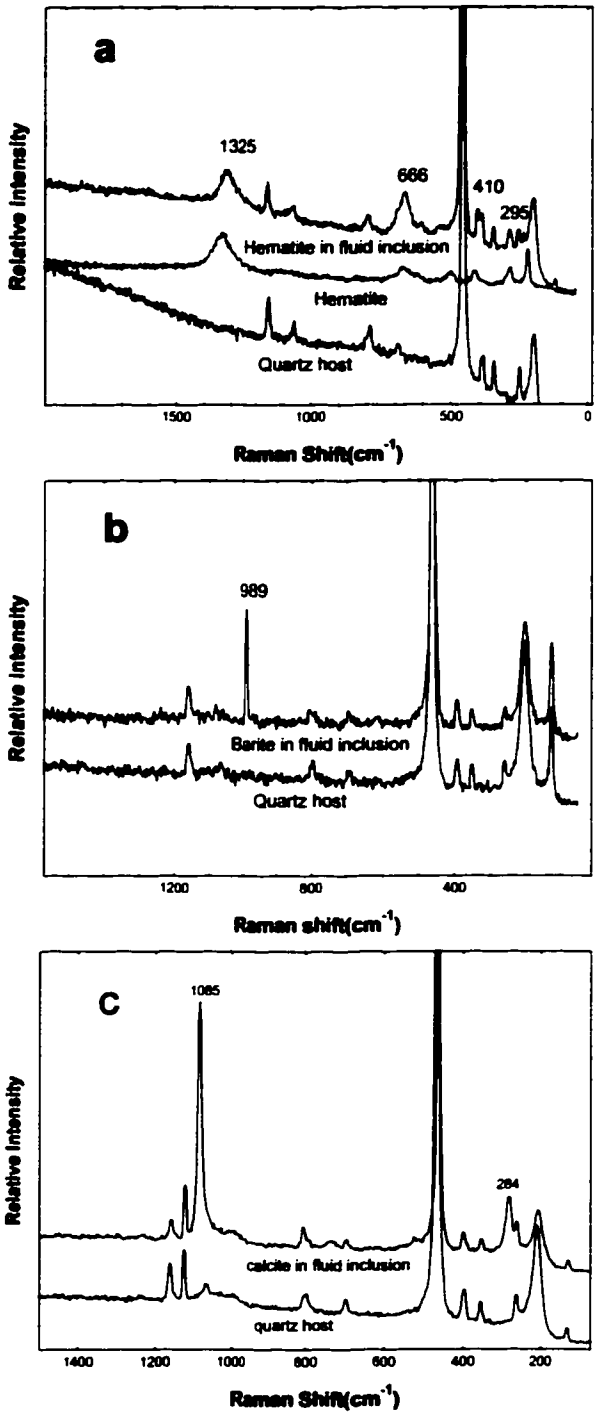

Figure 14 Ramam spectra. a. Hematite in fluid inclusions in quartz from silicified zone (PR95-28). b. Sulphate in fluid inclusion in quartz from amphibole zone (PR95-25), which has the strong peak of 989 cm^{-1} and it is derived from barite. c. Calcite in fluid inclusion in quartz from silicified zone (PR95-28).

Unidentified solids An opaque mineral with irregular shape often occurs in LVS and LVHS inclusions as a trapped phase and has not been identified. Given the mineralogy of the Pea Ridge deposit and the opacity of the crystals, it might be magnetite. Some LVHS inclusions also contain unidentified transparent solids which did not yield a Raman spectrum, either because they are too small or because they are Raman inactive.

Gases Raman spectra of the fluid phases in type C inclusions only indicate the presence of CO_2, with peaks at 1285 and 1388 cm^{-1} (Figure 15a). No N_2 or CH_4 was detected within these fluid inclusions. This is consistent with the $TmCO_2$ values that are close to the CO_2 triple point at -56.6°C. In one two phase C inclusion, water was detected (Figure 15b).

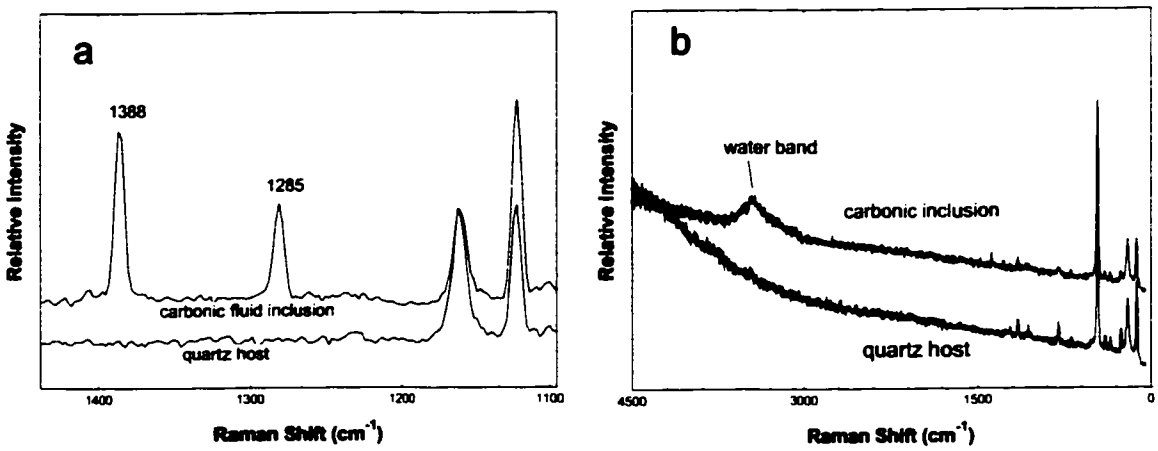

Figure 15 Raman spectra of carbonic fluid inclusions from quartz vein. a. Raman spectra of a C inclusion and its quartz host showing the two CO_2 peaks at 1388 and 1285 cm^{-1}. b. Raman spectrua of a C inclusion and its quartz host showing the water band.

Dissolved molecular species such as SO_4^{2-} within individual inclusions were looked for, however, none were detected.

5 Discussion

5.1 Fluid evolution

5.1.1 Pressure Corrections

In order to estimate the true trapping temperatures for the fluid inclusions, it is necessary to correct the Th values. Several methods can be used and their results are listed in Table 6.

Using the salinity and Th data for LV inclusions, isochores were calculated using the FLUIDS computer code (Bakker, 2001) and the equation of state of Brown and Lamb (1989) (Figure 16). Isochores for halite-bearing fluid inclusions that homogenize by halite dissolution are not as well constrained as for halite-undersaturated fluids. The only experimental data is that of Bodnar (1994), who presents isochoric projections for the 40 wt. % NaCl-H_2O system. This compositional system closely approximates the LVH inclusions in this study and has therefore been used to draw isochores for the Pea Ridge LVH inclusions.

Geological reconstructions suggest a maximum burial depth of 3000 m for the Pea Ridge deposit (Kisvarsanyi, 1974), which is equivalent to about 800 bars of lithostatic pressure. Brecciation in the late stages of deposit formation indicates a shallow depth of emplacement, probably at pressures less than 1 kbar, and possibly less than 0.5 kbar (Kerr, 1998). If we were to assume a pressure of 1 kbar, the pressure corrections that would need to be applied to the Th values for inclusions from the the amphibole-apatite and hematite stages would be around 50°C, and for the breccia pipe stage (quartz host) would be around 90°C (Figure 16).

Actinolite is stable in geothermal and metamorphic systems at temperature over 300°C (Turner, 1981; Fridleifsson and Albertsson, 2000). This implies that the presence of actinolite in the amphibole-apatite stage at the Pea Ridge deposit requires that this assemblage formed at minimum temperatures of 300°C. Using the isochore projections, this requires a minimum pressure of 3.4 kbar for this stage of mineralization (Figure 16). Assuming that the fluid inclusions have been correctly interpreted, such pressures suggest that either the depth estimates

of Kisvarsanyi (1974) are considerably underestimated and/or that significant overpressures existed during the early stages of deposit development. The pressure estimates of Kerr (1998) for breccia formation are also significantly lower than this value and, if correct, would require significant uplift and erosion during the life of the deposit. The least well-constrained data here are the depth estimates of Kisvarsanyi (1974) and the pressure estimates of Kerr (1998). Thus, in the following text, it is assumed that the early stages of deposit development occurred under approximately 3 kbar of lithostatic pressure. Veining and brecciation in the silicicificaton and breccia pipe stages implies that conditions were more likely to have been hydrostatic later in deposit development, and pressures may have dropped to around 1.2 kbar.

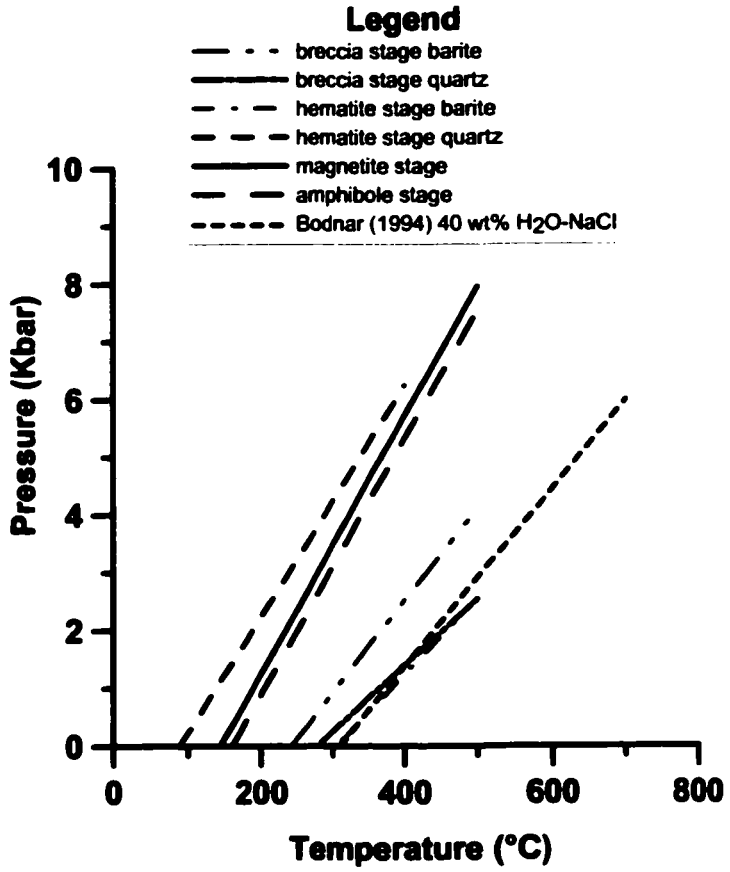

Figure 16 Isochore for fluids of various mineralization stages

Table 6 Comparison of corrected trapping temperature using various methods

Stage	Th	1 Kbar (geological)	3 Kbar (actinolite)
Breccia	230	320	320(1kbar)
Silicification	240-420	380-490	270-450
Hematite	100	150	150
Magnetite	140	190	280
Amphibole	160	210	300

5.1.3 Fluid Characteristics

Amphibole-apatite stage The data collected in this study indicate that the salinities of the fluids responsible for the amphibole apatite stage of deposition range from 19 to 25 wt. % with an average of 22 wt. %. These salinities are significantly lower than the salinities estimated by Sidder et al. (1993) (Figure 19), which were 51 to > 56 wt. %. The high salinity estimates of Sidder et al. (1993) result from their interpretation that LVH inclusions in quartz from this stage are primary. The petrographic observations reported in this study indicates that all of the LVH inclusions in this stage are secondary. Furthermore, much, and possibly all of the quartz in this zone post-dates the amphibole and apatite.

As noted above, the temperatures during this stage must have been at least 300°C as indicated by actinolite stability. Given the Th values for this stage, the pressures would have been at least 3 kbar. Higher temperatures would have required higher pressures to explain the observed Th values. Whether this is reasonable to expect is not known, however, 3 kbar is already significantly higher than the depth estimates of Kisvarsanyi (1974), i.e. 3 kbar is already on the high side and it may be unreasonable to suggest that they were any higher. The isotopic temperature of Sidder et al (1993) for the amphibole-apatite stage is 680 °C, much higher than the temperatures estimated from the fluid inclusion data in this study, i.e., 300 °C (Figure 18).

Sidder et al. (1993) used a magnetite-quartz pair to calculate a temperature for this zone (stage), however, there are two pieces of evidence to indicate that their temperature is wrong. The first is that the magnetite clearly post-dates deposition of amphibole and apatite in these samples, and the second is that the quartz and magnetite are most likely not in equilibrium.

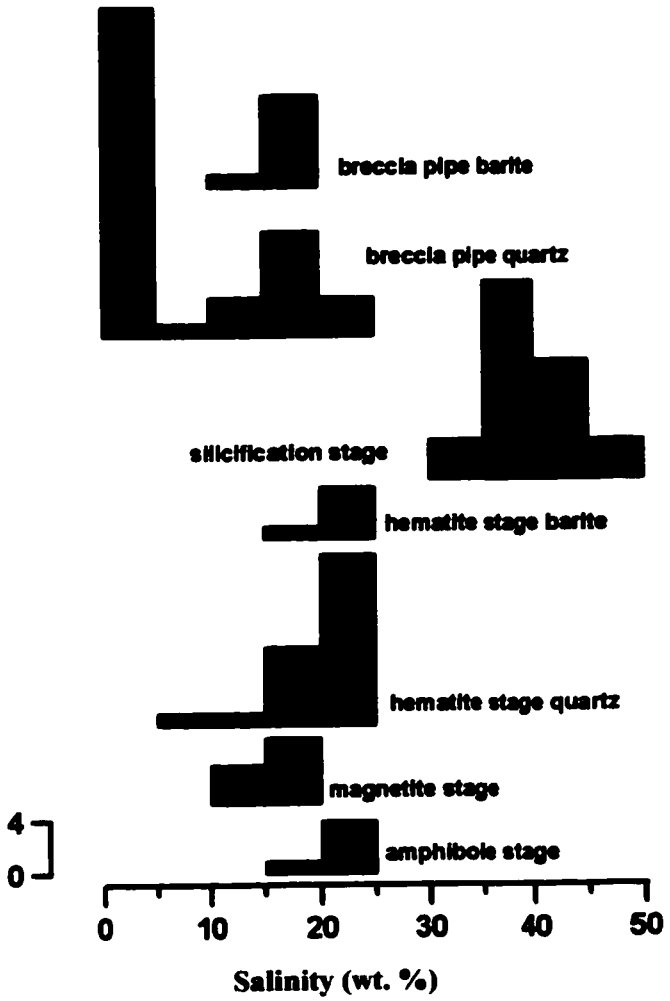

Figure 17 Fluid salinity of various mineralization stages

Magnetite zone Microthermometry results for this zone were obtained from apatite, which is interpreted to have formed during the amphibole stage and is therefore a relic. Therefore, the temperatures obtained from this apatite do not represent the temperatures of magnetite formation and consequently this study has not provided temperatures for the magnetite stage. Although Sidder et al. (1993) calculated magnetite-quartz isotopic temperatures for the magnetite stage, very little, if any, magnetite appears to be in equilibrium with quartz, implying that their temperatures may be wrong. The salinities obtained from LV inclusions in apatite are similar to those of LV inclusions hosted in apatite from the amphibole stage, but again are notthought to represent the magnetite-depositing fluid.. Sidder et al (1993) interpret LVH inclusions in quartz

from the magnetite zone to be the magnetite-forming fluid. However, this conclusion is called into question because the quartz and magnetite were not co-precipitated and only secondary LVH inclusions were observed in magnetite zone quartz.

Hematite stage The salinities of primary fluid inclusions in minerals (quartz and barite) that were co-precipitatetd with hematite in hematite-zone sample range from 14 to 23 wt. %, with an average value of 21 wt. %. As with the amphibole-apatite stage, these salinities are lower than those measured by Sidder et al (1993) (Figure 19). The reason for this discrepancy is the same as that given for the earlier stages, i.e., that the "primary" fluid inclusions interpreted by Sidder et al. (1993) may not be primary. It is actually difficult to assess the interpretations of Sidder et al. (1993) because they do not provide detailed petrographic descriptions of their samples.

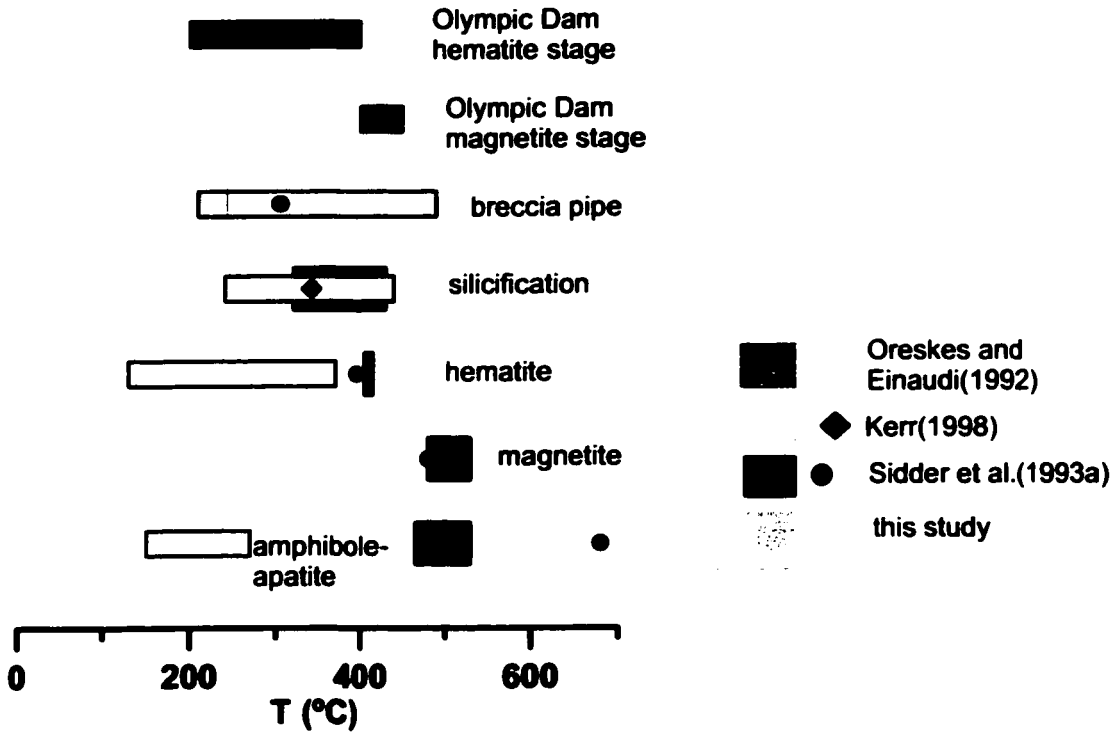

Figure 18 Temperature comparison with previous work on the Pea Ridge deposit and the Olympic Dam deposit

Nevertheless, no primary LVH inclusions were observed in hematite zone samples in this study, although one sample contained secondary LVH inclusions. The occurrence of hematite in growth zones with primary L and LV inclusions (Figure 6D through 6G) is conclusive evidence that these moderate salinity fluids precipitated hematite. The salinity of the hematite-depositing fluids is similar to the salinity of the fluids responsible for the early amphibole-apatite stage, which suggests that these two stages were formed from fluids from the same source.

Homogenization temperatures of LV inclusions in quartz and barite from the hematite stage cover a large range. In some growth zones, L inclusions make up over 90 % of the inclusions, which indicates that these inclusions would have had low homogenization temperatures, probably less than 80 °C, had they nucleated vapour bubbles (cf. Roberts and Spencer, 1995; Wilson et al., 2002). In other growth zones, L inclusions are less abundant, and LV inclusions occur together with the L inclusions. The LV inclusions are invariably larger, which may

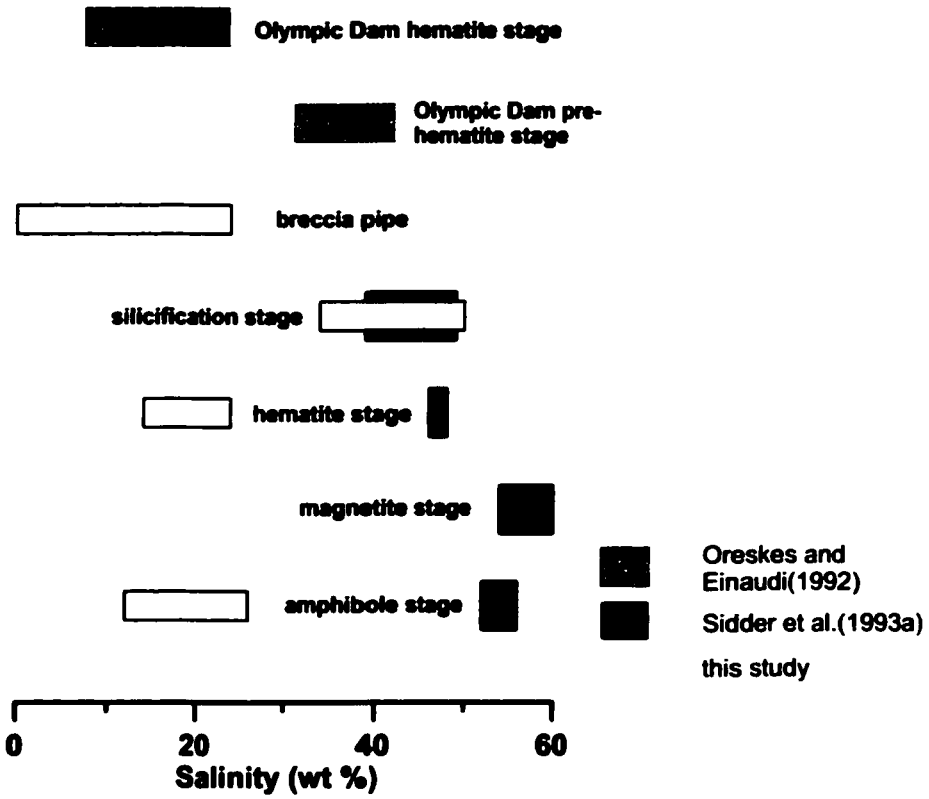

Figure 19 Salinity comparison with previous work on the Pea Ridge deposit and the Olympic Dam deposit

be the reason why they have nucleated vapour bubbles. However, in many cases, L inclusions are associated spatially with the LV inclusions, suggesting that necking has occurred (Figure 6F). Where Th values for LV inclusions show some consistency in a group or growth zone, Th values are invariably low, and are represented by the mode at ~100°C on Figure 9. The higher Th values are likely to be the result of necking. If the hematite zone formed at pressures of 3 kbar, true trapping temperatures for the LV inclusions were 150°C. This temperature is much lower than the isotopic temperature of 395°C calculated for the hematite stage by Sidder et al. (1993). As with the earlier stages, this may reflect that fact that very little quartz appears to have been co-precipitated with the hematite and their quartz-hematite pair may not have been at equilibrium.

Silicification Stage The fluids responsible for the silicification and quartz veins are very different from those responsible for the earlier stages. Salinities are much higher, ranging from 31 to 50 wt. %, averaging 40 wt. %. The presence of calcite, hematite, opaque solids (possibly magnetite) in addition to halite in LVHS inclusions from the silicification stage might infer that the fluid for the silicification stage is rich in Cl, Na, Ca, Fe, Ba, CO_3^{2-}, and SO_4^{2-}.

The lack of CH_4 in the carbonic inclusions (C) is consistent with a relatively oxidizing fluid, which is not surprising given the abundance of magnetite and hematite in the deposit. The association of the C inclusions with the halite-bearing inclusions and the presence of mixed LVHC inclusions is strong evidence that heterogeneous entrapment of carbonic and saline, aqueous fluids occurred during this stage, most likely as a result of immiscibility of an originally homogeneous fluid. This immiscibility may be the result of a decrease in pressure and/or temperature, and resulted from in the partitioning of CO_2 into a vapor phase, and salt to the liquid phase (e.g., Bowers and Helgeson, 1983).

The salinities calculated for the silicifcation stage are the same as those estimated by Sidder et al. (1993) because, in both studies, LVH inclusions are considered to be primary inclusions. However, Sidder et al. (1993) did not report the presence of CO_2-rich fluids.

The Th values for these inclusions range from 245°C to 422°C, averaging 311 °C. Assuming pressures of 1.2kbar, trapping temperatures for the inclusions in quartz from the silicification

stage is 380°C using the isochore for 40 wt % H_2O-NaCl by Bodnar (1994). This is consistent with the results of Sidder et al. (1993) (Figure 18). The presence of andalusite in the silicified zone requires temperatures of at least 341°C (Shade, 1974; Hemley et al., 1980; Kerr, 1998) (Figure 18). Seeger (1989) proposed that the fluids for silicification were also responsible for the hematitzation of magnetite. The results of this study indicate that this idea may not be correct because the fluids responsible for the two stages are very different.

Breccia pipe stage The salinity of the fluids responsible for this stage of mineralization ranges from 0 to 22 wt. %. These salinities fall into two populations; one is moderately saline (~ 20 wt. %) and has a similar range to the salinities of inclusions from early amphibole-apatite and hematite stages, and the other is very dilute (0 to 5 wt. %) (Figure 17). Sidder et al. (1993) did not report salinity data for the breccia pipe stage.

Homogenization temperatures for the inclusions from the core of the quartz crystals cover a wide range, from 120°C to 400°C. Some of the measured inclusions show evidence of necking and produced Th values over 300°C; those without evidence of necking produced more consistent values, averaging 230°C. Using this latter temperature and 1.2 kbar to calculate a pressure correction, the trapping temperature for breccia pipe inclusions is 320°C. Sidder et al. (1993) gave no fluid inclusion temperatures for the breccia pipes, however, they used a barite-pyrite pair to calculate an isotopic temperature of 305°C for the breccia pipe stage that is close to the temperatures calculated in this study. Unfortunately, they provide no detailed information about the occurrence of the mineral pair. Kerr (1998) used a variety of chlorite geothermometers to calculate the precipitation temperatures of chorite-bearing assemblages and got results ranging from 161°C to 243°C for chlorite from the silicification and breccia pipe stages, with the highest temperature occurring in the breccia pipe stage. These temperatures are lower than the temperatures calculated for quartz deposition, but are consistent with the paragenesis and overall late-stage cooling in that chlorite post-dates quartz in the paragenesis (Kerr, 1998). The chlorite may also be related to a regional alteration event identified by Wenner and Taylor (1976) that occurred within the St. Francois Mountains (Kerr, 1998).

5.1.4 Fluid evolution

The overall evolution of the fluids in the Pea Ridge deposit started with a fluid with a temperature of ~ 300°C and a salinity of ~ 22 wt. % that formed the amphibole-apatite assemblages. This event was followed by the formation of the main magnetite ores. The hematite assemblage was subsequently formed from a similar fluid to that which formed the amphibole assemblage, but at temperatures of ~ 150°C. Temperatures and salinity then increased to over 310°C and 40 wt. %, respectively, to form the silicification stage. The final, breccia pipe stage resulted from fluids that had temperatures of 320°C and lower and had a bimodal salinity with populations at ~ 0 and 20 wt. %.

Previous workers have proposed that hematite is the product of magnetite oxidization (e.g., Sidder et al., 1991; Seeger et al., 2001). Hematite is stable in oxidizing environments (high fO_2) and magnetite, on the other hand, is stable under more reducing conditions (low fO_2) (Haas and Robie, 1973). However, at constant oxygen fugacity, decreasing temperature will cause magnetite to convert to hematite (Haas and Robie, 1973). Thus, hematization of the magnetite could have been produced by the infiltration of a fluid with a lower temperature and/or higher fO_2, or simply by gradual cooling of the hydrothermal system. These possibilities cannot be distinguished at this point, however, the fluids responsible for hematite precipitation appear to have been chemically similar and cooler that those responsible for amphibole-apatite, and possibly magnetite, precipitation. Thus, the influx of an "oxidizing" fluid is not necessary to cause the hematization.

The high temperature, high salinity fluid population in the breccia pipe stage is very similar to that seen in the amphibole-apatite and hematite stages. All three have salinities between 15 and 25 wt. % and temperatures of between 150 and 320°C. This suggests that the fluid responsible for the early stages was again present during breccia pipe formation. In addition, a low salinity fluid (~ 0 wt. %) was also present that is not seen at any other time during the evolution of the deposit.

5.2 Comparison with the Olympic Dam Class Deposits

Among the many members of the Olympic Dam class of deposits listed by Hitzman et al. (1992), the Olympic Dam deposit in South Australia has the most similar paragenesis to the Pea Ridge deposit. Oreskes and Einaudi (1992) summarized the principal paragenetic stages for the Olympic Dam deposit as follows: (1) magnetite stage (magnetite-pyrite association), (2) hematite and breccia stage (hematite-uraninite-fluorite-REE minerals), (3) sulphide stage (Cu-Fe sulphides intergrown with sericite, fluorite, uraninite or hematite), and (4) barite stage (barite as fragments and intergrown with fluorite, siderite and Cu-Fe sulphides in veins). It can be seen that both the Pea Ridge and the Olympic Dam deposits have a magnetite stage, then hematite and REE mineralization and late-stage sulphate veining.

Oreskes and Einaudi (1992) studied fluid inclusions hosted in quartz clasts and hydrothermal minerals in the hematite breccia stage. They reported that within the quartz clasts there are two types of secondary fluid inclusions: LVH(S) and LV(S). Solids within these inclusions are mostly hematite, and occasionally Fe chlorides in addition to halite. These inclusions represent the early fluids that predate the hematite brecciation stage. Within the hydrothermal quartz and fluorite, primary and secondary fluid inclusions are observed and are all liquid-rich (LV), two-phase inclusions. These are interpreted to represent the fluids that were responsible for the main hematite stage and the associated brecciation, as well as late-stage hydrothermal veins. Their microthermometric data indicate that the hematite breccias formed at between 120°C and 380°C and that salinities ranged from 7 to 24 wt. %. These temperature and salinity values are very similar to those of the fluids responsible for the breccia pipe and hematite stages at Pea Ridge (Figure 18 and Figure 19). One notable difference, however, is that the silicification stage is thought to occur between the hematite and breccia pipe stages at Pea Ridge (Nuelle et al., 1989a,b; Seeger et al., 2001). Such an event is absent at Olympic Dam.

Measurements on the secondary fluid inclusions from quartz fragments in the breccias at Olympic Dam reveal that there were early, saline fluids present there. These fluids can be grouped into two populations: one had temperatures of between 200 and 390°C and salinities of 31 to 42 wt. %, and the other had temperatures of 170 to 210°C and salinities of 10 to 23 wt. %.

These fluids resemble the fluids responsible for the silicification and amphibole-apatite stages at Pea Ridge (Figure 18 and Figure 19).

Crushing experiments confirm the presence of noncondensable gases in all of the fluid inclusion types studied at Olympic Dam. Oreskes and Einaudi (1992) infer that the gases are dominated by CO_2 because of high ice melting temperatures (4 to 6°C). The estimated CO_2 pressure in the inclusions increases from 1 to 2 bars in the early fluid inclusions, to 10 bars in the hematite breccia stage, to 20 bars in the late post-breccia barite stage. Crushing tests were not carried out on the Pea Ridge inclusions so that the gas content of the aqueous inclusions is not known. However, CO_2-rich inclusions occur widely in quartz from the silicification and magnetite zones, which suggests that the fluids that were present at Pea Ridge during silicification had higher CO_2 contents than those at Olympic Dam or that conditions were such that immiscibility occurred at Pea Ridge but not at Olympic Dam.

Although fluids with similar characteristics are present in both deposits (see above discussion), there are notable differences in the evolution of those fluids with respect to the stages of mineralization. Most notably, the hypersaline fluids at Olympic Dam are interpreted to have formed the early magnetite mineralization, whereas at Pea Ridge these fluids post-date the Fe oxide mineralization, and appear to only be responsible for silicification and quartz veining.

Appendix VI contains a compilation of fluid inclusion data on Fe-oxide Cu-Au-REE deposits. The deposits included in this table all have iron oxide (magnetite or hematite) and Cu-Au mineralization stages.

Most fluid inclusion data on Fe-oxide Cu-Au deposits are from the Cloncurry mining district, Northwest Queensland, Australia (Appendix VI). This district occurs within the Eastern Fold Belt of the Mount Isa inlier (Williams et al., 1999). The Fe-oxide Cu-Au mineralization was formed by hydrothermal activity in brittle-ductile shear zones in metamorphosed supracrustal rocks after the peak of regional metamorphism (1550 Ma), and was broadly coeval with the emplacement of 1530-1500 Ma I-type granitoids (Williams et al., 1999). Fluid inclusion studies have been conducted at Eloise (Baker, 1998), Starra (Rotherham et al., 1998), Lighting Creek

(Perring et al., 2000), Osborne (Adshead (1995), Mount Elliot (Garret, 1992; Xu, 2000), and Maramungee Creek, Little Eva, and Ernest Henry (Xu, 2000).

The pre-mineralization stage includes hb-bio –qtz veins at Eloise (Baker, 1998), Na-Ca alteration (qtz-ab-scp-act) at Starra (Rotherham et al., 1998), and silica alteration at Osborne (Adshead et al., 1998). Primary fluid inclusions in the pre-mineralization stages comprise LVHS (hypersaline) and CO_2-rich types. These kinds of inclusions indicate temperatures of 450 to 600°C and salinities of 32 to 60 wt. % for the Eloise deposit (Baker, 1998), and over 450°C and salinities of 60 to 70 wt. % for the Osborne deposit (Adshead et al., 1998) (Figure 20).

The pre-mineralization mineral assemblages in the Cloncurry district may be comparable to the amphibole-apatite stage at Pea Ridge, however, the high temperature-high salinity fluids are not observed.

The mineralization stage includes qz-cal-act and chl-cp-po-py-mt vein assemblages at the Eloise deposit (Baker, 1998),), K-Fe metasomatism (bio-mt-hm-qtz-py) and qtz-anh-bar-hm-cal-Au-py-ccp-bn-cc-chl-ms assemblages at the Starra deposit (Rotherham et al., 1998), and qtz-mt ± py±ab veins at the Lighting Creek Fe-Cu-Au prospect (Perring et al., 2000). The primary fluid inclusions present in the mineralization stages contain LVHS and CO_2 types.

Microthermometric measurements infer temperatures and salinities of 300°C and 20 to 37 wt. % at the Osborne deposit (Adshead, 1995), 100 to 500°C and 30 to 47 wt. % at the Eloise deposit (Baker, 1998), 345 to 615°C and 34 to 52 wt. % for the K-Fe metasomatism at the Starra deposit, and 225 to 360°C and 30 to 42 wt. % for the Fe-Au-Cu ore-forming stage at Starra (Rotherham et al., 1998) (Figure 20 and Figure 21). The ore-stage mineral assemblages in these deposits are comparable to the magnetite and hematite stages at Pea Ridge. However, fluid temperatures and salinities are both much higher than in the hematite stage at Pea Ridge. Rather, fluids equivalent to those responsible for mineralization in the Cloncurry deposits are seen in the silicification stage at Pea Ridge.

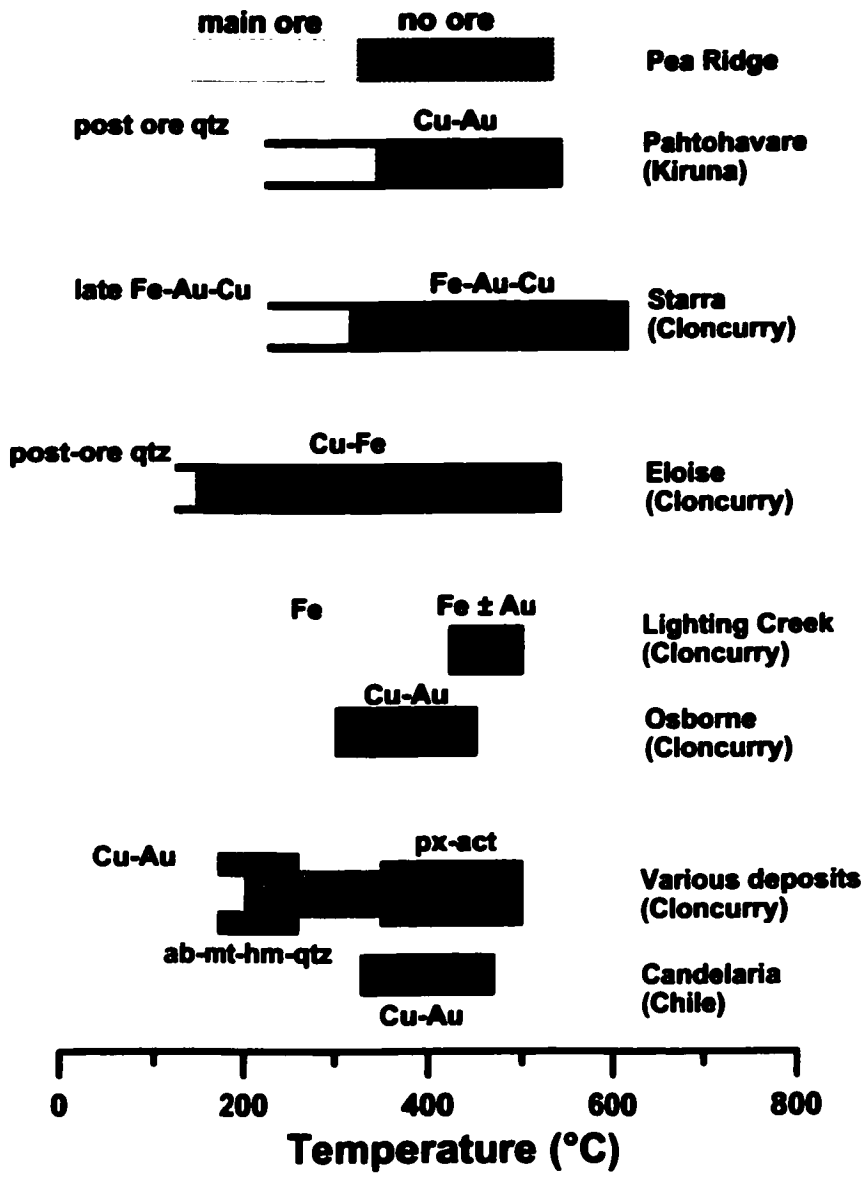

Figure 20 Temperature of other Fe-oxide Cu-Au deposit. Data for Candelaria, Chile (Marschik et al. (2000), Maramungee Creek, Little Eva, Ernest Henry, Mount Elliot, Cloncurry district (Xu, 2000), Osborne , Cloncurry district(Adshead et al., 1998; Adshead, 1995), Lighting Creek, Cloncurry district (Perring et al. (2000), Eloise, Cloncurry district (Baker, 1998), Starra, Cloncurry district (Rotherham et al., 1998), and Pahtohavare, Kiruna, Sweden (Lindblom et al., 1996). Floating bars of the same Y-axis position represent fluids of the same deposit. Black color refers to high temperature fluids for the early mineralization stages and light gray refers to low temperature fluid for the late or post-ore mineralization stages of the same deposit. Among them, Candelaria, Chile and Osborned, Cloncurry do not have data on low temperature fluids.

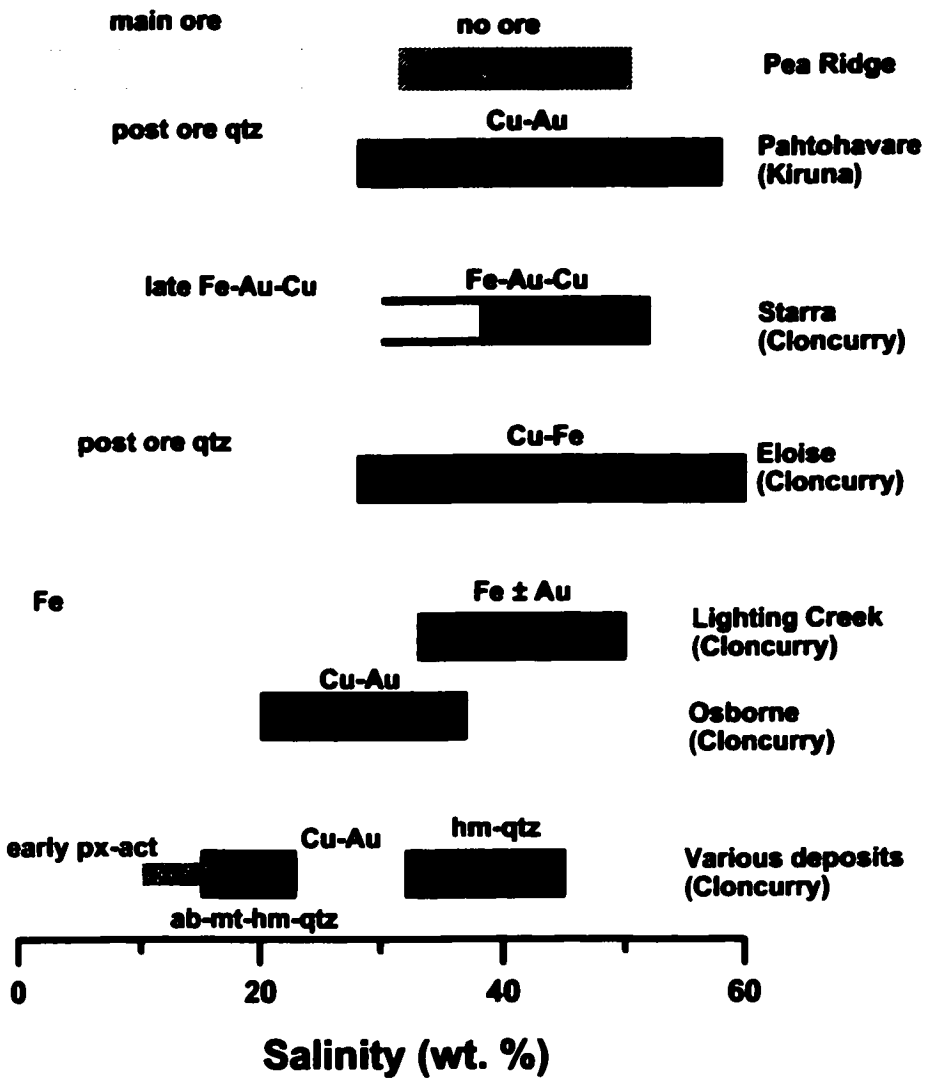

Figure 21 Salinity of other Fe-oxide Cu-Au deposit. Data for various deposits (e.g., Maramungee Creek, Little Eva, Ernest Henry, Mount Elliot, Cloncurry district, Xu, 2000), Osborne, Cloncurry District (Adshead et al., 1998; Adshead, 1995), Lighting Creek, Cloncurry district (Perring et al. (2000), Eloise, Cloncurry district (Baker, 1998), Starra, Cloncurry district (Rotherham et al., 1998), and Pahtohavare, Kiruna, Sweden (Lindblom et al., 1996). Floating bar of the same Y-axis position represent fluids of the same deposit. Black color refers to high salinity fluids for the early main mineralization stages and light gray refers to low salinity fluids for the late mineralization stages or post-ore stages of the same deposit. Among them, Osborne, Cloncurry does not have data on low salinity fluids.

In the Cloncurry district, post-ore mineralization includes the quartz veins at Eloise (Baker, 1998). Primary inclusions in these stages are mainly LV. Data from these inclusions indicate temperatures and salinities of 100 to 150°C and 4 to17 wt. % at Eloise (Baker, 1998) (Figure 20 and Figure 21). These mineral assemblages are comparable to the mineral assemblages of the silicification stage at Pea Ridge, however, the fluids are very different, in that, at Pea Ridge, the fluids in this stage are more saline, higher temperature, and include a carbonic component.

To summarize, in the Cloncurry district, the fluids responsible for the pre-mineralization and mineralization (Fe-oxide and Cu-Au) stages are dominated by hypersaline and CO_2 fluids, which form the mineralization. In comparison, the fluids responsible for the amphibole and hematite stages at Pea Ridge are moderately saline and do not contain detectable CO_2. However, hypersaline and carbonic fluids existed during the silicification stage but do not appear to be associated with the Fe-oxide mineralization. The post ore-stage fluids in the Cloncurry district had lower temperatures and lower (low to moderate) salinities than the ore-stage fluids, and are comparable to the fluids responsible for the amphibole and hematite stages at Pea ridge. It is clear that the fluids responsible for equivalent stages of mineralization in the Cloncurry district and at Pea Ridge are different from one another, and indicates the fluid responsible for the Pea Ridge deposit had different sources from those in the Cloncurry district.

Xu (2000) also carried out a fluid inclusion study of several deposits in the Cloncurry district, but gave different results from other Cloncurry workers. This author studied pyroxene-actinolite alteration, magnetite-hematite-quartz veins, and sulphide-quartz-calcite veins at Maramungee Creek, Ernest Henry, Mount Elliot and Little Eva. Xu (2000) concluded that the fluids were high temperature (350-500°C) and moderate salinity (10-22 wt. %) in the early alteration stage, moderate temperature (170-260°C) and moderate salinity (15-23 wt. %, average 19 wt. %) for the albite-magnetite-hematite-quartz veins, and low temperature (80-200°C) and salinity (14-28 wt. %, average 22 wt. %) for the late sulphide-quartz-calcite stage (Figure 20 and Figure 21). However, the author also reported that there are a few primary LVH inclusions in the hematite-quartz veins with salinities of 32 to 45 wt. %. Thus, the data of Xu (2000) differs from other studies on the Cloncurry district in that the main ore stage fluids are moderate salinity and

moderate temperature, and quite similar to the fluids responsible for the early stages at Pea Ridge.

So the salinity is decreasing instead of increasing as the author said from early hematite-quartz vein to the late sulphide-calcite vein and the temperature does decrease significantly from early to late stages. The fluids responsible for these deposits more closely resemble in salinity the fluids at Pea Ridge for the early alteration and Fe-oxide mineralization. However, their temperature is much higher than those of the three stages of the Pea Ridge deposit.

The Candelaria iron oxide Cu-Au (-Zn-Ag) deposit in Chile occurs as veins in the matrix of hyrothermal breccias or superposed on massive magnetite replacement bodies (Marschik and Fontbote, 2001). Parageneses include early albitization, then potassic alteration and silicification associated with intense iron metasomatism, then the main Cu-Au mineralization in which chalcopyrite ± pyrite cut magnetite and hematite (Marschik and Fontbote, 2001). Fluid inclusion data indicate that the fluids for the Cu-Au mineralization stage had temperature of 330 to 470°C. In post-Cu-Au stage mineralization, the fluids had lower temperatures, less than 180°C (Figure 20). No salinity data was reported. It can be seen that the Candelaria deposits differs from the Pea Ridge deposit in that hematite formed early and was converted to magnetite, possibly because of the increasing temperature. This is the converse of the sequence at Pea Ridge and indicates a very different fluid evolution.

The Pahtohavare Cu-Au mineralization is hosted by albitized rocks in the Kiruna greenstone belt (Lindblom et al., 1996). Quartz veins and carbonate veins occur as irregular masses within the ores and surrounding altered rocks. Pyrite, chalcopyrite, and gold are the main ore minerals and are found in the albitized rocks as veinlets and in breccia matrices with carbonate and quartz. Fluid inclusion data indicate that in the Cu-Au mineralization stage, the fluids were hot (>490°C) and hypersaline (33-58 wt. %), but became cooler (120-170°C) and dilute (0.5-25 wt. %) in the later stages (Figure 20 and Figure 21). This deposit is included in the Fe oxide-Cu-Au class by Pollard (2001), however, magnetite-rich horizons are syngenetic and the relationship between the Fe-oxide and epigenetic Cu-Au mineralization is unclear.

The Bayan Obo deposit was also included as an Olympic Dam class deposit by Hitzman et al. (1992). However, it has a very different geological evolution from the other Olympic Dam class deposits. Cao et al. (1995) proposed that the original iron bodies are sedimentary deposits and the REE ores are formed by mantle fluid metasomatism that was superimposed on the preexisting iron ores. They believed that the REE ores are related to an intracontinental hot spot. Smith and Henderson (2000) studied the fluid inclusions at Bayan Obo and demonstrated that the ore-forming fluids are quite different from the fluids responsible for Olympic Dam-type deposits. Their results show that in the early, disseminated, monazite mineralization, the fluids are represented by the system H_2O-CO_2-NaCl with salinities ranging from 1 to 5 wt. % NaCl equivalent and that temperatures ranged from 280°C to 330°C. In the main-stage banded ores, the fluids forming the apatite and bastnasite are aqueous, with salinities ranging from 6 to 10 wt. % NaCl equivalent and a temperature of 300°C to >400°C. Inclusions in late-stage fluorite and barite have homogenezation temperatures of 150°C to 240°C and 130°C to 200°C respectively, and their salinities decrease from about 15 to 5 wt. % down to less than 1 wt. %. The low salinities and temperatures of the fluids in the Bayan Obo deposit indicate that this is not an Olympic Dam type deposit.

As the above discussion demonstrates, the Pea Ridge fluids have some features in common with deposits of the "Olympic Dam class", namely, the fluid inclusion types present, the coexistence of high temperature, hypersaline aqueous fluids with carbonic fluids, and the presence of lower temperature, moderately saline fluids. However, a major difference is that, unlike the other Olympic Dam-type deposits, the high temperature, hypersaline fluids were not responsible for the formation of either Fe oxide or REE mineralization at Pear Ridge. Rather, the amphibole-apatite alteration (and possibly the magnetite mineralization), and hematite stages at Pea Ridge were formed from moderate salinity, low temperature fluids. It has been suggested that magmatic fluids have played a significant role in the formation of many Fe-oxide Cu-Au deposits (e.g., Xu, 2000; Pollard, 2001), however, the difference noted above suggest that this may not be the case for Pea Ridge. This will be discussed more fully in the next section.

5.3 Fluid Sources

Fluid salinities and temperatures indicate that there were two fluids involved in the formation of the amphibole-apatite alteration, the hematite stage and the breccia pipes (Figure 22). One of these fluids had a moderate salinity (10 to 25 wt. %, average 20 wt. %) and a temperature 150 to 320°C; and the second fluid had a low salinity of 0 to 5 wt. % and a temperature of 120 to 250°C. A third fluid, with a temperature of 270 to 450°C and a salinity of 30 to 50 wt. %, which coexisted with carbonic fluids, formed the silicification assemblage.

Three fluid sources have been invoked to explain the Pea Ridge deposit specifically, and Olympic Dam-type deposits in general: (1) fluids derived from a silicate magma (magmatic fluids); (2) fluids derived from meteoric water; and (3) fluids derived from evaporite brines.

1) Magmatic Fluids

In many Fe-Oxide Cu-Au deposits a high temperature fluid assemblage comprising hypersaline brines and immiscible carbonic fluids has been identified and is invariably interpreted as representing magmatic fluids (Adshead, 1995; Lindblom et al., 1996; Adshead et al., 1998; Rotherham et al., 1998; Baker, 1998; Ullrich and Clark, 1999; Marschik et al., 2000; Perring et al., 2000). This conclusion is supported by isotopic evidence (Oreskes and Einaudi, 1992; Pollard et al., 1997).

At Pea Ridge, hypersaline plus carbonic fluids are present in the silicification stage, and it is therefore reasonable to suggest that these fluids are magmatic. An alternative explanation is that the earlier moderately saline fluids seen in the amphibole-apatite and hematite stages may evolve into the hypersaline fluids during silicification. Halite-saturated aqueous inclusions in which halite is the final phase to disappear can be formed from aqueous immiscibility of a moderate salinity fluid (halite undersaturated) at magmatic temperatures with subsequent cooling of the hypersaline brine (Samson, 1990; Bodnar, 1994). This model is, however, untenable at Pea Ridge because the temperature increased from the early stages to the silicification stage. In addition, the CO_2-rich fluids in the silicification stage cannot be easily explained through this model because no CO_2 has been detected in the early fluids. These arguments suggest that the

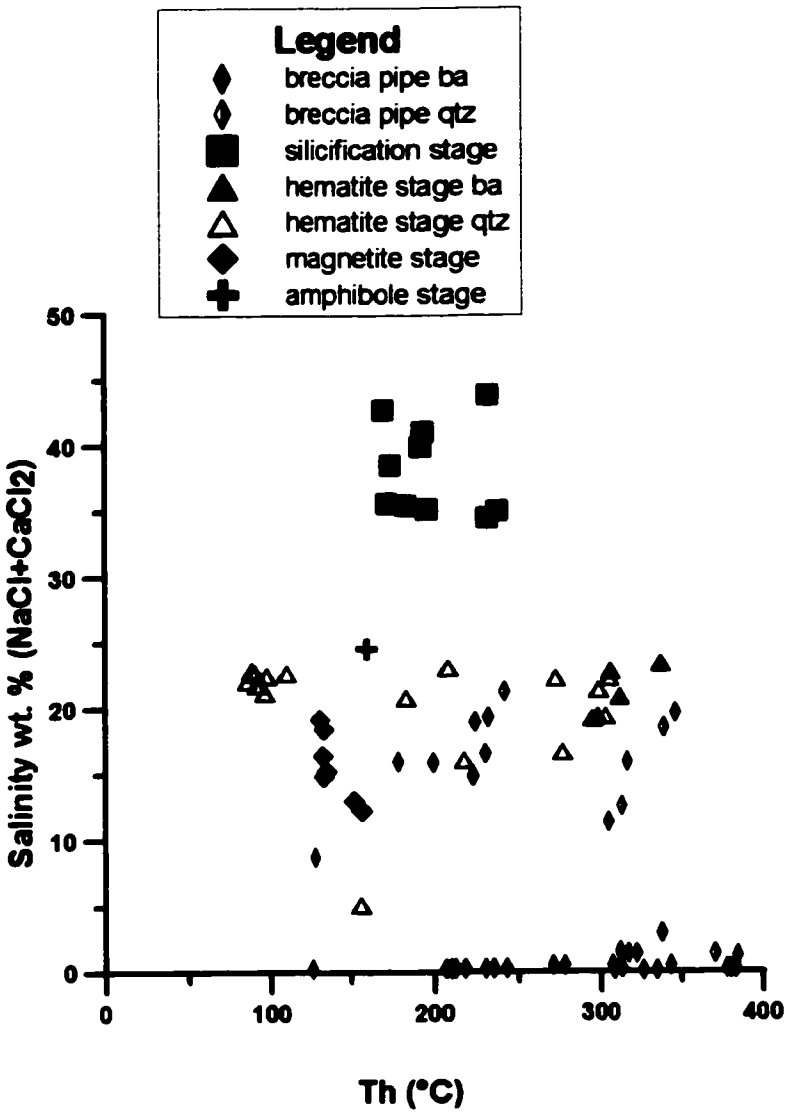

Figure 22 Plot of homogenization temperature Th versus salinity of primary fluid inclusions, indicating three fluids responsible for the formation of these stages.

moderate salinity fluids responsible for the three early stages could not have evolved into the hypersaline-carbonic assemblage, and that they had separate origins.

The temperature range of the moderate salinity fluids at Pea Ridge (150-320°C) is low compared to that of the magmatic fluids (400-600°C) seen in many other Fe-oxide deposits. If the silicification was indeed produced by high temperature, magmatic fluids, and assuming the same magma is the putative source for the moderate salinity fluids, the latter should also be high temperature. Also, by analogy with the other deposits (and most porphyry deposits), the salinities are too low to be of magmatic origin. The same arguments apply to the late, low salinity fluids seen in the breccia pipes.

2) Meteoric waters

Fluids derived from meteoric water are generally low temperature, have low salinities, are mildly oxidizing, and have low $\delta^{18}O$ signatures. At Pea Ridge, the fluids responsible for the amphibole-apatite, hematite and silicification stages do not fit these characteristics. However, one of the two population of fluids present in the breccia pipes is very low in salinity (0-5 wt. %) and low temperature (about 100°C) (Figure 9), which is consistent with their being meteoric in origin. The abundant hematite and barite in the breccia pipes is consistent oxidizing fluids and with the involvement of meteoric fluids.

3) **Evaporite brines**

Barton and Johnson (1996) presented a model in which the fluids responsible for Fe- Oxide Cu-Au-REE deposits are derived from evaporate brines. For this model to be valid there is a requirement of coeval or older evaporates, a correlation with arid belts or evaporate-bearing basins, and the presence of saline fluids (>20 wt. % NaCl). In their model, the nature of associated igneous rocks has a second-order control, mainly on the alteration mineralogy and on element abundances. Barton and Johnson (1996) require an intrusion to provide the necessary heat to drive the thermal circulation of the saline evaporitic fluids. The evaporite provides the necessary chloride for metal transport and sodium for the sodic alteration that is typically associated with these deposits.

The salinity of the fluids responsible for the amphibole-apatite, possibly the magnetite, and hematite stages, and a component of the fluids in the breccia pipe stages, are between 10 and 25 wt. % (Figure 17). The formation temperature for amphibole-apatite, hematite and breccia pipe stages are about 300°C, 150°C, and 320°C, respectively (Figure 9 and Figure 12). These fluid characteristics are consistent with the involvement of evaporite-derived brines in the formation of the amphibole-apatite stage, possibly the magnetite stage, the hematite stage and breccia pipe stage.

Barton and Johnson (1996) contend that Mesozoic and Mesoproterozoic Fe oxide-rich hydrothermal deposits and districts are most commonly associated spatially and temporally with arid environments and low- to mid-latitudes. The St. Francois Mountains region at 1.4 to 1.5 Ga was within the 20° of the equator (Buchan et al., 2000) which is consistent with conditions that might be favorable for the formation of evaporites, even though coeval or older evaporate are not found in the strategraphic column of the St. Francois Mountains area (Kisvarsanyi et al., 1981).

To summarize, it is possible that moderate salinity (~20 wt. %) fluids, derived from evaporite surface waters, circulated in the igneous rocks that host the Pea Ridge deposit, were heated to around 300°C, dissolved Fe and REE from the volcanic rocks, and generated the early amphibole-apatite alteration assemblage and the magnetite ores. Then, possibly due to decreasing temperatures in the hydrothermal system, the magnetite was converted to hematite at about 150°C. Silicification and quartz vein formation then occurred due to an influx of magmatic fluids (hypersaline-carbonic assemblage), which temporarily overwhelmed the early fluid system. As the magmatic system waned, the evaporite-derived fluid became dominant again, forming the breccia pipes. During this stage, more dilute, possibly meteoric, waters also became involved in the hydrothermal system. These latter fluids may possibly have mixed with the more saline fluids causing dilution and possibly an increase in the fO_2 of the system, the end result being the precipitation of sulphates and REE.

6 Conclusion

The Pea Ridge iron oxide-REE deposit is hosted by the Mesoproterozoic St. Francois granite-rhyolite terrane in Southeast Missouri and is considered to be an example of an Olympic Dam class deposit. Primary aqueous, liquid-vapour (LV) inclusions in apatite from the early amphibole stage has salinities of 14 to 24 equiv. wt. % $NaCl+CaCl_2$ and Th (L-V) values of 130°C to 180°C. Primary LV fluid inclusions in quartz from the post-magnetite hematite stage have salinities of 21 ± 3 equiv. wt. % $NaCl+CaCl_2$ and Th(L-V) values of 100°C, however, there are many primary liquid-only inclusions within the quartz growth zone of the hematite stage, which may suggest a very low temperature.

Primary inclusions in quartz from the silicification stage, which surrounds the magnetite and hematite zones, comprise liquid-vapour-halite (LVH) inclusions that have salinities between 34 and 48 equiv. wt. % NaCl. These inclusions homogenize by halite dissolution with TmH values of between 245°C and 422°C. These high salinity inclusions also occur as secondary inclusions in the earlier amphibole, magnetite, and hematite stages. LVH inclusions may also contain trapped hematite or calcite crystals. CO_2-bearing inclusions occur as secondary inclusions in quartz of the silicification stage. These comprise both halite-bearing, aqueous, liquid-rich inclusions and CO_2-rich, aqueous-poor inclusions. No CH_4 has been detected by Raman spectroscopy.

Primary inclusions in quartz from late-stage REE-rich breccia pipes consist of LV inclusions that exhibit two salinity populations; one is moderately saline (~20 wt. %) and one is dilute (0-5 wt. %). Th (L-V) values for these inclusions have a consistent mode at 230°C. There are also abundant liquid-only primary fluid inclusions within the quartz growth zones of the breccia pipes indicating low formation temperature.

Microthermometry data suggest that there are three types of fluids responsible for the formation of the Pea Ridge deposit. A moderate salinity fluid (~20 wt. %) formed the amphibole-apatite and hematite zones and was also present during formation of the breccia pipes. The temperature

of this fluid was at least 300°C during amphibole formation, decreased to 150°C or less during hematite formation and increased again to approximately 320°C during breccia pipe formation. Between hematite and breccia pipe formation, a high salinity (average 40 wt. %), high temperature (270°C to 450°C) fluid formed the silicification stage. During breccia pipe formation, a low salinity fluid infiltrated the system.

These data suggest the following. a) the fluid responsible for hematitic alteration of the magnetite zone was similar to that which deposited the amphibole and possible magnetite, except that it must have been more oxidizing; this fluid is moderately saline and low temperature and may be derived from evaporite surface water. b) a second fluid was responsible for silicification and was hypersaline. The common occurrence of CO_2-rich inclusions in these samples suggests that immiscibility occurred during infiltration of this hypersaline fluid. c) The third fluid responsible for the REE-rich breccia pipes is a mixture of the first fluid with a distinct, late, lower-salinity fluid, possible meteoric water.

These results differ from preliminary fluid inclusion data obtained by Sidder et al. (1993), which indicated that the salinity of the fluids responsible for the early stages (amphibole, magnetite, and hematite) were significantly higher than the estimates reported here. This is likely due to a different interpretation of the origin of LVH inclusions in the early zones and/or to the timing of the quartz from which they obtained their data.

Comparison on the ore-forming fluids of the Pea Ridge deposit with other Proterozoic Fe-Oxide Cu-Au-(REE) deposits suggest that they have the same types of fluids present, i.e., (1) high temperature and hypersaline aqueous fluids coexisting with carbonic fluids, which are thought to be magmatic, and (2) low temperature and very dilute fluids, which are thought to be derived from meteoric water. However, the Pea Ridge deposit differs in that it has moderate salinity and low to moderate temperature fluids in the early alteration, possibly magnetite, and hematite stages. This requires that the Pea Ridge deposit has more than two fluid sources. The characteristics of this fluid are consistent with a fluid derived from evaporate brine.

Suggestions for further study

This study comprises a detailed fluid inclusion petrographic, microthermometric, and Raman spectroscopic study on fluid inclusions from the Pea Ridge deposit. The discovery of the three fluids for the different stages suggests more work should be done to better constrain their sources. Although a preliminary laser ablation ICP-MS study was carried out on some fluid inclusions, few usable results were obtained. Acquisition of more laser ablation ICP-MS data on the fluid inclusions from the different stages will help better understand the chemistry of these three fluids, and, given that the chemistry of fluids from the three putative sources will be different, such analyses will place constraints on the origin of the fluids. Further stable isotopic work on the fluid inclusions and minerals should be carried out to further constrain the sources of the three fluids.

As for the magnetite stage, as fluid inclusion data from apatite of this stage might not represent the fluids responsible for magnetite precipitation, more work needs to be done on identifying the character of the fluids responsible for magnetite deposition.

The relative timing of the silicification and hematite stages is an important question and is still uncertain. It might be possible that there are two modes of hematite formation, one oxidizing magnetite to hematite and occurring before the silicification stage, and one formed from the same fluids as for the breccia pipe and occurring possibly later than silicification. It is also possible that the same fluid oxidized magnetite to hematite and precipitated the specular hematite. Therefore, timing of various stages is needed so as to exactly determine the ages of different stages.

The presence of abundant liquid-only fluid inclusions in all stages, but particularly in the hematite and breccia pipe stages, suggests these two stages were formed under low temperatures. Further analysis of these inclusions is required, including homogenization temperature measurements, assuming that vapour bubbles can be induced to nucleate.

References

Adshead, N. D., 1995, Alteration, geochemistry and paragenesis of the Osborne Cu-Au deposit,NW Queensland, PhD Thesis, James Cook University, Townsville

Adshead, N. D., Voulgaris, P., Muscio, V. N., 1998, Osborne copper-gold deposit. In: Geology of Australian and Papua New Guinean Mineral Deposits (Eds. D.A. Berkman, and D.H. Mackenzie), pp.793-799 (The Australasian Institute of Mining and Metallurgy, Melbourne).

Baker, T., 1998, Alteration, mineralization, and fluid evolution at the Eloise Cu-Au deposit, Cloncurry District, Northwest Queensland, Australia, Economic Geology, 93, 8, 1213-1236.

Bakker, R.J., 2001, FLUIDS: new software package to handle microthermometric data and to calculate isochores. XVI ECROFI European Current Research on Fluid Inclusions, Porto 2001, Abstracts (eds. F. Noronha, A. Doria, A. Guedes) Faculdade de Ciencias do Porto, Departamiento de Geologia, Memoria 7, 23-25.

Barton, M.D. and Johnson, D.A., 1997, A comparison of Fe-oxide (-Cu-Au-REE-U-Co-Ag) mineralization, Abstracts with Programs - Geological Society of America, 29(6), 51.

Barton, M.D. and Johnson, D. A., 1996, Evaporitic-source model for igneous- related Fe oxide – (REE-Cu-Au-U) mineralization, Geology, 24, 3, 259-262.

Bickford, M.E. 1988. Formation of continental crust: Part 1. Review of some principles; Part 2. An application to the Proterozoic evolution of southern North America. Geological Society of America Bulletin, 100, 9, 1375-1391.

Bodnar, R.J.,1994, Synthetic fluid inclusions; XII, The system H_2O-NaCl; experimental determination of the halite liquidus and isochores for a 40 wt% NaCl solution, Geochimica et Cosmochimica Acta, 58(3).1053-1063.

Bowers, T.S., Helgeson, H.C., 1983, Calculation of the thermodynamic and geochemical consequences of non-ideal mixing in the system H_2O-CO_2-NaCl on phase relations in geologic systems: equation of state for H_2O-CO_2-NaCl fluids at high pressures and temperatures. Geochimica Cosmochimica Acta 47:1247-1275.

Brown, P.E., 1989, FLINCOR; a microcomputer program for the reduction and investigation of fluid-inclusion data, American Mineralogist, 74(11-12), 1390-1393.

Brown, Philip E; Lamb, William M., 1989, P-V-T properties of fluids in the system H_2O + or – CO_2 + or - NaCl; new graphical presentations and implications for fluid inclusion studies, Geochimica et Cosmochimica Acta, 53(6), 1209-1221.

Buchan, K.L., Mertanen, S., Park, R.G., Pesonen, L.J., Elming, S.A., 2000, Comparing the drift of Laurentia and Baltica in the Proterozoic : the importance of key palaeomagnetic poles, Tectonophysics, 319:167-198.

Cao, R., Zhu, S., and Wang, J., 1995, Source of ore-forming substances and theoretical problems of metallogeny relevant to the Bayan Obo fe-REE ore deposits in Inner Mongolia, China. Science in China (Series B), 38, 8, 1003-1014.

Crawford, M L., 1981, Phase equilibria in aqueous fluid inclusions, In: Hollister, L.S., Crawford, M.L., (Eds.), Short Course in Fluid Inclusions: Applications to Petrology, Mineralogical Association of Canada, Short Course Handbook, 6, 75-100.

Day, W.C., Kisvarsanyi, E.B., Nuelle, L.M., Marikos, M.A. and Seeger, C.M. 1989a. New data on the origin of the Pea Ridge iron-apatite deposit, Southeast Missouri; implications for Olympic dam-type deposits. GSA Abstracts with Programs, St. Louis, Missouri, 1989, 21,6, A132.

Day, W.C., Sidder, G.B., Rye, R.O., Nuelle, L.M. and Kisvarsanyi, E.B. 1989b. The Middle Proterozoic rhyolite-hosted Pea Ridge iron and rare-earth-element deposit: a magmatic source for Olympic Dam-type deposits in the mid-continent region of the U.S.A, GSA Abstracts with Programs.21, 6, A132.

Day, W.C., Sidder, G.B., Rye, O., Nuelle, L.M., and Kisvarsanyi, E.B., 1991, The middle Proterozoic rhyolite-hosted Pea Ridge iron and rare earth element deposit: A magmatic source for Olympic Dam-type deposits in the mid-continent region of the U.S.A. In: Second hutton Symposium on Granites and Related Rocks (ed. B.W. Chappell). 409.

Emery, J.A. 1968. Geology of the Pea Ridge iron ore body. In Ore deposits of the United States, 1933-1967 (Graton-Sales Volume), V. 1, Am. Inst. Mining, Metall. and Petroleum Engineers, New York, 359-369, illus., 1968.

Einaudi, M.T. and Oreskes, N., 1990, Progress toward an occurrence model for Proterozoic iron oxide deposits; a comparison between the ore provinces of South Australia and Southeast Missouri. In: The Midcontinent of the United States; permissive terrane for an Olympic dam-type deposit? Pratt-Walden-P (editor); Sims-P-K (editor) U.S. G. S. Bulletin 1932. 58-69.

Fortowski, D.B. and McCracken, S.J.A., 1998, Mount Elliott copper-gold deposit, In: Geology of Australian and Papua New Guinean Mineral Deposits (Eds. D.A. Berkman, and D.H. Mackenzie), pp.775-782 (The Australasian Institute of Mining and Metallurgy, Melbourne).

Fridleifsson, Q. O. and Albertsson, A., 2000, Deep geothermal drilling on the Reykjanes Ridge opportunity for international collaboration. proceedings world geothermal congress 2000 Kyushu - Tohoku, Japan, May 28 - June 10, 2000. p. 3701-3706

Garret, S.J.M., 1992, The geology and geochemistry of the Mount Elliot copper gold deposit, Northwest Queensland, MSc thesis (unpublished), University of Tasmania, Hobart.

Gleason, J.D., Marikos, M. A., Barton, M.D., and Johnson, D.A., 2000, Neodymium isotopic study of rare element sources and mobility in hydrothermal Fe oxide (Fe-P-REE) systems, Geochimica et Cosmochimica Acta, 64,6,1059-1068.

Gow, P.A., Wall,V.J., Oliver, N.H.S.,and Valenta, R.K.,1994, Proterozoic iron oxide (Cu-U-Au-REE) deposits; further evidence of hydrothermal origins. Geology (Boulder).22, 7, 633-636.

Griffith, W.P., 1969, Raman spectroscopy of minerals. Nature, 224, 264-266.

Hagni, R.D. and Brandom, R.T., 1990, Mineral assemblages and paragenetic sequence of the iron-copper-cobalt ores at Boss-Bixby, Missouri and their mineralogical similarities to the ores at Olympic Dam, South Australia, In: 8th IAGOD symposium in conjunction with international conference on Mineral deposit modeling; program with abstracts. Boyle-R-W (chairperson) Proceedings of the Quadrennial IAGOD Symposium.8; Pages A195-A196.

Haas, J.L., Jr. and Robie, R.A., 1973, Thermodynamic data for wustite, Fe0.947O, magnetite, Fe_3O_4, and hematite, Fe_2O_3 [abs]: transactions of the American Geophysical Union, 54, 483.

Hauck, S.A., Hinze, W.J., Kendall, E.W., and Adams, S.S., 1989, A conceptual model of the Olympic Dam Cu-U-Au-REE-Fe deposit; a comparison of central North American and South Australian terranes, Abstracts with Programs - Geological Society of America, 21(6), A32-A33.

Hauck, S. A.,1990, Petrogenesis and tectonic setting of middle Proterozoic iron oxide-rich ore deposits; an ore deposit model for olympic dam-type mineralization. In: The Midcontinent of the United States; permissive terrane for aan olympic dam-type deposit? Pratt-Walden-P (editor); Sims-P-K (editor) SOURCE: U. S. Geological Survey Bulletin 1932. 4-39.

Haynes, F.M., 1985. Determination of fluid inclusion compositions by sequential freezing. Economic Geology, 80, 1436–1439.

Haynes, D. W., Cross, K.C., Bill, R. T., Reed, M. H., 1995, Olympic Dam ore genesis; a fluid mixing model. Economic Geology, 95, 281-307.

Hemley, J.J., Montoya, J.W., Marinenko, J.W., and Luce, R.W. 1980. Equilibria in the system Al_2O_3-SiO_2-H_2O and some general implications for alteration/mineralization processes. Economic Geology, 75, 210-228.

Hitzman, M.W., Oreskes, Naomi, and Einaudi, M.T., 1992, "Geological characteristics and tectonic setting of Proterozoic Fe-REE deposits," Precambrian Research, 58,241-287.

Holmgren D.C., 1985, Antecedentes para un modelo genetico del yacimiento El Soldado, V Region. Antecedents for the genetic model of the El Soldado Deposit, Region V, Actas - Congreso Geologico Chileno, vol.4, no.4, pp.3.626-3.650.

Husman, J.R., 1989, Gold, rare earth element, and other potential by-products of the Pea Ridge iron ore mine, Washington County, Missouri, Contribution to Precambrian Geology, Report: 21; OFR-89-78-MR, 18 pp.

Johnson, J.P. and McCulloch, M.T., 1995, Sources of mineralizing fluids for the Olympic Dam deposit (South Australia): Sm-Nd isotopic constraints, Chemical Geology, 121,177-199.

Kerr, I., D.,1998, Mineralogy, chemistry and hydrothermal evolution of the Pea Ridge Fe-oxide-REE deposit, Missouri, USA. 1998 Master's University of Windsor. Windsor, ON, Canada. 113p.

Kerr, I., D., Samson, I., M., 1998, REE mineralogy of the Pea Ridge Fe-REE deposit, Missouri. Abstracts with Programs - Geological Society of America. 30; 7, Pages 370.

Kisvarsanyi, E.B. 1990. General features of the St.Francois and Spavinaw granite- rhyolite terranes and the Precambrian metallogenic region of southeast Missouri. In The mid-continent of the United States- Permissive terrane for an Olympic Dam Type Deposit? Edited by W.P. Pratt and P.K. Sims. U.S. Geological Survey Bulletin 1932, 48-57.

Kisvarsanyi, E.B. and Kisvarsanyi, G. 1989a. Alkaline granite ring complexes and metallogeny in the middle Proterozoic St.Francois Terrane, southeastern Missouri, USA, in Mid-Proterozoic Laurentia-Baltica Edited by C.F. Gower, T.River , B. Ryan, Geological Association of Canada, Special Paper 38, 433-446.

Kisvarsanyi, E.B. and Kisvarsanyi, G. 1989b. Alkaline granite ring complexes and hotspot activity in the Middle Proterozoic St. Francois terrane, southeastern Missouri, USA Geological Association of Canada Special Paper 38, 14p.

Kisvarsanyi, E.B., Hebrank, A.W., and Ryan, R.F., 1981, Guidebook to the geology and ore deposits of the St. Francois Mountains, Missouri. Contribution to Precambrian Geology No. 9, Missouri Department of Natural Resources, Division of Geology and Land Survey.

Kisvarsanyi, E.B. and Proctor, P.D. 1967. Trace element content of magnetites and hematites, southeast Missouri iron metallogenic province, USA. Economic Geology, 62, 449-471.

Lindblom, S., Broman, C., Martinsson, O., 1996, Magmatic-hydrothermal fluids in the Pahtohavare Cu-Au deposit in greenstone at Kiruna, Sweden, Mineralium Deposita, 31(4), 307-318.

Marikos, M.A., Nuelle, L.M. and Seeger, C.M. 1990. Geologic Mapping and Evaluation of the Pea Ridge Iron Ore Mine (Washington County, Missouri) for Rare-Earth Element and Precious Metal Potential - A Progress Report. In The Mid-continent: Permissive Terrane for an Olympic Dam Type Deposit? Edited by W.P. Pratt and P.K. Sims. United States Geologic Survey Bulletin 1932, 77-81.

Marschik, R., Leveille, R.A., and Martin, W., 2000, La Candelaria and the Punta del Cobre district, Chile: Early Cretaceous iron oxide Cu-Au (Zn-Ag) mineralization, In: Porter,T. M., ed., Hydrothermal iron-oxide copper-gold & related deposits: A global perspectives: Adelaide, Australian Mineral Foundation, p. 163-175.

Marschik, R. and Fontbote, L., 1996, Copper (-iron) mineralization and superposition of alteration events in the Punta del Cobre Belt, northern Chile. Special Publication - Society of Economic Geologists, 5, 171-190.

Marschik, R. and Fontbote, L., 2001, The Candelaria-Punta del Cobre iron oxide Cu-Au(-Zn-Ag) deposits, Chile. Economic Geolog,96(8), 1799-1826.

Marschik, R., Singer, B.S., Munizaga, F., Tassinari, C., Moritz, R., and Fontbote, L., 1997, Age of Cu(-Fe)-Au mineralization and thermal evolution of the Punta del Cobre district, Chile, Mineralium Deposita, 32: 531-546.

Menuge, J.A., Seeger, C.M. and Brewer, T.S. 1997. Origin of the Pea Ridge Fe oxide-REE-Au ore deposit, S.E. Missouri. Geofluids II '97 extended abstracts. 194-196.

Nuelle, L.M., Day, W.C., Sidder, G.B., and Seeger, C.M. 1989a. Geology and mineral paragenesis of the Pea Ridge iron ore mine, Washington County, Missouri; origin of the rare-earth-element and gold-bearing breccia pipes. U.S Geological Survey Bulletin,1989, A1-A11.

Nuelle, L.M., Marikos, M.A., Seeger, C.M. and Day, W.C. 1989b. Hydrothermal aspects of amphibole and magnetite emplacement in the Pea Ridge Fe-REE deposit, Washington County, Missouri. GSA Abstracts with Programs, St. Louis, Missouri, 1989, 21,6,248.

Nuelle, L.M., Kisvarsanyi, E.B. and Seeger, C.M. 1991a. Structural setting and control of the Pea Ridge magnetite deposit, middle Proterozoic St. Francois terrane, Missouri. GSA abstracts with programs, San Diego, California, 23,5,A292.

Nuelle, L.M., Seeger, C.M., Day, W.C. and Sidder, G.B. 1991b. Rare earth element and gold bearing breccia pipes of the Pea Ridge iron ore mine, Washington County, Missouri. Society for mining metallurgy and exploration, Inc. Preprint no. 91-109, 14p.

Oakes, C.S., Bodnar, R.J., Simonson, J. M., 1990, The system $NaCl-CaCl_2-H_2O$; 1, The ice liquidus at 1 atm total pressure. Geochimica et Cosmochimica Acta,54,3, 603-610.

Oreskes, N. and Einaudi, M.T. 1990. Origin of rare earth element-enriched hematite breccias at the Olympic Dam Cu-U-Au-Ag Deposit, Roxby Downs, South Australia. Economic Geology, 85, 1-28.

Orekes, N. and Einaudi, M.T. 1992. Origin of hydrothermal fluids at Olympic Dam: Preliminary results from fluid inclusions and stable isotopes. Economic Geology, 87, 64-90.

Oreskes, N. and Hitzman, M.W. 1993. A model for the origin of Olympic Dam type deposits. In Mineral Modeling. Edited by R.V. Kirkham, W.D. Sinclair, R.I. Thorpe and J.M. Duke. Geological Association of Canada, special paper 40, 615-633.

Roberts, S.M., Spencer, R.J., 1995. Paleotemperatures preserved in fluid inclusions in halite. Geochim. Cosmochim. Acta 59, 3929–3942.

Perring, C.S., Pollard, P.J., Blake, K.L., Dong, G., Nunn, A.J., 1999, Metallogeny of the lighting Creek Cu-Au prospect, mount Isa Inlier, Australia. In: Stanley, c.J., Rankin, A.H., Bodnar, R.J. et al.(eds) Mineral deposits: process to processing, vol. 1. Balkema, Rotterdam, 413-416.

Perring, C.S., Polland, P.J., Dong, G., Nunn,A.J., and Blake, K.L., 2000, The lighting Creek Sill Complex, cloncurry District, Northwest Queensland : A source of fluids for Fe oxide Cu-Au mineralization and sodic-cacic alteration, Economic Geology, 95,5,1067-1090.

Pollard, P.J., Blake, K.L., Xu, G., 1997. Sodic -calcic alteration in the Cloncurry district, eastern Mount Isa Inlier, Australia: fluid inclusion and stable isotope constraints on fluid sources. In: Pollard, P.J. compiler , AMIRA p438 Cloncurry Base metals and Gold Annual Report 1997, section 6.

Pollard, P.J., 2001, Sodic (-calcic) alteration in Fe-oxide-Cu-Au district; an origin via unmixing of magmatic H_2O-CO_2 –NaCl ± $CaCl_2$ -KCl fluids, Mineralium Deposita, 36(1) 93-100.

Pratt, W. P. (editor) and Sims, P. K. (editor), 1990, The Midcontinent of the United States; permissive terrane for an Olympic dam-type deposit?. United States Geological Survey Bulletin 1932.

Rabbia, O.M., Frutos, J., Pop, N., Isache, C., Sanhueza, V., Edelstein, O., 1996, Caracteristicas isotopicas de la mineralizacion de Cu (-Fe) de Mina Carola, distrito minero Punta del Cobre, norte de Chile. Isotopic characterization of the copper (iron) mineralization at Carola Mine, Punta del Cobre mining district, northern Chile, Actas del Congreso Geologico Argentino, vol.13, Vol. III, pp.241-253.

Reeve, J.S., Cross, K. C., Smith, R.N., Oreskes, N., 1990, Olympic Dam copper-uranium-gold-silver deposit. In: Geology of the mineral deposits of Australia and Papua New Guinea; Volume 2. Hughes-F-E (editor) Monograph Series - Australasian Institute of Mining and Metallurgy. 14; Pages 1009-1035. 1990. Australasian Institute of Mining and Metallurgy. Melbourne, Victoria, Australia. 1990.

Robert, D.E. and Hudson, G.R.T., 1983, The Olympic Dam copper-uranium gold-silver deposit, Roxby Downs, South Australia. Economic Geology, 78,799-822.

Rotherham, J. F., Blake, K. L., Cartwright, I., Williams, P.J., 1998, Stable isotope evidence for the origin of the Mesoproterozoic Starra Au-Cu deposit, Cloncurry District, Northwest Queensland, Economic Geology, 93(8)1435-1449.

Samson, I. M., 1990, Fluid evolution and mineralization in a Subvolcanic Granite Stock: the Mount Pleasant W-Mo-Sn deposits, New Brunswick, Canada. Economic Geology, 85, 145-163.

Samson, I.M., Kerr, I.D. and Seeger, C., in prep., Genesis of the Pea Ridge Fe oxide-REE desposit, Missouri: Constraints from paragenesis and mineralogy.

Samson, I. M and Walker, R.T., 2000, Cryogenic Raman spectroscopic studies in the system $NaCl-CaCl_2-H_2O$ and implications for low-temperature phase behavior in aqueous fluid inclusions. The Canadian Mineralogist, 38, 1, 35-43.

Seeger, C M; Nuelle, L M; Day, W C; Sidder, G B; Marikos, M A; Smith, D C., 2001, Geologic maps and cross sections of mine levels at the Pea Ridge iron mine, Washington County, Missouri, http://greenwood.cr.usgs.gov/pub/mf-maps/mf-2353/ Miscellaneous Field Studies Map - U. S. Geological Survey, Report: MF-2353, 6 pp., 5 sheets, 2001.

Seeger, C.M., Nuelle, L. M., Marikos, M. A.,1989, Massive silicification and late stage quartz veining in the Pea Ridge Fe-REE deposit, Southeast Missouri. In: Geological Society of America, 1989 annual meeting. Dymek-Robert-F (chairperson); Shelton-Kevin-L (chairperson) Abstracts with Programs - Geological Society of America. 21; 6, A34.

Shade, J.W. 1974. Hydrolysis reactions in the SiO_2-excess portion of the system $K_2O-Al_2O_3-SiO_2-H_2O$ in chloride fluids at magmatic conditions. Economic Geology,69 : 218-228.

Sidder, G.B., Day, W.C., Nuelle, L.M., Seeger, C.M., and Kisvarsanyi, E.B. 1993a. Mineralogic and fluid-inclusion studies of the Pea Ridge iron-rare-earth-element deposit, Southeast Missouri. U.-S.-Geological-Survey-Bulletin 2039, 205-216.

Sidder-G-B; Day-W-C; Rye-R-O, 1993b, Fluid inclusion and stable isotope data for the Pea Ridge Fe-REE orebody, Missouri. In: Geological Society of America, North-Central Section, 27th annual meeting. Abstracts with Programs - Geological Society of America. 25; 3, Pages 81. 1993.

Sidder, G.B., Nuelle, L.M., Day, W.C., Rye, R.O., Seeger, C.M., and Kisvarsanyi, E.B. 1991. Paragenesis and conditions of formation of the Pea Ridge iron and rare earth element deposit, Missouri. GSA abstracts with programs, San Diego, California, 23,5, A292.

Sims, P.K., Kisvarsanyi, E.B., and Morey, G.B. 1987. Geology and metallogeny of Archean and Proterozoic basement terranes in the northern Midcontinent, U.S.A.-an overview. U.S G. S. Bulletin 1815, 51p.

Smith, M.P. and Henderson, P., 2000, Preliminary fluid inclusion constraint on fluid evolution in the Bayan Obo Fe-REE-Nb deposit, Inner Mongolia, China. Economic Geology, 95, 1371-1388.

Sterner, H.D.L., Michael, S., Bodnar, R.J., 1988, Freezing point depression of NaCl-KCl-H_2O solutions. Economic Geology, 83, 97-202.

Turner, F.J., 1981, Metamorphic petrology : mineralogical, field, and tectonic aspects. Hemisphere Pub. Corp.; New York, 1981

Ullrich, T.D. and Clark, A.H., 1999, The Candelaria copper-gold deposit, Region III, Chile: Paragenesis, geochronology and fluid composition, In: Stanley, c.J., Rankin, A.H., Bodnar, R.J. et al.(eds) Mineral deposits: process to processing, vol. 1. Balkema, Rotterdam, 201-204.

Wenner, D.B. and Taylor, H.P., Jr. 1976. Oxygen and hydrogen isotope studies of a Precambrian granite-rhyolite terrane, St. Francois Mountains, southeastern Missouri. Geological Society of America Bulletin 61107. v.87, pp.1587-1598.

Williams, P.J., Dong, G., Pollard, P.J., and Perring, C.S., 1999, Fluid inclusion geochemistry of Cloncurry (Fe)-Cu-Au deposit, In: Stanley, c.J., Rankin, A.H., Bodnar, R.J. et al.(eds) Mineral deposits: process to processing, vol. 1. Balkema, Rotterdam, 111-114.

Wilson, N., Cline, J., and Amelin, Y., 2002, low temperature fluid inclusion microthermometry and age constraints for secondary mineral formation at Yucca Mountain, Nevada. In:Program with Abstract, Eighth Binebbial Pan-American Conference on Research on Fluid inclusions, D.J. Kontak and A.J. Anderson (eds.),July 22-25, 2002, Halifax, Nova Scotia, Canada

Xu, G., 2000, Fluid inclusions with NaCl-CaCl2-H2O composition from the Cloncurry hydrothermal system, NW Queensland, Australia. Lithos, 53, 21-35.

Appendix I

Sample locations and types

Sample	Level /Drill	Type
PR01-01	2275	quartz vein
PR01-02	2275	magnetite ore
PR01-03	2275	quartz in magnetite ore
PR01-04	2275	quartz in magnetite ore
PR01-05	2275	sulfide vein in magnetite ore
PR01-06	2275	altered host rock in magnetite ore
PR01-07	2275	Quartz & Calcite vein in magnetite ore
PR01-08	2370	massive actinolite with apatite & Quartz
PR01-09A	2370	quartz-hematite vein cutting silicified rhyolite
PR01-09B	2370	quartz-hematite vein cutting silicified rhyolite
PR01-10	2370	massive actinolite
PR01-11	2440	barite vein in breccia pipe
PR01-12	2440	breccia
PR01-13A	2440	silicified zone
PR01-13B	2440	silicified and hematite altered rock
PR01-13C	2440	hematite
PR01-14	954-8	magnetite and amphibole
PR01-15	954-8	magnetite and amphibole
PR01-16	954-8	magnetite ore
PR01-17	954-8	magnetite ore
PR01-18	954-8	magnetite ore
PR01-19	954-8	magnetite in amphibole
PR01-20	954-8	amphibole and rhyolite transition
PR01-21	954-8	amphibole
PR01-22	954-9	magnetite
PR01-23	954-9	magnetite
PR01-24	954-9	magnetite and amphibole transition
PR01-25	954-9	amphibole and rhyolite transition
PR01-26	954-9	magnetite and apatite
PR01-27	954-9	magnetite and rhyolite
PR01-28	954-9	magnetite and apatite ore
PR01-29	954-9	amphibole and rhyolite
PR01-30	954-9	magnetite and amphibole
PR01-31	954-9	amphibole andapatite
PR01-32	954-14	magnetite and apatite
PR01-33	954-14	magnetite and apatite
PR01-34	954-14	magnetite
PR01-35A	961-11	magnetite and apatite

Sample	Level /Drill	Type
PR01-35B	961-11	magnetite and apatite
PR01-36	961-11	magnetite and apatite
PR01-37A	961-11	magnetite and apatite
PR01-37B	961-11	magnetite and apatite
PR01-38	961-11	magnetite and amphibole
PR01-39	961-11	amphibole and magnetite
PR01-40	961-11	magnetite and apatite
PR01-41	961-11	magnetite and amphibole
PR01-42	962-26	magnetite
PR01-43	962-26	magnetite and rhyolite
PR01-44	962-26	magnetite and amphibole
PR01-45	962-26	magnetite and amphibole
PR01-46	962-26	magnetite and amphibole
PR01-47	962-26	magnetite and amphibole
PR01-48	962-26	massive magnetite
PR01-49	964-5	apatite and magnetite and amphibole
PR01-50	964-5	apatite and amphibole
PR01-51	964-5	amphibole and magnetite
PR01-52	964-5	amphibole and magnetite
PR01-53	964-5	magnetite and amphibole
PR01-54	964-5	amphibole,magnetie & apatite
PR01-55	964-5	magnetite and amphibole
PR01-56A	964-5	magnetite , amphibole and apatite
PR01-56B	964-5	magnetite , amphibole and apatite
PR01-56C	964-5	magnetite , amphibole and apatite
PR01-57	2475 DH8	breccia and rhyolite
PR01-58	2475 DH8	breccias
PR01-59	2475 DH8	silicified rhyolite
PR01-60	2475 DH8	rhyolite
PR01-61	2475 DH8	rhyolite replaced by amphibole
PR01-62	2475 DH8	amphibole
PR01-63	2475 DH8	amphibole(+magnetite+ hematite)
PR01-64	2475 DH8	hematite
PR01-65	2475 DH8	hematite in silicified rhyolite
PR01-66	2475 DH8	hematite vein in silicified rhyolite
PR01-67	2475 DH8	hematite
PR01-68	2475 DH8	hematite
PR01-69	2475 DH8	hematite

Sample #	Level/ Drill	Type
PR01-70	2475 DH8	Hematite
PR01-71	2475 DH8	Hematite
PR01-72	2475 DH8	Hematite
PR01-73	2475 DH12	carbonate vein
PR01-74	2475 DH12	amphibole and apatite
PR01-75	2475 DH12	Hematite and amphibole and rhyolite
PR01-76	2475 DH12	amphibole and rhyolite
PR01-77	2475 DH12	rhyolite and amphibole
PR01-78	2475 DH12	Rhyolite
PR01-79	2475 DH12	Barite
PR01-80	2475 DH12	Barite
PR01-81	2475 DH9	altered rhyolite
PR94-1	2275	Breccia pipe
PR94-2	2275	Hematite zone
PR94-3	2275	Magnetite zone
PR94-4	2370	Amphibole zone
PR94-6	2370	Quartz vein
PR94-7	2370	Pseudobreccia
PR94-8	2440	Breccia pipe
PR94-9	2440	Breccia pipe
PR95-01	2275	Porphyry
PR95-02	2275	Breccia pipe
PR95-03	2275	Breccia pipe
PR95-04	2275	Breccia pipe
PR95-05	2275	Hematite zone
PR95-06	2275	Hematite zone
PR95-07	2275	Hem/Mag zone
PR95-08	2275	Magnetite zone
PR95-09	2275	Hematite zone
PR95-10	2275	Amphibole zone
PR95-11	2275	Amphibole zone
PR95-12	2275	Magnetite zone
PR95-13	2275	Magnetite zone
PR95-14	2275	Heterolithic breccia
PR95-15	2275	Breccia pipe
PR95-16	2275	Breccia pipe
PR95-17	2275	Aplite dike
PR95-18	2275	Porphyry
PR95-19	2275	altered porphyry
PR95-20	2275	Porphyry
PR95-21	2275	Pseudobreccia
PR95-22	2275	Qtz vein
PR95-23	2275	Silicified pseudobreccia?
PR95-24	2275	Silicified zone

Sample #	Level/ Drill#	Type
PR95-25	2370	Amphibole zone
PR95-26	2370	Breccia pipe
PR95-27	2370	Quartz vein
PR95-28	2370	Silicified zone
PR95-29	2370	Silicified zone
PR95-30	2370	Breccia pipe
PR95-31	2370	Quartz vein
PR95-32	2370	Magnetite zone
PR95-33	2370	Pseudobreccia
PR95-34	2370	Pseudobreccia
PR95-35	2370	Breccia pipe
PR95-36	2370	Quartz vein
PR95-37	2370	Silicified zone
PR95-38	2370	Silicified zone
PR95-39	2370	Quartz vein
PR95-40	2440	Breccia pipe
PR95-41	2440	Breccia pipe
PR95-42	2440	Breccia pipe
PR95-43	2440	Qtz vein
PR95-44	2440	Qtz vein
PR95-45a	2440	Qtz vein
PR95-45b	2440	Qtz vein
PR95-45c	2440	Qtz vein
PR95-46	2440	Breccia pipe
PR95-47	2440	Breccia pipe
PR95-48	2440	Breccia pipe
PR95-49	2440	Breccia pipe
PR95-50	2440	Breccia pipe
PR95-51	2440	Silicified zone
PR95-52	2505	Silicified zone
PR95-53	2505	Pseudobreccia
PR95-54	2505	Breccia pipe
PR95-55	2675	Breccia pipe
PR95-56	2675	Hem. breccia
PR95-57	2675	Silicified zone
PR95-58	2675	Mafic dike
PR95-59	2675	Silicified zone
PR95-60	2675	altered porphyry
PR95-61	2675	altered porphyry
PR95-62	2675	altered porphyry
PR95-63	2675	altered porphyry
PR95-64	2675	Silicified zone

Appendix II

Primary LV fluid inclusion microthermetry results

Sample #	Inclu-sion #	Stage	Mineral	Origin	Type	Tn	Te	Tm ICE	Th (L-V)	Salinity $NaCl + CaCl_2$(wt%)	Salinity Used (wt%)	Density at Th (g/cm^3)
PR01-56A	1-3-4	amphibole	apatite	primary	lv			-27.5	159.4	24.6	24.6	1.1
PR01-56A	1-3-5	amphibole	apatite	primary	lv				153.4			
PR01-56A	1-3-10	amphibole	apatite	primary	lv				205.1			
PR01-56A	1-3-12	amphibole	apatite	primary	lv				154.8			
PR01-56A	1-3-15	amphibole	apatite	primary	lv				174.2			
PR01-56A	1-3-16	amphibole	apatite	primary	lv				154.8			
PR01-56A	1-3-17	amphibole	apatite	primary	lv				152.1			
PR01-56A	1-3-18	amphibole	apatite	primary	lv				168.6			
PR01-56B	chip1	amphibole	apatite	primary	lv			-22.1		22.4	22.4	1.3
PR01-56B	chip1	amphibole	apatite	primary	lv			-21.2		22.0	22.0	1.3
PR01-56B	chip1	amphibole	apatite	primary	lv			-19.3		21.0	21.0	1.2
PR01-56B	chip1	amphibole	apatite	primary	lv			-16.5		19.4	19.4	1.2
PR01-56B	chip1	amphibole	apatite	primary	lv				142.8			
PR01-56B	chip1	amphibole	apatite	primary	lv				146.8			
PR01-56B	chip1	amphibole	apatite	primary	lv				148.7			
PR95-12	8-1-1	magnetite	apatite	primary	lv	-70.9	-34.9	-16.2	130.3	19.2	19.2	1.1
PR95-12	8-1-2	magnetite	apatite	primary	lv	-65.1	-35.9	-15.1	133.0	18.5	18.5	1.1
PR01-33	chip1	magnetite	apatite	primary	lv	-59.0	-40.0	-11.1	134.7	15.2	15.2	1.0
PR01-33	chip1	magnetite	apatite	primary	lv	-62.0	-39.0	-12.5	132.6	16.5	16.5	1.0
PR01-33	chip1	magnetite	apatite	primary	lv	-58.0		-10.7	133.1	14.8	14.8	1.0
PR01-33	chip1	magnetite	apatite	primary	lv			-8.9	151.4	13.0	13.0	1.0
PR01-33	chip1	magnetite	apatite	primary	lv			-11.9		15.9	15.9	1.1
PR01-33	chip1	magnetite	apatite	primary	lv	-52.0			117.5			
PR01-33	chip1	magnetite	apatite	primary	lv			-8.2	156.1	12.3	12.3	1.0
PR01-33	chip1	magnetite	apatite	primary	lv				146.4			
PR01-33	chip1	magnetite	apatite	primary	lv				160.3			
PR01-33	chip1	magnetite	apatite	primary	lv				159.1			

Sample #	Inclu-sion #	Stage	Mineral	Origin	Type	Tn	Te	Tm ICE	Th (L-V)	Salinity NaCl + $CaCl_2$(wt%)	Salinity Used (wt%)	Density at Th (g/cm^3)
PR01-33	chip1	magnetite	apatite	primary	lv				150.2			
PR01-33	chip1	magnetite	apatite	primary	lv				146.4			
PR01-33	chip1	magnetite	apatite	primary	lv				146.4			
PR01-33	chip1	magnetite	apatite	primary	lv				155.7			
PR01-33	chip1	magnetite	apatite	primary	lv				156.7			
PR01-69	5-1	hematite	quartz	primary	lv		-54.0					
PR01-69	5-2	hematite	quartz	primary	lv			-12.1	217.6	16.1	16.1	1.0
PR01-69	5-6	hematite	quartz	primary	lv				229.4			
PR01-69	5-13	hematite	quartz	primary	lv		-55.0	-10.1		14.3	14.3	1.1
PR01-69	5-15	hematite	quartz	primary	lv		-58.0	-16.5		19.4	19.4	1.2
PR01-69	5-16	hematite	quartz	primary	lv	-74.0	-52.0	-23.7	207.8	23.1	23.1	1.0
PR01-69	6-1	hematite	barite	primary	lv	-79.0	-53.0	-23.0	305.9	22.8	22.8	0.9
PR01-69	6-2	hematite	barite	primary	lv	-80.0	-57.0	-18.8		20.8	20.8	1.2
PR01-69	6-3	hematite	barite	primary	lv			-16.2	294.8	19.2	19.2	0.9
PR01-69	6-4	hematite	barite	primary	lv				315.6			
PR01-69	6-5	hematite	barite	primary	lv		-56.0	-24.4	337.9	23.4	23.4	0.9
PR01-69	6-6	hematite	barite	primary	lv		-56.0	-18.9	311.8	20.8	20.8	0.9
PR01-69	6-7	hematite	quartz	primary	lv			-19.9	298.4	21.4	21.4	0.9
PR01-69	6-8	hematite	quartz	primary	lv			-21.7	272.8	22.2	22.2	1.0
PR01-69	6-9	hematite	quartz	primary	lv	-78.0	-49.0	-21.7	305.3	22.2	22.2	0.9
PR01-69	6-10	hematite	quartz	primary	lv	-78.0	-49.0	-12.8	276.7	16.7	16.7	0.9
PR01-69	6-11	hematite	quartz	primary	lv		-37.0	-16.5	297.7	19.4	19.4	0.9
PR01-69	6-12	hematite	quartz	primary	lv		-55.0	-16.5	302.8	19.4	19.4	0.9
PR01-69	7-1-1	hematite	quartz	primary	lv	-70.0	-65.0	-19.7	96.1	21.3	21.3	1.1
PR01-69	7-1-2	hematite	quartz	primary	lv	-40.0	-67.0					
PR01-69	7-1-3	hematite	quartz	primary	lv	-50.0	-37.0	-22.0		22.4	22.4	1.3
PR01-69	7-1-5	hematite	quartz	primary	lv	-66.0	-33.0	-16.1		19.1	19.1	1.2
PR01-69	3-1-1	hematite	quartz	primary	lv			-22.2	97.3	22.5	22.5	1.1
PR01-69	3-1-2	hematite	quartz	primary	lv			-22.8	109.7	22.7	22.7	1.1
PR01-69	3-1-4	hematite	quartz	primary	lv	-50.0		-23.2	88.4	22.9	22.9	1.2

Sample #	Inclu-sion #	Stage	Mineral	Origin	Type	Tn	Te	Tm ICE	Th (L-V)	Salinity $NaCl + CaCl_2$(wt%)	Salinity Used (wt%)	Density at Th (g/cm^3)
PR01-69	8-1	hematite	quartz	primary	lv	-43.0	-55.0	-2.9	155.6	5.1	5.1	0.9
PR01-69	9-1	hematite	quartz	primary	lv	-68.3	-50.0	-20.8	91.6	21.8	21.8	1.1
PR01-69	9-2	hematite	quartz	primary	lv	-69.0	-50.0	-21.4	85.3	22.1	22.1	1.1
PR01-69	9-3	hematite	quartz	primary	lv	-65.0	-50.0	-22.8	90.0	22.7	22.7	1.2
PR01-69	9-5	hematite	quartz	primary	lv	-85.0		-18.9	183.4	20.8	20.8	1.0
PR95-54	1-1-1	breccia	barite	primary	lv	-68.0		-17.0	346.3	19.7	19.7	0.9
PR95-54	1-1-2	breccia	barite	primary	lv			-15.9	224.1	19.0	19.0	1.0
PR95-54	1-2-1	breccia	barite	primary	lv			-12.7	230.1	16.6	16.6	1.0
PR95-54	1-2-2	breccia	barite	primary	lv	-61.2		-11.9	316.6	15.9	15.9	0.9
PR95-54	1-2-3	breccia	barite	primary	lv	-69.9		-12.0	178.6	16.0	16.0	1.0
PR95-54	1-2-4	breccia	barite	primary	lv	-48.5	-33.9	-11.9	199.4	15.9	15.9	1.0
PR95-54	1-2-5	breccia	barite	primary	lv			-16.5	231.8	19.4	19.4	1.0
PR95-54	1-2-6	breccia	barite	primary	lv	-75.8		-10.7	222.8	14.9	14.9	1.0
PR95-35	1-1-1	breccia	quartz	primary	lv			-0.8	311.9	1.6	1.6	0.7
PR95-35	1-1-2	breccia	quartz	primary	lv	-32.9		-1.6	338.2	2.9	2.9	0.6
PR95-35	1-1-3	breccia	quartz	primary	lv			-0.7	322.6	1.4	1.4	0.7
PR95-35	1-1-4	breccia	quartz	primary	lv			-0.7	370.8	1.4	1.4	0.5
PR95-35	2-1-1	breccia	quartz	primary	lv			-0.1	377.6	0.3	0.3	0.5
PR95-35	2-2-1	breccia	quartz	primary	lv			-5.4	127.4	8.8	8.8	1.0
PR95-35	2-3-1	breccia	quartz	primary	lv			-0.7	317.3	1.4	1.4	0.7
PR95-35	2-3-2	breccia	quartz	primary	lv	-32.0		-0.6	384.4	1.2	1.2	0.5
PR95-35	2-3-3	breccia	quartz	primary	lv			-0.2	343.3	0.5	0.5	0.6
PR95-35	2-4-1	breccia	quartz	primary	lv			-0.1	242.6	0.3	0.3	0.8
PR95-35	2-4-2	breccia	quartz	primary	lv			0.0	326.7	0.1	0.1	0.6
PR95-35	2-4-3	breccia	quartz	primary	lv			0.0	334.9	0.1	0.1	0.6
PR95-35	2-5-1	breccia	quartz	primary	lv			-0.1	125.7	0.3	0.3	0.9
PR95-35	2-6-1	breccia	quartz	primary	lv				200.4			
PR95-35	2-7-1	breccia	quartz	primary	lv	-34.9		-0.1	210.0	0.3	0.3	0.9
PR95-35	2-7-2	breccia	quartz	primary	lv			-0.1	212.3	0.3	0.3	0.9
PR95-35	2-7-3	breccia	quartz	primary	lv			-0.2	270.9	0.5	0.5	0.8

Sample #	Inclu-sion #	Stage	Mineral	Origin	Type	Tn	Te	Tm ICE	Th (L-V)	Salinity NaCl + $CaCl_2$(wt%)	Salinity Used (wt%)	Density at Th (g/cm^3)
PR95-35	2-7-4	breccia	quartz	primary	lv			-0.2	278.0	0.5	0.5	0.7
PR95-35	3-1-1	breccia	quartz	primary	lv			-0.1	206.5	0.3	0.3	0.9
PR95-35	3-1-2	breccia	quartz	primary	lv			-0.1	383.0	0.3	0.3	0.5
PR95-35	3-2-1	breccia	quartz	primary	lv			-0.1	312.8	0.3	0.3	0.7
PR95-35	3-3-1	breccia	quartz	primary	lv			-0.1	380.0	0.3	0.3	0.5
PR95-35	3-4-1	breccia	quartz	primary	lv	-26.1		-8.5	312.7	12.6	12.6	0.8
PR95-35	3-4-2	breccia	quartz	primary	lv			-7.4	304.7	11.4	11.4	0.8
PR95-35	4-1-1	breccia	quartz	primary	lv	-29.0			324.3			
PR95-35	4-2-1	breccia	quartz	primary	lv	-69.0		-19.8	241.3	21.3	21.3	1.0
PR95-35	5-1	breccia	quartz	primary	lv	-38.8		-0.1	217.9	0.3	0.3	0.8
PR95-35	5-4	breccia	quartz	primary	lv	-31.0		-0.2	306.8	0.5	0.5	0.7
PR95-35	5-3	breccia	quartz	primary	lv	-65.1	-43.6	-21.2		22.0	22.0	1.3
PR95-35	5-5	breccia	quartz	primary	lv			0.0	308.4	0.1	0.1	0.7
PR95-35	5-6	breccia	quartz	primary	lv				219.3			
PR95-35	5-7	breccia	quartz	primary	lv	-40.7	-30.0	-0.1	230.0	0.3	0.3	0.8
PR95-35	5-8	breccia	quartz	primary	lv				262.4			
PR95-35	5-9	breccia	quartz	primary	lv	-69.0	-48.5	-20.8		21.8	21.8	1.3
PR95-35	5-12	breccia	quartz	primary	lv				316.2			
PR95-35	5-13	breccia	quartz	primary	lv			-0.1	235.2	0.3	0.3	0.8
PR95-35	5-14	breccia	quartz	primary	lv				215.5			
PR95-35	5-11	breccia	quartz	primary	lv	-65.1	-46.6	-15.2	339.2	18.5	18.5	0.9

Appendix III

Primary LVH(S) fluid inclusion microthermometry results

Sample #	Incl #	Zone	Mineral	Origin	Type	Tn	Te	Tm ICE	Th (L-V)	Tm NaCl	Salinity (N)	salinity used	mol NaCl	d at Th
PR95-31	6-1-1	quartz vein	quartz	primary	lvh					247.0	34.5	34.5	9.0	
PR95-31	6-1-3	quartz vein	quartz	primary	lvh					245.1	34.4	34.4	9.0	
PR95-31	6-1-2	quartz vein	quartz	primary	lvh					276.2	36.4	36.4	9.8	
PR95-31	6-1-4	quartz vein	quartz	primary	lvh					259.2	35.3	35.3	9.3	
PR95-31	7-1-11	quartz vein	quartz	primary	lvh					284.8	37.0	37.0	10.1	
PR95-31	7-1-12	quartz vein	quartz	primary	lvh					314.1	39.3	39.3	11.1	
PR95-31	7-1-13	quartz vein	quartz	primary	lvh				193.5	334.8	41.0	41.0	11.9	1.5
PR95-31	7-1-14	quartz vein	quartz	primary	lvh					333.5	40.9	40.9	11.8	
PR95-31	7-1-15	quartz vein	quartz	primary	lvh					277.9	36.5	36.5	9.8	
PR95-31	7-1-16	quartz vein	quartz	primary	lvh				192.1	322.5	40.0	40.0	11.4	1.4
PR95-31	7-1-17	quartz vein	quartz	primary	lvh					273.3	36.2	36.2	9.7	
PR95-31	7-1-18	quartz vein	quartz	primary	lvh					325.1	40.2	40.2	11.5	
PR95-31	7-1-19	quartz vein	quartz	primary	lvh					282.1	36.8	36.8	10.0	
PR95-31	7-1-20	quartz vein	quartz	primary	lvh				183.5	262.3	35.5	35.5	9.4	1.3
PR95-31	7-1-21	quartz vein	quartz	primary	lvh					276.1	36.4	36.4	9.8	
PR95-31	7-1-22	quartz vein	quartz	primary	lvh					313.0	39.2	39.2	11.0	
PR95-31	8-1-8	quartz vein	quartz	primary	lvh	-85	-45		232.1	364.6	43.8	43.8		0.8
PR95-31	8-1-1	quartz vein	quartz	primary	lvhs	-81	-28	-28.0	231.5	247.2	34.5	34.5		0.8
PR95-31	8-1-2	quartz vein	quartz	primary	lvhs	-67	-47	-47.0	196.0	258.2	35.2	35.2		0.9
PR95-31	8-1-3	quartz vein	quartz	primary	lvhs		-50							
PR95-31	8-1-4	quartz vein	quartz	primary	lvhs		-50							
PR95-31	8-1-5	quartz vein	quartz	primary	lvhs	-80	-46							
PR95-31	8-1-6	quartz vein	quartz	primary	lvhs	-82	-57		237.6	255.1	35.0	35.0		0.8
PR95-31	8-1-7	quartz vein	quartz	primary	lvhs	-77	-56		173.5	305.0	38.6	38.6		0.9
PR95-28	6-1-1	silicified	quartz	primary	lvh					422.0	49.9	49.9	17.1	5.2
PR95-28	6-1-4	silicified	quartz	primary	lvh					383.4	45.7	45.7	14.4	3.7
PR95-28	6-1-7	silicified	quartz	primary	lvh					344.6	41.9	41.9	12.3	2.9
PR95-28	6-1	silicified	quartz	primary	lvh					419.6	49.6	49.6	16.9	5.0
PR95-28	6-1	silicified	quartz	primary	lvh					375.3	44.9	44.9	13.9	3.5

Sample #	Incl #	Zone	Mineral	Origin	Type	Tn	Te	Tm ICE	Th (L-V)	Tm NaCl	Salinity (N)	salinity used	mol NaCl	d at Th
PR95-28	6-1	silicified	quartz	primary	lvh					355.1	42.9	42.9	12.8	3.1
PR95-28	6-1	silicified	quartz	primary	lvh					358.4	43.2	43.2	13.0	3.2
PR95-28	6-1	silicified	quartz	primary	lvh									
PR95-57	6-1-1	silicified	quartz	primary	lvhs	-60	-30		150.3					
PR95-57	6-1-2	silicified	quartz	primary	lvhs	-60			171.3	265.0	35.7	35.7	9.5	1.3
PR95-57	6-1-3	silicified	quartz	primary	lvhs	-58	-58		169.7	353.2	42.7	42.7	12.8	1.7
PR95-57	7-1-1	silicified	quartz	primary	lvhs	-74	-40							
PR95-57	7-1-2	silicified	quartz	primary	lvhs	-78	-30							
PR95-57	7-1-3	silicified	quartz	primary	lvhs		-36							

Appendix IV

Secondary fluid inclusion microthermometry results

Sample #	Incl #	Zone	Host Mineral	Type	Tn	Te	Tm ICE	Th (L-V)	Tm Hh	Salinity NaCl + CaCl2	salinity Hh melting	salinity used	mol NaCl	Density at Th
PR95-11	1-1-1	amphibole	quartz	lv			-9.7			13.8		13.8	2.7	
PR95-11	1-1-2	amphibole	quartz	lv	-46.6		-2.0			3.6		3.6	0.6	
PR95-11	1-1-3	amphibole	quartz	lv	-48.5		-4.9			8.1		8.1	1.5	
PR95-11	1-3-1	amphibole	quartz	lv	-44.6	-19.3	-4.7			7.8		7.8	1.5	
PR95-11	1-3-2	amphibole	quartz	lv	-43.6		-3.6			6.3		6.3	1.1	
PR95-11	1-3-3	amphibole	quartz	lv	-45.6		-2.4			4.3		4.3	0.8	
PR95-11	1-3-4	amphibole	quartz	lv	-56.3		-12.1			16.1		16.1	3.3	
PR95-11	1-3-5	amphibole	quartz	lv	-55.3		-10.4			14.6		14.6	2.9	
PR95-11	2-1-1	amphibole	quartz	lv	-55.3	-41.2	-21.1	166.5		21.9		21.9	4.8	1.1
PR95-11	2-1-2	amphibole	quartz	lv		-23.2	-20.3	184.3		21.5		21.5	4.7	1.0
PR95-11	2-1-3	amphibole	quartz	lv	-67.0	-26.1	-20.0	197.9		21.4		21.4	4.7	1.0
PR95-11	2-1-4	amphibole	quartz	lv	-60.8	-24.2	-11.6	153.5		15.7		15.7	3.2	1.0
PR95-25	1-1-1	amphibole	quartz	lv			-8.9			13.0		13.0	2.6	
PR95-25	1-1-2	amphibole	quartz	lv	-49.5		-10.6			14.8		14.8	3.0	
PR95-25	1-1-3	amphibole	quartz	lv			-10.0			14.2		14.2	2.8	
PR95-25	1-1-4	amphibole	quartz	lv			-7.4			11.4		11.4	2.2	
PR95-25	1-2-1	amphibole	quartz	lv			-17.4			19.9		19.9	4.3	
PR95-25	1-3-1	amphibole	quartz	lv	-42.7		-2.4			4.3		4.3	0.8	
PR95-25	1-3-2	amphibole	quartz	lv			-2.0	175.5		3.6		3.6	0.6	0.9
PR95-25	1-3-3	amphibole	quartz	lv			-1.6			2.9		2.9	0.5	
PR95-25	1-4-1	amphibole	quartz	lv			-0.5	295.7		1.0		1.0	0.2	0.7
PR95-25	1-4-2	amphibole	quartz	lv			-0.5	289.9		1.0		1.0	0.2	0.7
PR95-25	1-4-3	amphibole	quartz	lv			-0.4	300.0		0.8		0.8	0.1	0.7
PR95-25	1-4-4	amphibole	quartz	lv			-0.5	301.2		1.0		1.0	0.2	0.7
PR95-25	2-1-1	amphibole	quartz	lv	-56.3		-6.6	201.8		10.4		10.4	2.0	0.9
PR95-25	2-1-2	amphibole	quartz	lv			-3.8	291.3		6.6		6.6	1.2	0.8
PR95-25	2-1-3	amphibole	quartz	lv			-1.2	182.3		2.3		2.3	0.4	0.9
PR95-25	2-1-4	amphibole	quartz	lv	-38.8	-26.1	-4.7	218.4		7.8		7.8	1.5	0.9

Sample #	Incl #	Zone	Host Mineral	Type	Tn	Te	Tm ICE	Th (L-V)	Tm Hh	Salinity NaCl + CaCl2	salinity Hh melting	salinity used	mol NaCl	Density at Th
PR95-25	2-1-5	amphibole	quartz	lv	-60.2		-19.3	257.8		21.0		21.0	4.6	1.0
PR95-25	2-1-6	amphibole	quartz	lv	-55.3		-24.6	183.1		23.5		23.5	5.3	1.1
PR95-25	2-1-7	amphibole	quartz	lv	-69.9	-33.9	-22.6	192.7		22.7		22.7	5.0	1.0
PR95-25	2-1-8	amphibole	quartz	lv		-57.3	-25.7	188.1		23.9		23.9	5.4	1.1
PR95-25	2-1-9	amphibole	quartz	lv	-56.3		-25.7	210.4		23.9		23.9	5.4	1.0
PR95-25	2-2-1	amphibole	quartz	lv	-57.3		-15.8	220.7		18.9		18.9	4.0	1.0
PR95-25	2-2-2	amphibole	quartz	lv	-50.5	-24.2								
PR95-25	2-2-3	amphibole	quartz	lv	-66.1		-16.0	215.2		19.1		19.1	4.0	1.0
PR95-25	2-2-4	amphibole	quartz	lv			-16.0	179.4		19.1		19.1	4.0	1.0
PR95-25	2-2-5	amphibole	quartz	lv			-16.7	215.2		19.5		19.5	4.1	1.0
PR95-25	2-3-1	amphibole	quartz	lv	-59.2	-38.8	-13.6	261.4		17.3		17.3	3.6	0.9
PR95-25	2-3-2	amphibole	quartz	lv	-61.2		-14.3	181.7		17.9		17.9	3.7	1.0
PR95-25	2-3-3	amphibole	quartz	lv	-69.9	-39.8	-14.1	190.2		17.8		17.8	3.7	1.0
PR95-25	2-4-1	amphibole	quartz	lv	-56.3	-38.8	-13.6			17.4		17.4	3.6	
PR95-25	6-1-2	amphibole	quartz	lv	-79.7	-51.4	-21.0	176.6		21.9		21.9	4.8	1.0
PR95-25	6-1-3	amphibole	quartz	lv	-79.7	-58.3	-22.2	287.2		22.5		22.5	5.0	0.9
PR95-25	6-1-4	amphibole	quartz	lv	-64.1	-48.5	-16.9	232.8		19.6		19.6	4.2	1.0
PR95-25	6-1-5	amphibole	quartz	lv			-20.0	292.1		21.4		21.4	4.7	0.9
PR95-25	6-1-6	amphibole	quartz	lv			-16.0	288.1		19.1		19.1	4.0	0.9
PR95-25	6-1-7	amphibole	quartz	lv	-58.3	-49.5	-16.2	283.0		19.2		19.2	4.1	0.9
PR95-25	6-4-1	amphibole	quartz	lv	-59.2	-58.3	-15.0	224.2		18.4		18.4	3.9	1.0
PR95-25	6-4-2	amphibole	quartz	lv	-53.4	-43.6	-14.7	185.9		18.2		18.2	3.8	1.0
PR95-25	6-4-3	amphibole	quartz	lv	-53.4	-43.6	-14.4	217.6		18.0		18.0	3.7	1.0
PR95-25	6-4-5	amphibole	quartz	lv	-60.2	-46.6	-15.6	213.1		18.8		18.8	4.0	1.0
PR95-25	6-4-6	amphibole	quartz	lv	-53.4	-59.2	-16.2	187.0		19.2		19.2	4.1	1.0
PR95-25	6-4-8	amphibole	quartz	lv		-60.2	-15.8	185.5		18.9		18.9	4.0	1.0
PR95-12	5-1-1	magnetite	quartz	lv	-38.8	-33.9	-1.9	118.5		3.4		3.4	0.6	1.0
PR95-12	5-1-3	magnetite	quartz	lv	-34.9	-40.7	-1.6	120.3		2.9		2.9	0.5	1.0
PR95-12	5-1-2	magnetite	quartz	lv	-54.4	-44.6	-10.9	103.5		15.1		15.1	3.0	1.0
PR95-12	5-1-4	magnetite	quartz	lv	0.2	-40.7	-2.1	198.2		3.8		3.8	0.7	0.9

Sample #	Incl #	Zone	Host Mineral	Type	Tn	Te	Tm ICE	Th (L-V)	Tm Hh	Salinity NaCl + CaCl2	salinity Hh melting	salinity used	mol NaCl	Density at Th
PR95-12	5-1-9	magnetite	quartz	lv	-46.6	-27.1	-1.8	297.5		3.3		3.3	0.6	0.7
PR95-12	5-1-5	magnetite	quartz	lv	-36.8	-29.0	0.2	226.7						
PR95-12	5-1-10	magnetite	quartz	lv	-34.9	-48.5	-2.3	289.0		4.1		4.1	0.7	0.8
PR95-12	6-1-1	magnetite	quartz	lv	-38.8		-1.8	112.8		3.3		3.3	0.6	1.0
PR95-12	6-1-2	magnetite	quartz	lv	-38.8		-1.6	109.7		2.9		2.9	0.5	1.0
PR95-12	6-2-1	magnetite	quartz	lv	-49.5		-2.4	171.8		4.3		4.3	0.8	0.9
PR95-12	6-2-2	magnetite	quartz	lv	-44.6	-53.4	-5.9	184.1		9.4		9.4	1.8	1.0
PR95-12	6-2-3	magnetite	quartz	lv			-2.0	184.1		3.6		3.6	0.6	0.9
PR95-7	5-2-6	hematite	quartz	lv	-48.5	-53.4	-10.9	101.3		15.1		15.1	3.0	1.0
PR95-7	5-2-8	hematite	quartz	lv	-48.5	-60.2	-11.0	115.6		15.1		15.1	3.1	1.0
PR95-7	5-2-11	hematite	quartz	lv	-53.4	-50.5	-10.9	112.3		15.1		15.1	3.0	1.0
PR95-28	5-2-6	silicified	quartz	lv	-64.1	-38.8		140.7	-22.5		23.0	23.0	5.1	1.1
PR95-28	5-2-1	silicified	quartz	lv	-57.3	-38.8		89.4	-18.4		23.6	23.6	5.3	1.2
PR95-28	5-2-5	silicified	quartz	lv	-58.3	-38.8		153.3	-22.5		23.0	23.0	5.1	1.1
PR95-28	5-2-3	silicified	quartz	lv	-61.2	-30.0		100.5	-14.9		24.1	24.1	5.4	1.2
PR95-28	5-2-2	silicified	quartz	lv	-58.3			137.7	-22.5		23.0	23.0	5.1	1.1
PR95-28	5-4-2	silicified	quartz	lv				192.7						
PR95-39	5-3-1	quartz vein	quartz	lv	-56.3	-48.5	-8.8	83.4		12.9				
PR95-39	5-3-2	quartz vein	quartz	lv	-60.2	-62.2	-21.7	85.6		22.3				
PR95-39	5-3-3	quartz vein	quartz	lv	-72.9	-25.1	-22.1	128.2		22.4				
PR95-39	5-3-4	quartz vein	quartz	lv	-54.4	-23.2	-18.8	110.5		20.8				
PR95-39	5-3-5	quartz vein	quartz	lv	-53.4	-47.5	-19.8	110.5		21.3				
PR95-39	5-2-1	quartz vein	quartz	lv	-55.3	-32.0	-14.2	106.5		17.8				
PR95-39	5-2-2	quartz vein	quartz	lv	-49.5	-20.0	-13.7	101.2		17.5				
PR95-39	5-2-3	quartz vein	quartz	lv	-51.4	-26.1	-13.5	107.3		17.2				
PR95-39	5-2-4	quartz vein	quartz	lv	-64.1	-32.9	-14.3	123.3		17.9				
PR95-39	5-2-5	quartz vein	quartz	lv	-63.1	-34.9	-14.2	122.2		17.8				
PR95-39	5-2-10	quartz vein	quartz	lv		-21.2	-20.2	331.3		21.5				
PR95-3	1-1-1	breccia	quartz	lv	-39.8			91.3						
PR95-3	1-1-2	breccia	quartz	lv	-68.0		-20.3	109.7		21.5		21.5	4.7	1.1

Sample #	Incl #	Zone	Host Mineral	Type	Tn	Te	Tm ICE	Th (L-V)	Tm Hh	Salinity NaCl + CaCl2	salinity Hh melting	salinity used	mol NaCl	Density at Th
PR95-3	1-1-3	breccia	quartz	lv	-74.8		-9.7	112.0		13.8		13.8	2.7	1.0
PR95-3	1-2-1	breccia	quartz	lv	-45.6	-2.3	-1.9	120.4		3.4		3.4	0.6	1.0
PR95-3	1-2-2	breccia	quartz	lv	-49.5	-4.2	-3.3	202.3		5.8		5.8	1.1	0.9
PR95-3	1-2-3	breccia	quartz	lv			-1.8	248.2		3.3		3.3	0.6	0.8
PR95-3	1-2-4	breccia	quartz	lv	-59.2	-14.2	-11.7	282.2		15.8		15.8	3.2	0.9
PR95-3	1-3-1	breccia	quartz	lv	-62.2	-25.7	-12.5	145.9		16.4		16.4	3.4	1.0
PR95-3	1-3-2	breccia	quartz	lv	-62.2	-31.0	-13.9	149.9		17.6		17.6	3.7	1.0
PR95-3	1-3-3	breccia	quartz	lv	-42.7		-3.4	154.5		6.0		6.0	1.1	1.0
PR95-3	1-3-4	breccia	quartz	lv	-60.2	-19.3	-12.8	143.2		16.7		16.7	3.4	1.0
PR95-3	1-3-5	breccia	quartz	lv			-3.2	136.1		5.7		5.7	1.0	1.0
PR95-3	1-4-1	breccia	quartz	lv	-62.2		-7.2	181.8		11.1		11.1	2.1	1.0
PR95-3	1-4-2	breccia	quartz	lv	-59.2	-19.3	-13.6	192.8		17.3		17.3	3.6	1.0
PR95-3	1-4-3	breccia	quartz	lv			-10.0	206.2		14.2		14.2	2.8	1.0
PR95-3	1-5-1	breccia	quartz	lv		-19.3	-3.2	237.9		5.7		5.7	1.0	0.9
PR95-3	1-5-2	breccia	quartz	lv	-37.8		-2.2	238.6		3.9		3.9	0.7	0.9
PR95-3	1-5-3	breccia	quartz	lv			-1.9	241.1		3.4		3.4	0.6	0.8

Sample #	Incl #	Zone	Mineral	Type	Tn CO2	Tn CLATH	Tm CO2	Tm CLATH	Th CO2	Salinity (clath)	salinity used	mol NaCl	density at Th
PR95-39	7-1-5	quartz vein	quartz	lv	-97.0		-57.3		28.0				
PR95-39	7-1-4	quartz vein	quartz	lv	-97.0		-57.3		28.0				
PR95-39	7-1-1	quartz vein	quartz	lv	-80.0		-57.3		25.9				
PR95-39	7-1-2	quartz vein	quartz	lv	-97.0		-57.3		25.9				
PR95-39	7-1-3	quartz vein	quartz	lv	-92.0		-57.3		28.1				
PR95-39	7-1-6	quartz vein	quartz	lv	-80.0		-57.0		24.5				
PR95-39	7-1-7	quartz vein	quartz	lv	-80.0		-57.3		21.5				
PR95-39	7-1-8	quartz vein	quartz	lv	-85.0		-57.3		21.5				
PR95-39	7	quartz vein	quartz	lv	-96.8		-56.4	8.6		2.8	2.8	0.5	1.0
PR95-39	7	quartz vein	quartz	lv	-83.9		-56.4	8.6		2.8	2.8	0.5	1.0
PR95-39	7	quartz vein	quartz	lv	-79.8		-56.5		24.9				
PR95-39	7	quartz vein	quartz	lv	-82.2		-56.5		21.6				
PR95-39	7	quartz vein	quartz	lv	-94.2		-56.5		25.6				
PR95-39	7	quartz vein	quartz	lv	-78.0		-56.3	7.5	21.8	4.9	4.9	0.9	1.0
PR95-39	7	quartz vein	quartz	lv	-94.5		-56.3		24.0				
PR95-39	7	quartz vein	quartz	lv	-78.3		-56.2		25.5				
PR95-39	7	quartz vein	quartz	lv	-78.3		-56.3		25.5				
PR95-39	5-1-1	quartz vein	quartz	lv	-92.0		-57.2		29.2				

Sample #	Incl #	Zone	Mineral	Type	Tn	Th (L-V)	Tm NaCl	Salinity (N)	salinity used	mol NaCl	d at Th
PR95-25	6-3-1	amphibole	quartz	lvh			304.6	38.5	38.5	10.7	
PR95-25	6-3-4	amphibole	quartz	lvh			278.6	36.6	36.6	9.9	
PR95-25	1-5-1	amphibole	quartz	lvh			395.3	46.9	46.9	15.1	
PR95-25	1-5-2	amphibole	quartz	lvh			314.8	39.3	39.3	11.1	
PR95-11	2	amphibole	quartz	lvh		120.0	222.5	33.1	33.1	8.5	1.4
PR95-11	2	amphibole	quartz	lvh		158.6	197.2	31.7	31.7	8.0	1.2
PR95-12	6-3-2	magnetite	quartz	lvh			172.9	30.6	30.6	7.5	
PR95-12	6-3-4	magnetite	quartz	lvh			168.2	30.4	30.4	7.5	
PR95-12	6-3-5	magnetite	quartz	lvh			168.2	30.4	30.4	7.5	
PR95-12	6-3-3	magnetite	quartz	lvh			349.7	42.4	42.4	12.6	
PR95-12	5-2-3	magnetite	quartz	lvh			445.7	52.7	52.7	19.1	
PR95-12	5-2-4	magnetite	quartz	lvh			510.0	61.1	61.1	26.9	
PR95-12	5-2-5	magnetite	quartz	lvh			420.0	49.7	49.7	16.9	
PR95-12	5-2-6	magnetite	quartz	lvh			534.8	64.6	64.6	31.2	
PR95-28	5-3-11	silicified	quartz	lvh	-78.7		222.3	33.0	33.0	8.4	1.8
PR95-28	5-3-6	silicified	quartz	lvh			338.5	41.4	41.4	12.1	2.8
PR95-28	5-3-16	silicified	quartz	lvh			337.2	41.2	41.2	12.0	2.8
PR95-28	6-1	silicified	quartz	lvh			190.2	31.4	31.4	7.8	1.7
PR95-28	6-1	silicified	quartz	lvh			188.5	31.3	31.3	7.8	1.7
PR95-28	6-1	silicified	quartz	lvh			199.4	31.8	31.8	8.0	1.7
PR95-39	6-1-5	quartz vein	quartz	lvh			273.9	36.3	36.3	9.7	

Appendix V

Results of Raman Spectroscopy

Scan #	Stage	Sample	object	Range	Integration	reads	lens	Details	Peaks and comments
JN01014	amphibole	PR95-25	red solid in apatite	4000-50	10	5	50	mineral inclusion	291& 432(Hematite)
JL01014	amphibole	PR95-25	red solid in lvhs	5000-50	10	5	50	red solid in a lvhs	1318, 613, 296, 247(Hematite)
JL01015	amphibole	PR95-25	red solid in quartz host	5000-50	10	5	50	red solid in quartz host	1510, 1329, 667,626, 413, 293, 225 (Hematite)
JL01017	amphibole	PR95-25	red solid in quartz host	5000-50	10	5	50	red solid in quartz host	1325, 670, 614, 414, 299, 246 (Hematite)
JL01002	magnetite	PR95-12	red solid in lvhs	5000-50	10	5	50	a red solid mineral in a lvhs	1318(Hematite)
JN01021	hematite	PR95-7	red solid in quartz	4000-50	10	5	50	red solid inclusion(hematite) in quartz	258, 313, 429, 625, 673, 1340(Hematite)
JN01024	hematite	PR95-57	red solid in quartz	4000-50	10	5	50	red solid (hematite) in quartz	1328 (Hematite)
JL01023	silicification	PR95-28	red solid in lvs	5000-50	10	5	50	a red solid mineral in a lvs	Water and 1311, 663, 409, 295, 242 (Hematite)
JL01027	silicification	PR95-28	red solid in lvs	5000-50	10	5	50	a red solid in lvs	1321, 606, 410, 299, 242(Hematite)
OC01040	silicification	PR95-28	solid	5000-50	10	5	100	transparent solid in lvhs	1088,1038, 416,381,293 1088 & 293(carbonate?), what are others?
JN01024	silicification	PR95-57	red solid in Qtz	4000-50	10	5	50	red solid (hematite) in quartz	1328(Hematite)
JL01035	quartz vein	PR95-39	cabonic lv?	5000-50	10	5	50	a lv carbonic fluid inclusion	1386 & 1281(CO2)
JL01037	quartz vein	PR95-39	a red solid in lvs	5000-50	10	5	50	a red solid in a lvs	1322, 613, 412, 298, 240(Hematite)
JN01025	quartz vein	PR95-39	vapor-rich inclusion in Qtz	4000-50	10	5	50	dark vapor-rich secondary lv	1285 &1388(CO2)
JN01026	quartz vein	PR95-39	solid in LVS	4000-50	10	5	50	a red solid in secondary lvs	Water and 1314(hematite)
JN01027	quartz vein	PR95-39	solid in LVS	4000-50	10	5	50	a rounded transparent solid in secondary lvs	Water and 284, 733, 1085, 1723(calcite or aragonite)
JN01028	quartz vein	PR95-39	LV carbonic	4000-50	10	5	50	liquid in lv carbonic	1285 & 1388(CO2)

Scan #	Stage	Sample	object	Range	Integration	reads	lens	Details	Peaks and comments
JN01029	quartz vein	PR95-39	vapor-rich carbonic LV	4000-50	10	5	50	a vapor-rich carbonic	1285 & 1388(CO2)
JN01030	quartz vein	PR95-39	carbonic lv in quartz	4000-50	10	5	50	liquid in lv carbonic	1285 & 1388(CO2)
JN01031	quartz vein	PR95-39	vapor in LVS carbonic	4000-50	10	5	50	gas of a lvs carbonic	1285 & 1388(CO2)
JN01032	quartz vein	PR95-39	liquid in LVS carbonic	4000-50	10	5	50	liquid of a lvs carbonic	1285 & 1388(CO2)
JN01033	quartz vein	PR95-39	solid in LVS carbonic	4000-50	10	5	50	solid of a lvs carbonic	Water,1006 (gypsum?), 1285 and 1388(CO2); 1052 may be SO2?. 438, 975, 1089, 1462, and 1508?
JN01034	quartz vein	PR95-39	vapor rich carbonic	4000-50	10	5	50	vapor-rich carbonic	1285 & 1388(CO2)
JN01036	quartz vein	PR95-39	LV carbonic	4000-50	10	5	50	liquid of a lv carbonic	1285 & 1388(CO2)
JN01038	quartz vein	PR95-39	vapor-rich carbonic LV	4000-50	10	5	50	vapor-rich carbonic	1285 & 1388(CO2)
JN01039	quartz vein	PR95-39	LV carbonic	4000-50	10	5	50	a lv carbonic	1388(CO2)
JN01040	quartz vein	PR95-39	solid in LVHS	4000-50	10	5	50	a red solid in secondary lvhs	Water and 1321 (hematite)
JN01041	quartz vein	PR95-39	LV carbonic	4000-50	10	5	50	vapor in a lv carbonic	1388(CO2)
OC01009	quartz vein	PR95-39	vappor in lv carbonic	5000-50	10	5	100	vapor in a lv carbonic	1382 & 1278(CO2)
OC01010	quartz vein	PR95-39	liquid in lv carbonic	5000-50	10	5	100	same flinc as above, on liquid	1383 & 1278(CO2)
OC01012	quartz vein	PR95-39	liquid in lv carbonic	5000-50	10	5	100	liquid in lv carbonic	1383 & 1278(CO2)
OC01013	quartz vein	PR95-39	liquid in lv carbonic	5000-50	10	5	100	liquid in lv carbonic	1383 & 1278(CO2)
OC01014	quartz vein	PR95-39	liquid in lv carbonic	5000-50	10	5	100	liquid in lv carbonic	1383 & 1278(CO2)
OC01016	quartz vein	PR95-39	liquid in lv carbonic	5000-50	10	5	100	liquid in lv carbonic	1385 & 1280 (CO2)

Scan #	Stage	Sample	object	Range	Integration	reads	lens	Details	Peaks and comments
OC01017	quartz vein	PR95-39	vapor in lv carbonic	5000-50	10	5	100	vapor in lv carbonic	1383 & 1280(CO2)
OC01019	quartz vein	PR95-39	vapor in lv carbonic	5000-50	10	5	100	vapor in lv carbonic	Water and 1383 & 1278(CO2)
OC01020	quartz vein	PR95-39	liquid in l only carbonic	5000-50	10	5	100	liquid in a liquid only carbonic flinc	1383 & 1279(CO2), 1822?
OC01052	quartz vein	PR95-39	solid	5000-50	10	5	100	transparent solid in lvhs	1088 & 283 (calcite)
OC01053	quartz vein	PR95-39	solid	5000-50	10	5	100	transparent solid in lvhs	1505(?), 1459(?), 1086(calcite), 1052? 1006(gypsum), 974?, 439?
OC01055	quartz vein	PR95-39	solid	5000-50	10	5	100	transparent solid in lvhs	1088 & 284 (calcite)
DC0108	quartz vein	PR95-25	solid	5000-50	10	5	100	on the solid of the previously identified sulphate	989(barite)
DC0110	quartz vein	PR95-25	liquid	5000-50	10	5	100	on the liquid near solid in the flinc	984(barite)
DC0113	quartz vein	PR95-39	solid	5000-50	10	5	100	repeat for OC01053, to verify the peaks	1505(?), 1459(?), 1086(calcite), 1052? 1006(gypsum), 974?, 439?
DC0114	quartz vein	PR95-39	solid	5000-50	10	5	100	solid in an lvhs flinc	1087 & 284 (Calcite)
DC0115	quartz vein	PR95-39	carbonic	5000-50	10	5	100	an carbonic lv in an lvh flinc	1386 & 1284(CO2)
DC0117	quartz vein	PR95-57	solid	5000-50	10	5	100	a solid in a lvhs flinc	Water and 1086, 283, 184(Calcite)
DC0120	quartz vein	PR95-57	solid	5000-50	10	5	100	a solid in a lvhs primary	Water and 1086 & 285 (Calcite)
DC0121	quartz vein	PR95-57	solid	5000-50	10	5	100	a solid in a lvhs	1086 & 283 (Calcite)

Appendix VI

Fluid inclusion data on some Iron-Oxide Cu-Au-(REE) deposits

Deposit	Metal	Stage	FI type	Other solids	Temperature (°C)	Salinity (wt. %)	Primary evidence	References
Candelaria, Chile	Fe-Cu-Au-Ag-(Zn)	main Cu mineralization	LV		340-470		no	Marschik et al. (2000) quoted by Marschik & Fontbote (2001)
			LVHC		330-400		no	Ullrich and Clark (1999)
		postore cal	LV		<=180		no	Marschik et al. (2000) quoted by Marschik & Fontbote (2001)
Maramungee Creek, Little Eva, Ernest Henry, Mount Elliot, Cloncurry	Fe-Cu-Au	px-act alter.	LV		350-500	10-22	yes	Xu (2000)
		ab-mt(-hm)			170-260	15-23	yes	
		Sulph.-qtz-cal			80-200	14-28	yes	
Osborne , Cloncurry district	Fe-Cu-Au	pre-ore	LVHS, CO_2		>450	60-70	no	Adshead et al. (1998) and Adshead (1995) - quoted by Pollard (2001)
		main Cu-Au	??, secondary		300	20-37	no	
Lighting Creek, Cloncurry district	Fe-Cu-Au	ab-mt-qtz sill and qtz-mt±py±ab.	LVHS, CO_2-rich	hl, Sylvite ± cb ± pyrosmallite±hm/mt	>420	33-50	No	Perring et al. (2000)
		Cu-Au	LV±H secondary?		122-178	15-28		
		associated with mt in veins	LV		A: 261->370 B: 178-283	A: <1.2; B: <4.6		
Pahtohavare, Kiruna, Sweden	Cu-Au	ore bearing qtz vein	LVHS	hl,sylvite,cal,hm, uniden. Solids	Th(L-V) 113-179, Tmh 221-486	33-58	Yes	Lindblom et al. (1996)
			LVH		125 – 170	28-30	Yes	
			CO_2-rich		Th -4.2 - +25.8; TmCO257.7 -57.9		Yes	
			secondary LV		80 – 344	0.5 – 25	Yes	

Deposit	Metal	Stage	FI type	Other solids	Temperature (°C)	Salinity (wt. %)	Primary evidence	References
Eloise, Cloncurry	Fe-Cu-Au-Ag	stage I albitization, stage II ± hbl ±bio ± qtz	LVHS	Hl±Fe-Mn-Cl-Si±Fe-chloride ±sylvite±unid.	277-540	32-60	Yes	Baker (1998)
		stage III qtz-cal-act,chl-cp-po, py, & mt	LVHS	Hl±sylvite±Fe-Mn-Cl-Si±Fe-Chloride ±unid.	101-330	30-40	yes	
		stage III	CO_2(LV) + H_2O					
		stage IV vein of (1) chl±Kfs±cal ±ms±cp± py±hm(2)sd-hm±py (3)cal ± fl± Kfs ± ms±chl ±sph ±gn±asp±py	LVHS	Hl±sylvite±Fe-chloride	137-258	29-35		
		stage III	LV±H	hl	127-199	30-32		
		syn to post III	secondary LV±H	hl	121-315	28-39		
		post ore	LV		101-145	4-17		
Starra, Cloncurry district	Fe-Au-Cu	stage 2 ironstone, breccia zones	CO_2-rich LV, CO_2. Minor CH_4		-20 to 24		poor	Rotherham et al. (1998)
		stage 2: bt-mt-hm-qz-py	LVHS	hl, cal+ mt+ ferropyrosmallite	345-615	34-52		
		stage 3: hm-Au-bar-qtz-anh-cal -> cal-Cu-py-chl-ms	LVHS	hl+bar+ferropy-rosmallite+Mn- chloride +anh	225-360	30-42		
			LV±H		97-315	8-38		
Olympic Dam	Fe-Cu-U-Au-Ag-REE	pre ore stage	LVH(S)	hl, Fe chlorides	198-389	31-42	Yes	Oreskes and Einaudi (1992)
			LV(S)	Hm	206-170	10-23	Yes	
		Hm-breccia	LV, CO_2		130-280	7-24	Yes	

VITA AUCTORIS

NAME:	Xinyu Song
PLACE OF BIRTH	Hebei, P.R.China
YEAR OF BIRTH	1965
EDUCATION	University of Windsor, Windsor, Ontario 2000-2002 M. Sc.
	China University of Geosciences, Beijing, China 1989-1992 M. Sc.
	Jilin University, Changchun, Jilin, China 1983-1987 B. Eng.